UNIVERSITY OF STRATHCLYDE

DEPARTMENT OF MECHANICAL ENGINEERING

AN INVESTIGATION INTO BASE BLEED FOR DRAG REDUCTION IN BLUFF TWO-BOX SPORTS UTILITY VEHICLES

ANDREW LAMOND

A thesis presented in fulfilment of the requirements for the degree of
MASTER OF PHILOSPHY in MECHANICAL ENGINEERING

SUPERVISOR: DR. M STICKLAND

2009

This thesis is the result of the author's original research. It has been composed by the author and has not been previously submitted for examination which has led to the award of a degree.

The copyright of this thesis belongs to the author under the terms of the United Kingdom Copyright Acts as qualified by University of Strathclyde Regulation 3.50. Due acknowledgement must always be made of the use of any material contained in, or derived from, this thesis.

Acknowledgements

The author would like to acknowledge and make thanks for the help of Dr. Matthew Stickland, senior lecturer at the University of Strathclyde, for his guidance throughout the project and assistance in its completion. His extensive knowledge was essential in the achievement of this project.

Thanks are also due to Adrian Gaylard, senior aerodynamicist at Jaguar Land Rover, for his comments and suggestions while the work was being completed.

The help and advice of Duncan Lindsay and David Cunningham was also appreciated during the use of the laser scanning equipment.

Alastair Duff is due thanks for his help when using the wind tunnel. He helped ensure the procedure was carried out correctly and undoubtedly improved the accuracy of the results.

The author would also like to thank all of the technicians in the Department of Mechanical Engineering at University of Strathclyde for their advice and assistance in building the wind tunnel model and rig - in particular, Jim Docherty and Frank McKenna.

Finally, a note of thanks must be made to all family and friends who offered support and encouragement throughout the project, particularly those who showed an interest in the work and questioned the methods used. This questioning often led to a greater understanding of the problem and was therefore invaluable.

Table of Contents

Table of Figures

Table of Tables

Table of Equations

Nomenclature

A	Reference Area
A_{base}	Base area of the vehicle
A_{bleed}	Area of the bleed outlet
C_d	Drag coefficient
C_f	Skin friction coefficient
Cm	Mass flow coefficient
Cq	Bleed ratio/bleed coefficient
D	Drag
F_A	Force on vehicle in wind tunnel tests
F_r	Wind tunnel balance reading
g	Force due to gravity
K_i	Turbulent kintetic energy at the inlet
$\dot{m}$	Mass flow rate
q	Dynamic pressure
P_1	Static pressure
P_2	Stagnation/total pressure
P_a	Ambient pressure
P_d	Dynamic pressure
R	Gas constant
Re	Reynolds number
S	Equivalent flat plate area
T_a	Ambient temperature
U_{in}	Velocity at the control volume inlet
V	Vehicle velocity
V_{bleed} or V_d	Bleed air velocity
V_∞	Free-stream velocity
β	Bleed deflection angle
ε_i	Turbulence dissipation rate at inlet
ρ	Fluid density
ρ_a	Ambient air density
μ	Fluid viscosity

Abstract

The purpose of this project was to investigate the concept of 'base bleed' when used on two-box bluff-body sports utility vehicles (SUVs). The project was set up in collaboration with Jaguar-Land Rover, with emphasis on the use of base bleed on a Land Rover Discovery Mk III. Base bleed is generally defined as a method of reducing the drag of an object in motion via the introduction of air or some other gas to the rearward low pressure region. In the case of this project, a supplementary air source was applied to test this effect.

The project involved computational fluid dynamics (CFD) and wind tunnel testing. A computer-model was generated through use of a Konica VI-9i Non-Contact 3-D digitizer and a scale model. Geomagic Studio 10 was used to manipulate the scanned point-cloud data into a useable 3-D model. Pre-processing for CFD was carried out in Gambit and CFD analysis was carried out using Fluent.

This paper shows that the reduction in drag increases to a certain point as the mass flow rate of air is increased and the flow is deflected at the outlet. By controlling the turbulent wake to the rear of the vehicle, it is shown in the paper that Cq of 0.035 (mass flow rates of under 0.76kg/s) can reduce drag coefficient by 9.1% with an outlet on the side of the vehicle, and that a Cq of 0.019 (mass flow rate of under 0.2kg/s) can reduce the drag coefficient by 5.5% for a small outlet on the upper section of the rear of the vehicle. It was also found through wind tunnel testing that the drag may be reduced further by the bleed outlet cavity that was not simulated in the CFD method employed.

Throughout the investigation, the feasibility of base bleed being applied to a production vehicle was considered.

1 Introduction

The purpose of this project was to investigate the concept of 'base bleed' when used on two-box bluff-body sports utility vehicles (SUVs). The project was set up in collaboration with Jaguar-Land Rover, with emphasis on the use of base bleed on a Land Rover Discovery Mk III.

In 2007/2008, the UK experienced a sudden and extreme rise in the cost of motoring fuel. In July 2008, the price of diesel reached over £1.30/litre, emphasising the importance of fuel efficiency when buying a new car to the consumer. Some believe that the cost of fuel will continue to rise significantly over the coming years.

Fuel efficiency is further sought after by manufacturers due to increasing environmental concerns from the UK government and consumers alike, as well as in the international market. Although the exact figures vary depending on the source, there is a clear trend showing that UK vehicle emissions are increasing simply due to the number of vehicles on the roads. As a result, major manufacturers are researching and utilising novel methods of improving vehicle efficiency. The introduction of electric and hybrid cars has become common, although the technology is still in its infancy. More traditional methods such as improving the engine design and vehicle aerodynamics could prove to be equally effective.

It must be noted, however, that the aim to increase fuel efficiency must be met while maintaining the practicality of the vehicle. Large 4x4 cars, or sports utility vehicles (SUVs), are desired by the consumer for aesthetic reasons, but also for their off-road ability and their high storage capacity. For these reasons, fuel economy must be increased without compromise to the power delivery from the engine or their interior space. Companies such as Jaguar-Land Rover are therefore investigating innovative drag reduction methods.

Aerodynamic drag contributes greatly to the amount of energy required by a vehicle. Figure 1.1 shows the contribution of aerodynamic drag to the total forces acting on a 1.5 tonne saloon car (Renault Laguna RT) [1]:

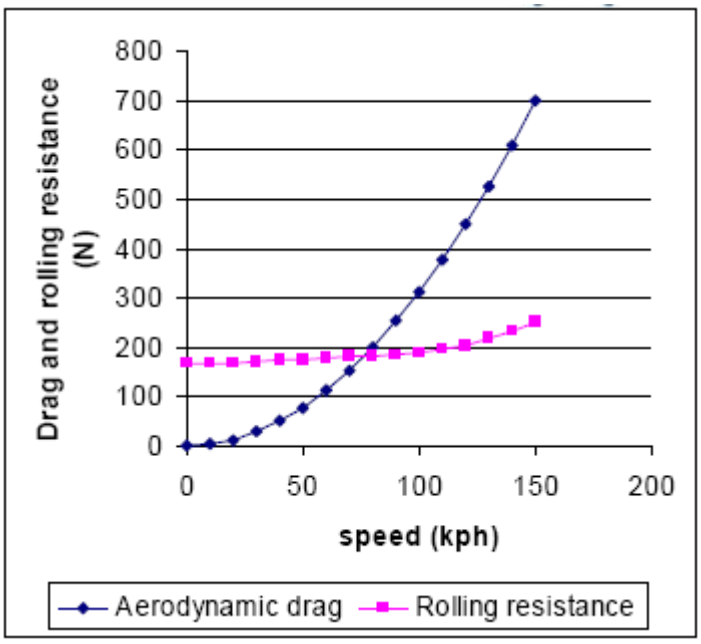

Figure 1.1 Graph of aerodynamic drag and rolling resistance

It can bee seen that above 70kph (19.44m/s) the aerodynamic force begins to dominate over the rolling resistance of the vehicle. As motorway speed limits in the UK tend to be 70mph (31.29m/s), reducing this force can significantly improve a vehicle's fuel economy. "For a full-size truck, a change in drag coefficient of 0.01 is approximately equal to an improvement in fuel economy of 0.1 mpg on the combined city/highway driving cycle," says Max Schenkel of General Motors. "The same drag coefficient reduction can improve a car's fuel economy by approximately 0.2 mpg."[2]

The drag coefficient referred to by Schenkel is a dimensionless parameter that can be used by engineers to calculate the total drag force acting on a vehicle, commonly written as C_d. However, a low drag coefficient does not necessarily translate to a low drag force. Famously, the Volkswagen Beetle had a lower drag coefficient than the Jaguar D type, but ultimately had a higher drag force for the same speed. To ensure

low drag, designers must also consider the cross-sectional area of the vehicle. Therefore, when improving an existing vehicle design, it is not C_d reduction that is important, but rather the reduction of C_d*A.

1.1 Base Drag and Lift Induced Drag

The total aerodynamic drag force acting on a vehicle can be considered to be a combination of a pressure (form) drag and skin friction drag.

Pressure drag due to flow separation constitutes more than 90% of the total drag of bluff bodies [3]. A considerable proportion of the drag of a 4x4, (that is not so prevalent in saloon cars, for example) is base drag. Base drag, a form of pressure drag, is caused as a low pressure region develops to the rear of the vehicle (the base region). This low pressure is caused by turbulence as the flow separates at the rear edges of the upper, lower and side surfaces of the car.

This is a particular problem in 4x4 vehicles due to the large flat rear section, causing a large turbulent wake. SUVs also have a tendency to have the four sides parallel to the flow at close to right angles with the rear surface. This sharp angle significantly affects the flow separation and the characteristics of the flow in the base region.

Another form of drag to be overcome is lift induced drag caused by adverse pressure gradients resulting in vortices. It has been suggested that in the case of road vehicles, it is not possible to define an induced drag and therefore the term ‘vortex drag’ is preferred [4]. However, the control of these vortices will have the effect of reducing the total drag of the vehicle.

In vehicle aerodynamics, it is much more difficult to differentiate between base drag and vortex drag than it is in aeronautics and therefore the distinction is useful mainly

to identify the primary source of the drag rather than to obtain quantitative predictions of each [5].

1.1.1 Common Base Drag Reduction Techniques

Vehicle aerodynamics research began not for reasons of economy, but for the realisation of faster sports and racing cars. In the 1930s manufacturers began to utilise the materials and processes that largely became available through developments in the aircraft industry to incorporate basic aerodynamic principles and streamlining into car design. This evolved from the 1960s onwards as a greater understanding of lift and drag was established in the automotive industry to create many of the novel ideas seen on the roads today. The benefits of aerodynamic innovation are widely known and recognised and should not be underestimated in the pursuit to improve modern road vehicle efficiency. Some common base drag reduction methods are illustrated in Figure 1.2 [6]:

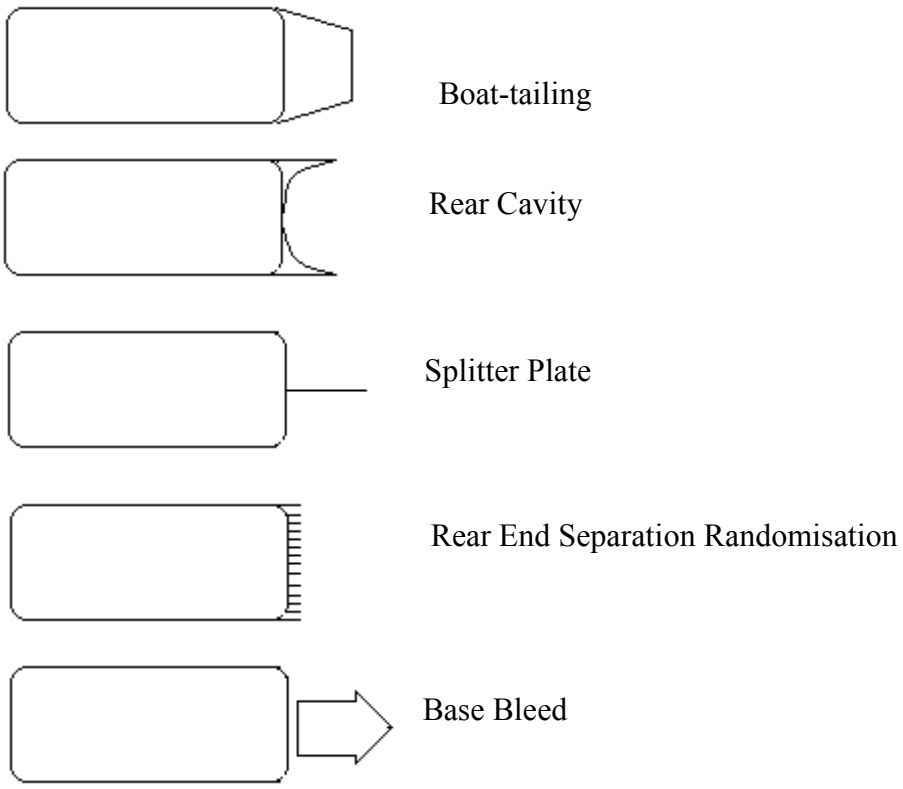

Figure 1.2 Common base drag reduction methods

All of these are practical methods of reducing base drag for certain, specific applications. However, only boat-tailing has, until recently, been seen as a practical solution in terms of SUVs (consider Porsche Cayenne, BMW X6 or Range Rover Sport).

This report details an investigation into base bleed as a drag reduction technique for bluff, two-box SUVs. Base bleed has the potential to reduce the drag coefficient with no effect on the projected area of the vehicle and could therefore reduce the overall drag force. This technique has had only limited exposure to road vehicles to date, and so a broad range of considerations will be made during the investigation.

1.2 Base Bleed

Base bleed can be defined as the reduction of drag via the introduction of air or some other gas to the rearward low pressure region. Drag reduction can be achieved through repressurisation of the base region, or the air or gas may be used to control the turbulent wake of the vehicle or the trailing vortices that cause drag. Although this may still result in repressurisation within the base region, repressurisation may not be the primary influence on the change in drag.

The air or gas used will be known as 'bleed air' for the duration of this report. This bleed air can be obtained in a number of different ways: In the case of artillery shells, base bleed is often implemented through use of a gas generator to the rear of the object, an example being the M864 [7]. The most detailed study of base bleed in vehicle design to date was carried out by Howell et. al. [8]. The experimental work carried out by Howell used a supplementary air source to simulate base bleed. Following Howell's work, this investigation's results were obtained by introducing a 'virtual' secondary flow to the system. However, consideration was given to bleed air being obtained through ducting from a high pressure region on the vehicle as this may be a more practical approach to a real system. This is commonly known as ventilation and is sometimes considered to be different from base bleed.

The point at which air is expelled into the base region will be known as the 'bleed outlet', positioned on the rear surface of the vehicle.

2 Literature Review

2.1 Base drag research

Diebler and Smith[9] state that existing models suggest that base drag is dependent on vehicle forebody drag, and that for certain configurations total drag can be reduced by increasing forebody drag. This fits most clearly with small projectiles but is not necessarily accurate for large vehicles and so studies were done to help predict the base drag of large vehicles.

Hoerner[10] was first to establish that the objects forebody shape directly influenced the base drag as a result of variation in the boundary layers and therefore the boundary layer separation at the rear. He quantified this with two equations, one for 2-dimensional analysis and one for 3-dimensional analysis. Based on these findings, it is important to consider that any modifications made to the front of the vehicle to implement base bleed may adversely affect the drag at the base region, regardless of the bleed configuration used and the effect of the bleed air. The system must be considered as a whole and the total drag reduction will be most significant.

It was found by Diebler and Smith through use of a specially designed ground based research vehicle (GRV) that the equations used by Hoerner could not be applied to large-scale vehicles and produced large errors in the base drag results. Although it appears part of the error produced was due to the boundary layer separation on the vehicle caused by the sharp leading edges, the errors are significant enough to dictate that these equations cannot be used in this report to compare forebody drag and base drag.

2.2 Base bleed

Base bleed has been studied in many different circumstances as it occurs accidentally in many practical applications. Some examples of this, also sited by Chin-Yi Wei and Jeng-Ren Chang[11], are flow between turbine blades and aerodynamic forces of high-rise buildings. Therefore, there have been many studies of a generic nature into base bleed to see how air flows react through bleed systems. Although these do not always concern pressure forces and drag reduction, these studies are particularly useful in predicting the results of various bleed configurations.

Chin-Yi Wei and Jeng-Ren Chang conducted an interesting study into the effects of base bleed in 2001. Their study involved two dissimilar bluff objects side-by side as air was forced towards them. Based on their literature review, they believed that there was a strong correlation between the geometry of the bluff bodies, the bleed outlet size and the observed biasing effect of the wake in the flow. Previous studies had found that for varying gap sizes, the vortex shedding frequency was different in the wake of the two objects, even where the objects are similar. The reasons are attributed to the differences of flow angle of the separated flow and of steadiness of the separation point.

Where only one bluff body is considered, with base bleed implemented through the centre of the body, it was found by Suryanarayana et. al.[12] that the drag of a sphere can be reduced significantly and that simultaneously, the flow field around the base is stabilised and made symmetric, leading to reduction of unsteady aerodynamic forces. The study investigates relatively high Reynolds numbers (8.5×10^5) and found that drag reductions in the region of 50-60% were observable.

The vented area in the sphere was set at 2.25% of the frontal area of the sphere. Experiments were conducted by reducing the vent area to 1% of the frontal area (by

reducing the hole size to 20 mm) using a parallel internal tube. Additionally, a venturi duct was placed in the internal flow. All tests resulted in a drag reduction of around 60%, and it was believed that any differences in the results were due to flow separation at the inlet.

Disturbances were introduced and it was found that the drag reduction achieved is highly sensitive to the quality of the external surface and relatively insensitive to disturbances in the internal flow. This is interesting as with a base bleed system involving a ducting system, it is very likely that the flow will be unsteady and liable to disturbances as the vehicle accelerates, changes direction, is influenced by wind or dirt in the atmosphere.

Wood [13] and Bearman [14] have studied the effect of bleeding a secondary stream of air into the wake of a 2-dimensional blunt based airfoil. Much of the work was carried out with consideration given to the non-dimensional bleed coefficient Cq, given by:

Equation 1

$$Cq = \frac{V_{bleed} \times A_{bleed}}{V_{\infty} \times A_{base}}$$

Where V_{bleed} is the velocity of the bleed air

A_{bleed} is the area of the bleed outlet

V_{∞} is the free-stream velocity

A_{base} is the base area of the vehicle

It was reported that by varying Cq, base bleed causes the base pressure to increase up to a certain limit and then the drag begins to increase with mass flow rate due to a drop in base pressure. The optimum value of Cq was found by Bearman to be around 0.13. Kohri[6] summarised Bearman's findings succinctly as follows:

"The flow visualization study reveals sporadic shedding of eddies similar to Kârmân vortices as long as Cq is small. Around the region where $Cq = 0.13$ in which C_{pB} [base pressure] becomes maximum, eddy forming positions are detached from the base causing random eddy formation. In other words, the vorticity becomes maximum at eddy formation points causing a decrease in pressure. When eddy formation locations are detached from the base by the base bleed, the base pressure is believed to increase causing the drag to decrease."

Wood and Bearman also found that the effect is greater when the area of the jet is large when compared with that of the base. These findings are of particular interest, and various bleed configurations were examined to test these findings on a 3-dimensional body.

Further work was done by Hiroshi Higuchi [15] when he investigated a number of passive controls, including base bleed (slotted disks), edge induced longitudinal vortices behind 3-d polygonal plates, the fineness ratio and surface protrusion. His paper demonstrates wake control of a slotted disk using base bleed, giving a brief explanation of the resulting flow pattern. This work does not draw any specific conclusions relevant to vehicle design, but demonstrates that base bleed can be used to control the wake of a bluff body and reconfirms its effectiveness.

2.3 Base bleed in vehicle design

The most extensive study of base bleed found for vehicle application was carried out by Howell et al.[8] Their study utilised a basic vehicle shape to test a number of base bleed configurations.

Howell et al. found that drag reduced linearly with flow rate.

It was also found that drag decreased asymptotically with bleed area, with the most effective bleed locations at the bottom, top and side of the body. Howell reported very poor results with a centrally located bleed outlet, but gave no explanation for these findings. To locate the outlet centrally, however, would likely be impractical for a production vehicle.

The lowest measured drag was obtained with porosities of 51% and 68%. "No attempt was made to see if an intermediate porosity would provide a drag minimum".

The tunnel speed was varied between 15m/s and 30m/s to assess the effects of Reynolds Number. It was found that base bleed was most effective at lower speeds (15m/s), but that it was only slightly dependent on Reynolds number. The effect appears to be due to the cavity created by the bleed outlet. Where the vehicle was examined with a bleed cavity but no outlet flow, "a reduction in the Reynolds Number from $Re = 2.2 \times 10^6$ to 1.1×10^6, where Re is based on model length and free-stream velocity, increased the drag benefit for the porous base [containing uniformly sized bleed outlet slots across the entire surface] from $\Delta C_D = 0.012$ to 0.015." Cavity depth was also examined and it was found that the presence of a bleed outlet alone caused drag reduction. "Optimum depth of cavity was investigated and was found to be the same regardless of porosity, around 10% of total length." These two points are of particular importance as the CFD methods used in this project do not simulate a cavity in the vehicle and therefore likely overestimate the total drag.

Cavity height was investigated in relation to vehicle height by altering the vehicle shape. These findings, however, were not relevant to this investigation as the intention was to apply base bleed to a specific production vehicle, leaving the vehicle geometry largely unaltered.

There were many features of the method used by Howell that would make it difficult to assess if base bleed could be applied to a production road vehicle. For example,

the study used bleed configurations that would be unfeasible to apply to the rear of a real vehicle, with porosities of up to 68%.

The study also considered only a fixed ground and the vehicle had no wheels and so the influence of turning wheels on the base region was not considered. A pump was used to create the bleed air and all tests were done using the MIRA model scale wind tunnel. The work of Howell et al. was strongly used as a basis for this study. To build on this work, the analysis was performed using CFD to try and give a clearer indication of the flow patterns around the vehicle. CFD also allowed simulation of turning wheels, interaction with a rolling road and analysis of a production vehicle shape at full-scale.

This report details how some of Howell's findings were tested with the geometry of a production vehicle to see if they still held true. Howell's findings were used to influence bleed configurations, but the configurations were independently investigated to see how the vehicle shape affected the results.

Howell neglected bleed outlet design and the angle of the outlet flow in his study and mainly considers repressurisation of the base region as a method of drag reduction.

For this investigation as in Howell's study, it was felt that presenting the bleed mass flow rate in kg/s was appropriate to give a clear understanding of the scale of the system and help establish the feasibility of creating the required airflow were the work to be continued. However, Howell did highlight that this could be non-dimensionalised. Bleed flow coefficients can be presented in either mass flow or momentum terms. A definition of the former is important to understand Howell's conclusions. The mass flow coefficient, Cm was defined as:

Equation 2

$$Cm = \dot{m} / \rho A V_{\infty}$$

Where $\dot{m}$ is the bleed mass flow rate,

V_∞ is the free stream velocity,

ρ is the air density

A is the reference area of the model.

The volume flow rate, v, is effectively given by $\dot{m} / \rho$. The maximum flow rate used in Howell's experiments of 10 litres/s converts to a mass flow coefficient of 0.0033 or 0.33%.

Although these variables were not addressed in this investigation, this non-dimensional coefficient may be particularly useful if studying varying scales or shapes of model or alterations in vehicle speed.

Howell highlighted the importance of considering the overall energy balance:

"For example consider a vehicle with a frontal area of 2.0 m^2 and travelling at 30m/s. If the base bleed produces a drag coefficient reduction of 0.01, then the power saved is 0.33 kW. If the air movement consumes more than this then the vehicle does not benefit."

It was concluded that the energy balance likely negates the effects of base bleed. The report suggests use of exhaust gases: "A 2.0 litre engine running at 3600rpm and driving the vehicle above at 30m/s produces a flow rate coefficient [Cm]of 0.1% at all speeds"; and cooling pack airflow "typically in the range 2 – 3%... essentially constant with speed", but the latter is impractical for front-engined vehicles.

In keeping with the idea of considering a complete base-bleed system, Kohri and Kataoka [6] investigated bleeding engine cooling air to the rear end of the body into the flow separation region. "With this design, it is possible to achieve a drastic

reduction in the aerodynamic drag resulting from engine cooling air, which has caused increased air resistance in the past."

Their study showed that when ducting is used to bleed air into the base region, base bleed affects the drag by changing the pressure distribution around the inlet as well as at the base. Although results in this investigation will only be concerned with the effect at the outlet, total drag, not only base drag, will be considered.

Kohri showed that changing the base configuration can have different effects on the front of the vehicle (or other inlet location) where no changes have been made. From this, it should be noted that consideration should ideally be given to the base bleed system as a whole when implementing a practical design. The work of Mair [16] further emphasises this. Mair states that, due to the drag of the device used to implement base bleed from a secondary flow, often the overall result will be negative as the resulting drag reduction from base bleed will not be sufficient to offset the initial drag increase from the device.

Kohri also shows that, where engine cooling air is a necessity, to discharging it to the base region is the most effective way to minimise drag.

The methods used by Kohri are interesting in that emphasis is given to the ratio of bleed velocity to free-stream velocity, V_d/V, and its effect on drag under various configurations. By tapering the base of a cuboid - more closely matching the geometry of a saloon passenger vehicle than the untapered configuration examined prior to this – it was found that the optimum value of V_d/V increased from 0.35 to 0.45. This underlines how subtle changes in geometry affect the overall result, and stresses that the findings of Howell et al. using a generic two-box bluff body shape cannot necessarily be applied to another two-box SUV geometry. What Kohri does not comment on, however, is that in changing the geometry of the parallelepiped, the geometry of the nozzle and therefore the speed and direction of the ducted air is also changed at the outlet and therefore would have influenced the wake differently.

While there was likely a significant effect due to the change in shape of the base region (the base pressure acting on a smaller surface area and in a different vector may have been two important factors), it was not quantified how much of the base pressure and overall drag changes were due to the body shape changing and how much was due to the outlet flow velocity changing.

As with Bearman [14], it was shown that 'the wake can be controlled with a relatively small amount of bleed by making the ratio of the bleed outlet area with respect to the base cross section larger" for a tapered configuration.

2.4 Further Drag Reduction Techniques for Two-Box SUVs

This short section has been included as studies carried out on other aspects of vehicle drag reduction have influenced the work in this investigation. Jung-Do Kee et al [17] considered reducing base drag by altering the shape of the rear of a vehicle to limit Coanda effects. This investigation was particularly relevant to saloon and coupe type cars where curved rear ends are both practical and aesthetically pleasing. However, Jung-Do Kee et al. did look at the application of spoilers on square back vehicles and found some interesting results.

Coanda effects can increase induced drag by accelerating air flow as the boundary layer remains attached. Two different spoilers were applied to a square backed vehicle – one with a gap between the spoiler and the vehicle and one without. It was found that the gap increased the Coanda effect, while removing the gap made an overall reduction in induced drag by 5%. The spoiler used had a 9° downward angle, which minimised the wake area and resulted in 47% reduced lift at the rear axle.

This control of the airflow into the rear wake had significant effects on the drag of the vehicle. The angle of the spoiler had a significant effect, suggesting that the outlet design and deflection of bleed air would also affect drag reduction.

3 Computational Fluid Dynamics

Computation Fluid Dynamics (CFD) is a modern method of allowing engineers to solve and analyse problems involving fluid flows using numerical techniques. First used in the aerospace industry in the 1960s, it also allows analysis of heat transfer and other associated phenomena such as chemical reactions. CFD has developed rapidly in aerodynamics engineering since the 1980s, meaning that current CFD codes can be solved on high-specification desktop computers. However, the underlying behaviour of fluid flows means that CFD problems are tremendously complex and care must be taken to ensure the results produced are sufficiently accurate for the problem being solved.

This chapter gives a background to CFD analysis and outlines the reasons that this method was selected for this investigation. Some detail of the programs and methods used is also included, but will be further expanded upon in later chapters.

3.1 CFD Method

CFD packages include three main elements and an understanding of what each of these elements does is essential to understanding the procedure for solving a problem using CFD. These are: a pre-processor; a solver; and a post-processor.

Pre-processors are used to define the geometry of the problem, known as the computational domain. These may be designed entirely within the pre-processor,

however more commonly the geometry is imported from another computer aided design (CAD) package. It is therefore important that a pre-processor is compatible with a host of other engineering programs. Pre-processors are then used to generate a mesh of the domain and apply boundary conditions.

The mesh applied in a pre-processor divides the system into a series of small sub-systems that are more easily solved. The solution to a flow problem is defined at nodes inside each cell, with the accuracy of the solution being dictated by the number of cells in the grid, or more accurately, the resolution of the mesh. Developing an appropriate mesh for a problem is extremely important in order to optimise the solution and time expense of a problem. Currently, pre-processors are being developed with self-adaptive meshing capability, which will be able to refine a mesh in areas of rapid variation of shape or detail [18].

Boundary conditions include specification of geometry type and physical properties of the domain. The pre-processor also allows specification of the fluid properties to be used within the problem. The pre-processor used in this investigation was Gambit version 2.4.6. This was developed by Fluent Inc. (a subsidiary of ANSYS Inc.) and so is specifically designed for use with the solver and post-processor Fluent.

Solvers and post-processors are often combined into one program. Fluent version 6.3.26, the solver and post-processor used in this investigation, is a general-purpose CFD code based on the finite volume method on a collocated grid. The solver generally follows three steps to produce a solution [18]:

1. Integration of the governing equations of fluid flow of all the (finite) control volumes of the domain
2. Discretisation – conversion of the resulting integral equations into a system of algebraic equations
3. Solution of the algebraic equations by an iterative method

The basis of almost all CFD is in solving the Navier-Stokes equations, named after Claude-Louis Navier and George Gabrile Stokes[0]. Newton's second law states that force equals mass times acceleration. This fundamental principle together with the assumption that the fluid stress is the sum of a diffusing viscous term (proportional to the gradient of velocity), plus a pressure term gives rise to Equation 3 [20]:

Equation 3

$$\frac{\partial \rho \phi}{\partial t} + \nabla \cdot \rho \boldsymbol{u} \phi - \nabla \cdot \Gamma \nabla \phi = S$$

This is usually referred to as the general transport equation for the variable ϕ (where ϕ can represent velocity components or scalar quantities such as energy, chemical species concentration etc). The first term refers to the fact that in an unsteady flow ϕ can vary with time throughout the flow field, often known as the time rate of change of ϕ. The second term accounts for changes in ϕ as a result of convective transport processes, which tend to dominate in fluids moving with relatively large velocities. The third term accounts for the diffusion of ϕ throughout the fluid. The presences of gradients or spatial variations in ϕ mean that diffusive processes can take place in a moving or stationary fluid. The term appearing on the right hand side is referred to as the source term and accounts for sources of momentum, energy and so on that are located within the flow field [21]. From this equation, the three Navier-Stokes equations arise in more complex form.

The CFD technique is based upon the idea that the Navier-Stokes equations can be discretised over some region or domain in which the flow is to be determined. Discretisation of the convective terms is the most challenging aspect of CFD software development because these terms are inherently nonlinear, for example, in the Navier-Stokes equations the convective terms involve products of the unknown velocities and velocity gradients.

This allows a set of linear algebraic equations to be produced, relating the flow field variable (velocity, pressure, temperature etc) values at the computational points to one and other. The user must then input boundary conditions to the solver (and initial conditions for any unsteady time dependent analyses), allowing the algebraic equations to be solved simultaneously, yielding the flow variable values at the computational points.

The nature of this method dictates that only an approximate solution can be produced. There are many factors that can influence the accuracy of the solution and it is important for the user to establish to how accurate the results are required to be. The only way to verify results is generally in comparison with experimental test work.

The post-processor is the tool by which results are analysed. Fluent has a powerful post-processor that can output coloured images of the three dimensional flowfield, displaying numerous properties of the system (e.g. static pressure, flow velocity, temperature or turbulence intensity). These can also be animated for transient problems. Post-processors can normally present numerical data such as forces acting on an object or heat transfer.

3.2 Turbulence model selection

Theoreticians have hoped for a century to produce a theory that could predict "the rate of energy transfer between the mean flow and the turbulence, the distribution of energy across the different eddy sizes, and the average rate of dispersal of a pollutant through turbulent mixing" [19**Error! Reference source not found.**]. There is, as yet, no general theory of turbulence. This means that in solving a problem involving turbulent flow (any real vehicle aerodynamics problem inherently involves turbulent flows) the use of either models or direct numerical simulation based on a multitude of theories are necessary. Direct numerical simulation is too computationally expensive to be viable for the Reynolds number range and geometric complexity required for automotive aerodynamics, therefore implementation of an appropriate turbulence model is required. When performing CFD analysis, the selection of the turbulence model can greatly affect the processing time and efficiency, but can also have a bearing on the results produced. The computational power available has a significant bearing on the choice made, but it is essential that the correct model is used for each specific application.

In the early stages of this investigation in particular, it was necessary only to use a simple turbulence model. Eddy-Viscosity Models approximate the Reynolds stresses through the Boussinesq relations. They are therefore less accurate than the alternative Second-Moment Stress Models which use a more complex equation to approximate the Reynolds stresses, but require far less processing power.

Two-equation models are the simplest complete models of turbulence, taking into account the convective and diffusive transport of the turbulence itself. At present, the most commonly used two-equation model in turbulent flow simulations is the k – ε model. The standard k – ε model has been used throughout this project. Although more accurate results may be achieved by utilising a more advanced model, such as the RNG k – ε model or the realized k – ε model which can perform better at the near-wall regions, the standard model solves more quickly and is therefore beneficial

where a large number of cases are being investigated, as was the case here. The accuracy of the results produced by the standard k – ε model were deemed sufficient, as the aim of the investigation was to produce general trends under varying conditions and allow comparison of the results to each other. For the duration of the project, initial estimates of k and ε were calculated as follows [23]:

Equation 4

$$K_i = 4.5 \times 10^3 (Uin)^2$$

Where K_i is the turbulent kinetic energy at the inlet

Uin is the velocity at the inlet

Equation 5

$$\varepsilon_i = (K_i^{1.5}) 0.1643 / (0.09 \times Height)$$

Where ε_i is the turbulence dissipation rate at the intlet

Height is the flow inlet dimension.

3.3 Advantages and Disadvantages of CFD

This section will describe the reasons that CFD was used as a primary method of analysis in this study. It will also highlight some of the problems associated with using CFD for a project of this nature and how this may have affected the overall results.

CFD as a tool for studying aerodynamics has developed significantly in recent years, and now has many strengths over more conventional methods. One of the most significant advantages was the ability to create a geometrically accurate model for analysis. As this study aimed to investigate base bleed on a production vehicle rather than a generic vehicle-shaped bluff body, CFD allowed for manipulation using CAD software of the level of detail required of the model. It is often the case the geometry of the vehicle to be tested can cause problems with other methods of testing (i.e. wind tunnel testing) due to the physical constraints of the tunnel. In this case, CFD allowed study of a full size vehicle where neither a large enough wind tunnel nor a suitable model would have been available.

Furthermore, provided that the vehicle geometry is accurate enough, modern CFD techniques can allow for practically complete characterisation of the flow around, and through, a vehicle.

One major advantage in terms of this investigation is that the base bleed system did not need to be manufactured. Using a computer model meant that the design of a base bleed system could be done precisely, giving consideration to the realistic constraints of the vehicle geometry. CFD allowed implementation of a supplementary air source where wind tunnel testing would have required manufacture and implementation of such a system which would have been significantly time consuming. In industry, CFD is particularly useful in the design process for these reasons. As a vehicle design evolves, for example, testing can be

carried out very quickly without the new design being manufactured, saving time and money. This is also true in optimisation of design, where the effect of new or different components can be implemented and analysed without affecting the existing system.

CFD also allows simulation of high Reynolds numbers, discussed in Chapter 5.3.

Another advantage of CFD, that was relevant to this project, was the ease with which driving conditions could be simulated for the model. It was felt necessary that the vehicle should be studied with a moving ground plane and no interference from surrounding objects. This was easily set-up in the CFD environment but would have been more difficult with the available wind tunnel facilities. CFD would also allow for study of unsteady wind conditions, cross winds or varying atmospheric conditions if it were felt necessary.

One of the most significant advantages of CFD for this investigation, however, was the ease with which parametric studies could be carried out. Incremental changes to the flow characteristics from the bleed outlet were easily and precisely implemented, the accuracy of which were crucial and would have been difficult to replicate in wind tunnel testing.

A final advantage that should be mentioned is the abundance of data produced from a single CFD test. Basic information about the system can be quickly calculated, such as the cross sectional area of the model or the mass-flow rate of fluid from a particular duct. CFD allows the user to instantly access data on forces in each individual surface of the model being examined. This can be broken down into pressure forces and skin friction forces very simply. CFD also allows simple analysis of the flow through use of static or animated full colour displays. The can be set to show velocity profiles, turbulence, fluid density or areas of high and low pressure among other things. Where relevant, CFD can then be used to examine heat

transfer characteristics within the flow, including changes to material properties that result.

This data can be saved and compared with other simulations allowing for a very complete analysis of the results.

There are, of course, some significant disadvantages to using CFD as an engineering tool. It has been estimated that suitable hardware for CFD would likely cost between £5,000 and £10,000, substantiated by the requirement for multiple CPUs utilised to decrease solving time with calculations being run in parallel. In addition to this, the "perpetual license fee for commercial software typically ranges from £10,000 to £50,000" [18]. Furthermore, the expertise required in using the programs and understanding the principles behind CFD can often be difficult to obtain – for an individual hoping to utilise the techniques or for an organisation looking to employ qualified staff. This is compounded by the growing trend towards using open-source CFD codes in the engineering industry, making the software particularly complex and requiring new but very specific skills for each challenge faced.

When analysing the CFD method it is apparent that there are further disadvantages that must be considered. Capturing the effects of turbulence is particularly difficult as discussed in chapter 3.2. However, when using CFD codes it must also be considered that the following may be analysed poorly [24]:

· Adequately resolving, or modelling, boundary-layers
· Correctly capturing flow separations in adverse pressure-gradients.
· Resolving vortex structures (RANS methods tend to under-predict vorticity; Lattice-Boltzmann solvers tend to over-predict vorticity.)
· Accounting for the influence of incidental flow paths and relatively small-scale roughness (i.e. tyre tread).
· Accounting for mechanical deformation of parts (e.g. tyre shape).

· Accounting for deformation of parts under aerodynamic load (e.g. wheel deflector deformation).
· Modelling laminar to turbulent transition in boundary layers (only relevant for vehicles with wings and, perhaps, aeroacoustic simulation of flow structures on external rear-view mirrors.)

As this investigation dealt primarily with incremental changes to a model and the effects of implementing base bleed in comparison with an initial test case, it was felt that any error produced by these weaknesses would be consistent or inconsequential and therefore the conclusions reached would not be affected.

A more significant disadvantage is the time taken to solve each particular case. Although wind tunnel testing may take significantly longer to set-up initially, it is possible to obtain results almost instantaneously and therefore parametric studies can often be carried out very quickly. With CFD, it is easier to accurately change a particular condition within the test, but to obtain results for each study may take several hours or even days in cases of complex geometries and flow patterns.

For this investigation, however, it was deemed important that boundary conditions were precisely monitored and that a complete depiction of the flow characteristics was obtained. For these reasons, CFD was the optimum means of investigation and was primarily used.

4 Model Generation

A computer model was required in order to carry out fluid analysis and gain an understanding of the flow patterns and pressure forces resulting from the introduction of these ideas. This chapter describes how the computer model was generated, what modelling techniques were used in each case, and explains the choices made at each stage.

As a drag reduction study on turning vanes was being carried out in parallel at the University of Strathclyde, an adaptable model was required that could be used for a variety of purposes and exported into a wide range of programs – critically, the commercial CFD code FLUENT 6.3.26 and GAMBIT 2.4.6, deemed the most appropriate pre-processor and meshing tool.

In the first instance, an IGES file was provided by Land Rover for use in CFD investigations.

The geometrical accuracy of this model was excellent; however the model was extremely complex. The model contained a vast amount of very small and obscurely shaped faces, necessary to create the intricate detail of the car. Irregular faces can cause problems when creating surface meshes in Gambit, and having many small faces can cause a significant increase in processing time when solving CFD problems. Therefore, time was spent trying to simplify this model to the point where it could be used for CFD analysis.

Figure 4.1 shows the resulting model. At this stage however, it was still not possible to create a mesh in Gambit due to the irregularity of some of the small surfaces. Therefore, a new model was required in order to proceed with the project.

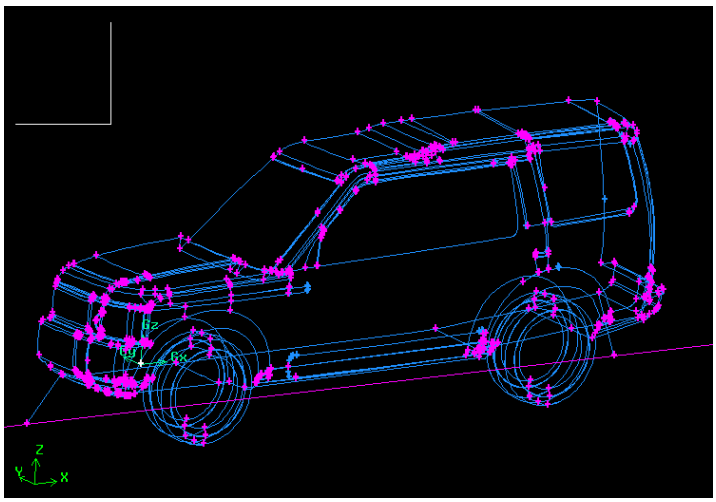

Figure 4.1 'Cleaned up' Land Rover model in Gambit

At this stage, it was felt necessary to create a very simple model, allowing some initial testing to be done. This allowed for a set of backup data to be produced that could be further investigated if a more accurate model could not be produced at a later date.

Dr. Stickland provided a CAD drawing of an SUV, similar in dimension to the Land Rover Discovery previously examined. This was successfully imported into Gambit and a coarse mesh was applied, as shown in Figure 4.2.

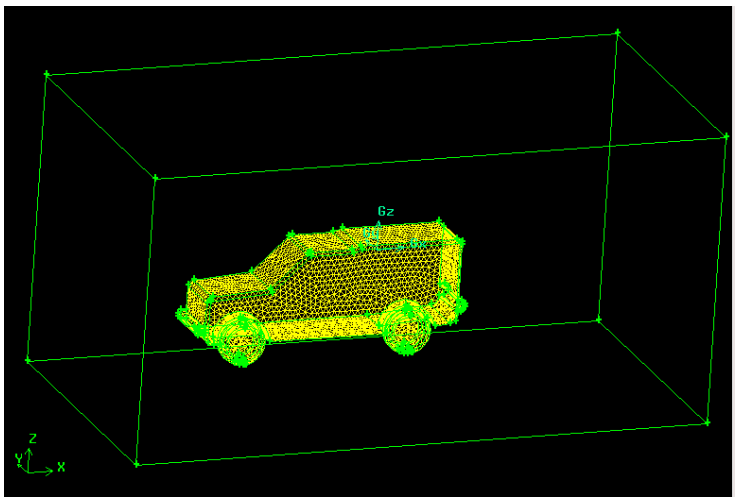

Figure 4.2 CAD model in Gambit with mesh

This mesh was then further refined in order to try to increase the accuracy of the results. Quadrilateral elements were used where possible to create a structured mesh, as shown in Figure 4.3. This was possible due to the simple nature of the geometry. A structured mesh has many advantages over an unstructured mesh (usually involving tetrahedral elements for 3-D problems). They allow more accurate results to be produced and generally have smaller data structures and therefore require less computer memory to store them. The mesh was also graded in order to make analysis on points of interest (the rear of the vehicle, in particular) more computationally intensive.

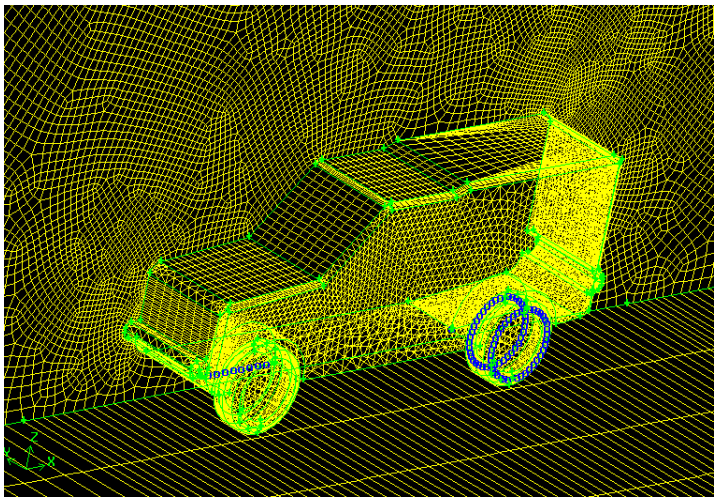

Figure 4.3 Structure mesh of CAD model

This model was imported to Fluent and the model was solved for a wind velocity of 25m/s, felt comparable to motorway driving speed in the UK. Calculation was then carried out to establish the drag coefficient of the model, C_d, using Equation 6.

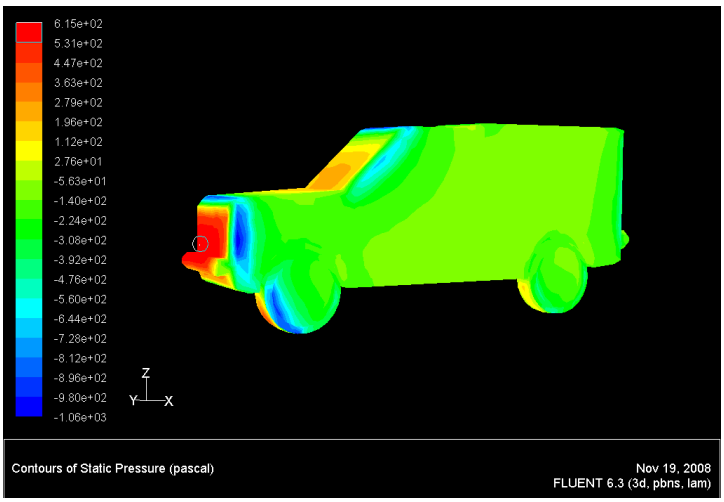

Figure 4.4 Fluent contour plot of static pressure for CAD model

Equation 6

$$D = \frac{1}{2}\rho A V^2 C_d$$

$$C_d = \frac{2(363.9585)}{1.225 \times 25^2 \times (1.567)}$$

$$C_d = 0.6071$$

It is common to use a half model in CFD to limit the processing time. The CFD solver was instructed to consider the inside surface of the vehicle to be a plane of symmetry, and therefore an appropriate solution is produced with half the number of calculations being required. However, this is only possible where the model being examined is symmetrical.

It was felt that the force values produced were realistic for this geometry; however the drag coefficient was higher than that of a production vehicle so modification of the model geometry would be required in order to continue using this model.

After failing to be able to test a model felt overly complex, and generating poor results from another of too simple geometry, it was decided that a laser scanner should be used to produce an ideal model. This model would be of sufficient detail to produce realistic drag readings and air flow patterns for the vehicle in question, while using simple surface shape designs so that pre-processing and solving could be done quickly and repetitively.

4.1 Laser Scanner

There are two main types of laser scanner: contact and non-contact. Non-contact scanners consist of active and passive scanners and are often called range scanners. Range scanners usually work via the triangulation method using a charge coupled device (CCD) camera, an apparatus designed to convert optical brightness into electrical amplitude signals using a plurality of CCDs, and then reproduce the image of a subject using the electric signals. By means of a laser passing across the surface of an object, the distance to the object can be obtained by the angle of reflection of the laser, the angle of incidence of the reflected light from the object into the CCD and the fixed distance between Laser and CCD camera. The National Research Council of Canada was among the first institutes to develop the triangulation based laser scanning technology in 1978 [25][26].

An alternative form of range scanner is a time-of-flight scanner, which measures the time taken for a photon to be reflected from the object and return to a sensor, allowing calculation of the distance to that particular point.

The image produced by a range scanner initially takes the form of a ‘point-cloud’ – a series of individual coordinates that can later be used to create a complete image of the model.

In this instance, a Konica VI-9i non-contact 3D digitizer was used for all scanning, shown in Figure 4.5. This is a free standing scanner suitable for scanning large

objects at variable distance, accurate to 50µm, ideally suited to reverse engineering applications such as this.

Figure 4.5 Konica VI-9i non-contact 3D digitizer

Konica Minolta non-contact 3D Digitizers are based on the principle of laser triangulation [27]. A fundamental limitation of what can be scanned with a triangulation system is having an adequate clear view for both the source and sensor to see the surface point currently being scanned.

4.2 Scale Model

A 1:6 scale model was used. Using a model of this size meant that it had many of the details such as windscreen wipers and door-mirrors that would affect the airflow around the car. However, a larger model or full-scale vehicle would have been more difficult to obtain and would have taken longer to scan. Another major advantage of using this scale of model was that the same model could be used for wind-tunnel testing, allowing accurate comparison to the CFD work. The model chosen is shown in Figure 4.6:

Figure 4.6 Scale model of Land Rover Discovery Mk. III

4.3 Laser Scanning Procedure

The general procedure for three dimensional modelling is shown in Figure 4.7 [28]. The left-hand side of the diagram shows the process from collecting the initial scans, known as 'range images', to aligning the scans and registering them as a single image, reducing the errors in the image to an acceptable level and then converting the image into a complete model. Each of these steps will be explained in more detail in the following sections. The right-hand side of the diagram shows how laser scanning equipment can also be used to create an image-map from intensity images of the colour and texture of the model, and how this would be integrated into the procedure if a true model were required. However, for the purposes of CFD, all intensity images were discarded.

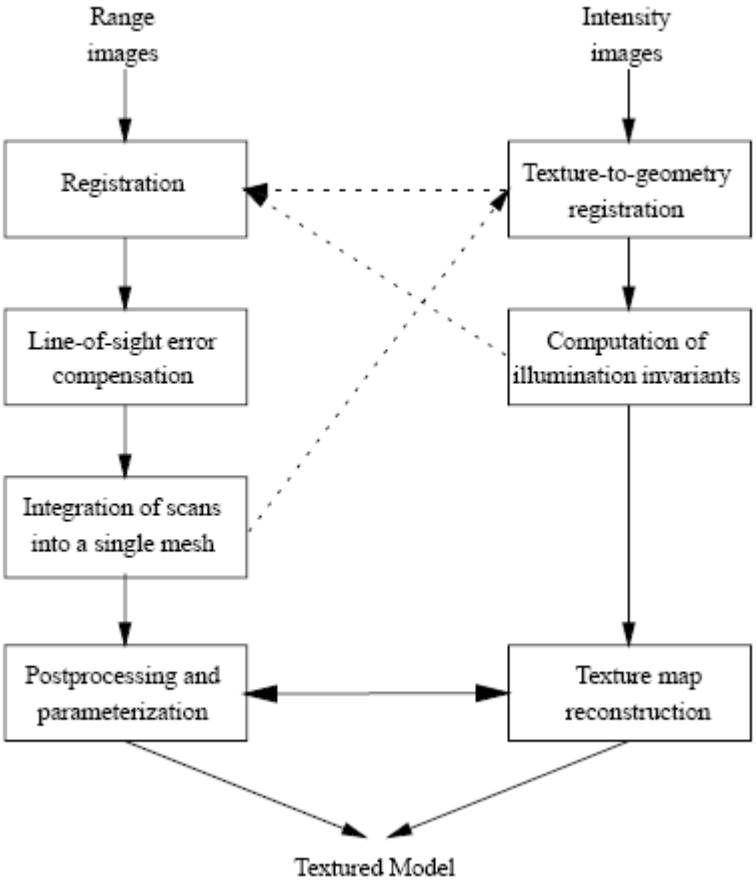

Figure 4.7 Image reconstruction process

4.3.1 Model Preparation

The colour and terrestrial albedo (the extent to which it diffusely reflects visible light) of the model were not suitable for scanning initially. The gloss black surface would not reflect adequate information back to the laser scanner. Therefore, the model was sprayed in a pale, matt colour to produce superior results.

Unwanted detail on the underside of the car was covered using masking tape. The wheels were removed to be scanned separately. The vehicle used for scanning is shown in Figure 4.8:

Figure 4.8 Prepared model for scanning

4.3.2 Scanning

To create the point-cloud, the model was positioned on top of a reflective black plastic sheet to avoid unwanted 'noise' data from the table/stand being collected. The final scan contained around 60 scans of the body work and chassis and around 15 scans of one wheel that was later added to the CAD model. The car was positioned approximately 1.5metres from the scanner. Konica Minolta Polygon Editing Tool (PET) was used to save and merge the scans into one model.

Each scan was taken at 20 º intervals turning the car through 360º (using the bottom of the chassis as a datum); the same process was repeated through pitch and yaw, using the same datum. Careful consideration was made to avoid holes in the final 3D image by creating extra scans of fine detail where necessary. The repeated data on the previous scan allowed for accurate supplemental scan stitching, and eventually a highly detailed point cloud.

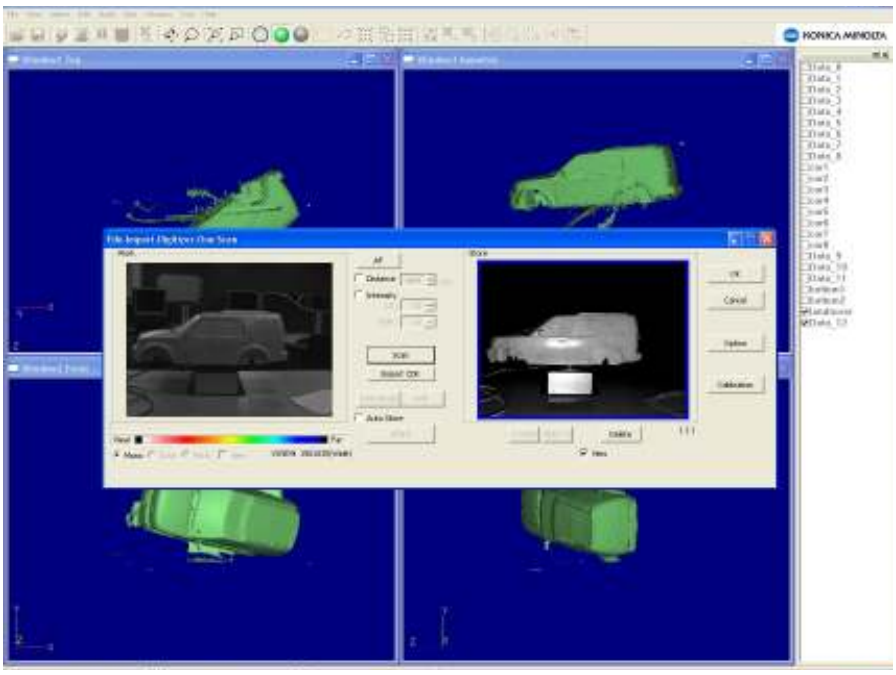

Figure 4.9 PET Laser scanning and stitching

Figure 4.9 shows the image of the car through the scanner on the left and the resulting scan on the right. The background images are various projections of the previous scans prior to being fully aligned.

Once aligned, the faces were stitched together using the 'merge scan' application. A detailed discussion of various scan registration and alignment methods is available in [28]. It should be noted that some peripheral detail, or 'noise data', was captured in the scan. Konica Minolta PET was used to delete this detail before the final point-cloud model was exported as an *.stp file.

4.3.3 Model Clean-up

The file was then imported into Geomagic studio 10, a leading reverse engineering and point-cloud management package.

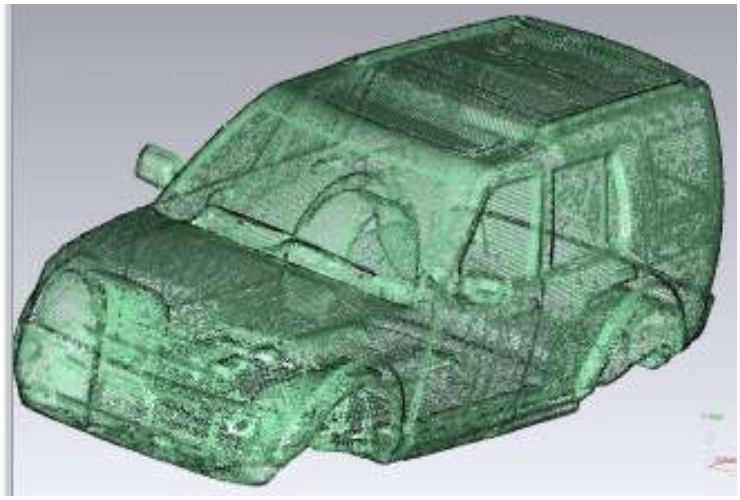

Figure 4.10 Initial detailed point cloud

From this initial, highly detailed point cloud (Figure 4.10), outliers were removed and then the vehicle was triangulated using the 'wrap' tool. The file could then be saved as a *.wrp file. Geomagic utilises a 'hole-filling' tool which was used to automatically patch up any gaps in the model. Geomagic was also used to remove any noise data left on the surface of the car. The 'remove feature' tool was used for large anomalous data, while the 'sandpaper' tool removed finer unwanted details. It was also possible to delete some of the fine detail around the windscreen wipers and front grill that might later cause problems in Gambit. The 'decimate triangles' tool allowed the triangulation to be simplified (decreasing the multiplicity of the knot vector), minimising the file size and thus providing a simplified point cloud suitable for NURBS surfacing.

4.3.4 Surface creation

NURBS surfaces were then created, an essential step for any model that will be used in a CAD program or CFD package. NURBS stands for Non-Uniform Rational Bézier-Spline. For a 2D surface, NURBS create curves with respect to control points and lines defined by the triangulation of the point cloud derived from the PET. Problems arise when the data reaches high complexity - the more complex the

surface (i.e. the multiplicity), the further the knot vector has to increase and the number of NURB patches has to increase.

4.3.4.1 Automatic surface creation

Both Catia V5R16 and Geomagic have point cloud NURBS surface creation work benches. Tests were done in each program using the auto-surface function, turning the point cloud into a series of patches (which would be turned into faces when the files was exported to Gambit) and, ultimately, a 3D volume.

In both programs, however, it was found that the patches created were highly irregular and would be difficult to mesh. Further to this, when the surfaces were applied much of the detail on the surface of the car was lost. Figure 4.11 and Figure 4.12 show the resulting patch layouts:

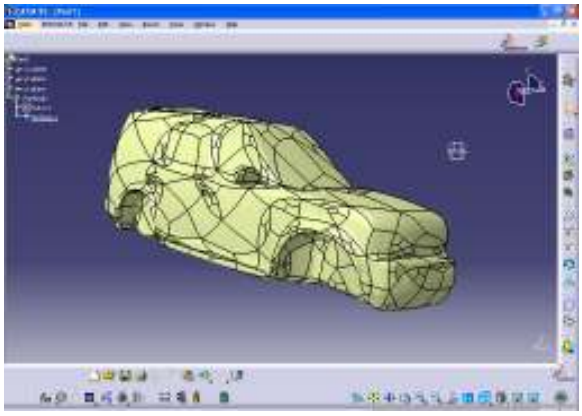

Figure 4.11 Catia automatic nurbs surfacing and patch layout

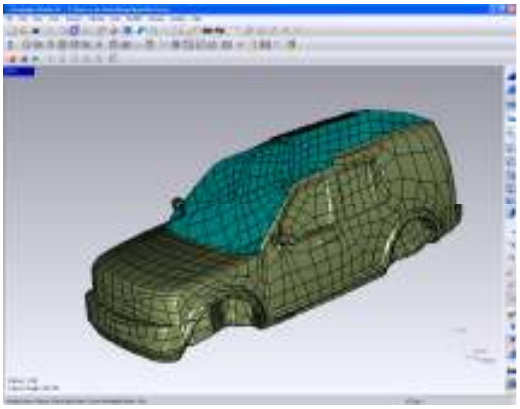

Figure 4.12 Geomagic automatic nurbs surfacing and patch layout

In each case, over 1000 patches were created. Although it was felt this would be unsuitable for the remainder of the project, further work was done to verify that the laser-scanned model could be used for analysis. The Catia model was chosen as more detail was retained. To apply a mesh in Gambit, some of the patch shapes had to be altered. This was time consuming, and, as the model was imported to Gambit

numerous times, the overall process was too slow using the auto-generated patch layout.

4.3.4.2 Manual Surface creation

To improve the accuracy of the model and shorten the time taken to apply a mesh, it was felt that manually creating a patch layout was necessary. Geomagic was used, initially with very large patches as larger patches are simpler for applying a uniform mesh. The initial layout is shown in Figure 4.13:

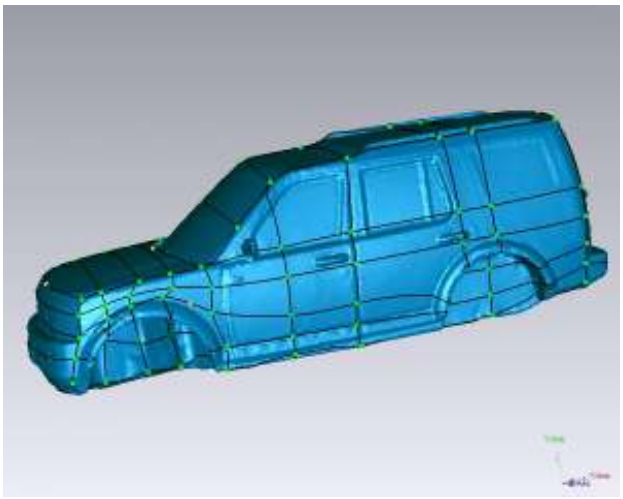

Figure 4.13 Initial patch layout

It was found that each of these patches contained too much detail, meaning it was lost when NURBS surfaces were applied. The patch number was increased to allow more detail to be retained. The patches were carefully aligned with main vehicle features to allow identification of the features during analysis and within a bulk-file where the geometry is easily interpreted.

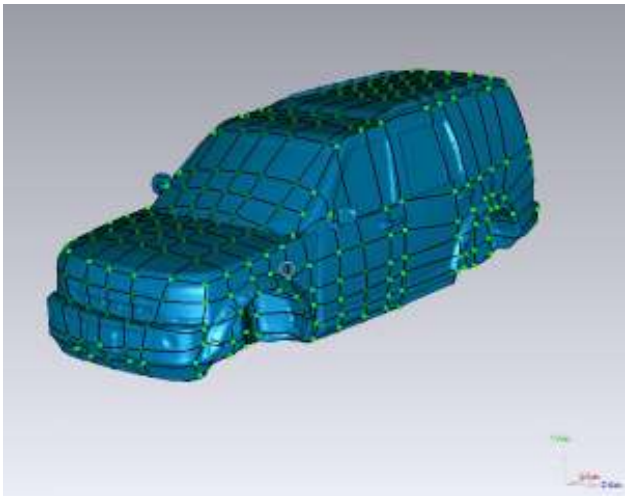

Figure 4.14 Final patch layout

Following this, Geomagic automatically applied a mesh for each patch that has been created. The surfaces are then laid over the meshes, creating a usable model for CFD. The grid pattern significantly reduced the number of skewed elements in Gambit.

4.3.5 Wheels

Figure 4.15 Image of final wheel design

The wheels were scanned using a similar process to that described previously. The same process followed for manual patch creation, keeping square faces to avoid

meshing errors in Gambit. Each wheel contains 155 faces, adding a significant amount of complexity to the model; however, the detail was retained in the tread and spokes of the wheel as this was expected to have a significant effect on the drag of the wheel as it spins.

4.4 Discussion of Model Generation Method

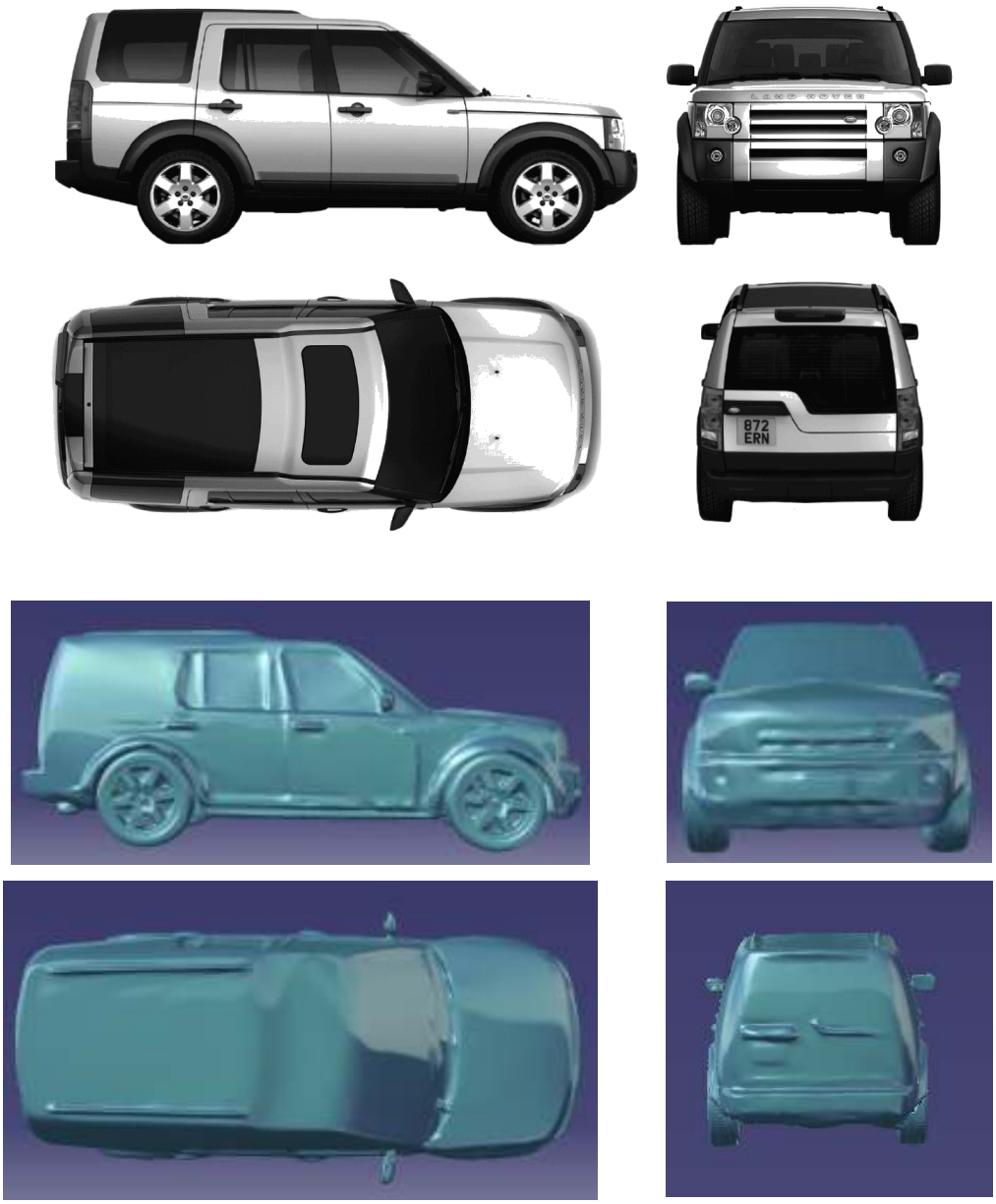

Figure 4.16 CAD 1/6th scale Discovery (shown in comparison with 1:1 scale Disco)

Figure 4.16 shows the CAD model obtained from the Laser scanning. It was felt that there were a number of significant advantages to using this laser scanned model for CFD analysis. The model was saved as an IGES file, meaning that this model is

fully capable of adaption and redesign within CAD programmes such as CATIA V5 or Pro Engineer, and allows transfer to fluid analysis packages such as Fluent and Gambit.

The vehicle body contained only 422 patches, making it simple to identify any faces with meshing errors – a particular problem with auto-generated patch designs. Another advantage of this patch layout was that the individual surfaces could be defined as boundary conditions in Gambit. By using uniform faces on the rear of the model, Gambit could create velocity (or mass flow) outlets from the faces for the purposes of base bleed. This meant that a number of different designs could be tested without having to alter the model. This is shown later in the base bleed development chapter (Figure 6.4 - Figure 6.6).

As the patch layout closely followed the contours of the vehicle, the faces could be assigned names in Gambit meaning that force readings could be produced for specific sections on the car (e.g. the pressure force on rear surface or front bumper with/without base bleed being implemented).

The disadvantages of this method mainly concern the time taken to produce the model. However, overall the amount of time saved in applying the mesh in Gambit far outweighs this cost. Furthermore the equipment required for this process is expensive, possibly prohibitively so for small projects.

5 Model Testing - CFD Analysis

5.1 Full Model

Numerous tests were done on the initial model to establish the best methods for conducting the study into base bleed. This section describes the various cases examined, the procedure and the reasons they were studied.

Firstly, a study of the full laser-scanned model was carried out to assess its suitability for CFD analysis. The model was easily imported into Gambit with no file conversion necessary. In Gambit, a small control volume (2000x750x750 - at this stage the model was dimensionless) was used to decrease solving time for this experimental session. A single volume was created from the faces of the vehicle geometry, which was then subtracted from the control volume using a Boolean command. A very coarse Tet/hybrid 3-D element shape unstructured mesh was then applied, with an element size of 20 and boundary conditions were set. The model was then exported to Fluent.

The 'scale' feature in Fluent was used to set the dimensions to millimetres. The convergence criteria of the residuals were set to $1x10^{-5}$ and k and ε were input:

$k_i = 2.8125$

$\varepsilon_i = 8.6106$

A velocity of 25 m/s was used again with the ground moving with the air flow to simulate movement of the vehicle. The air was considered to be incompressible, and atmospheric pressure was set at 101.325 kPa. Sea level air density of $1.225 kg/m^3$ was used, with a viscosity of $1.7894x10^{-5} kg/m\ s$. These values were used throughout the investigation.

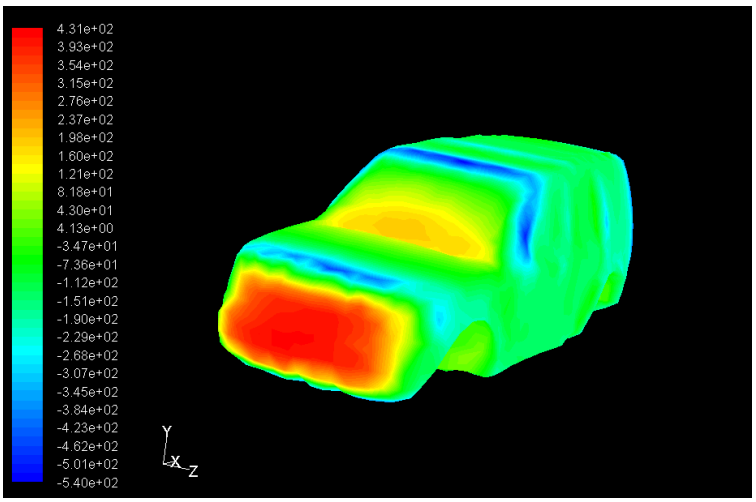

Figure 5.1 Contour plot of static pressure for laser-scanned model initial test

Figure 5.1 shows a pressure plot of the vehicle after it was solved. This was used to judge qualitatively whether the solution was realistic.

A brief study was then done to ensure that the wheels would not adversely affect the solution procedure. The wheels were imported in Gambit and aligned with the vehicle. Care was taken to ensure that the vehicle height was realistic as ground interaction may have affected the overall result if the vehicle were set too low. Four separate volumes were created for each of the wheels, and a Boolean command was used to subtract the wheels and car from the control volume. Again, a coarse mesh was applied in Gambit to decrease solving time (Figure 5.2), with the same control volume dimensions as used previously.

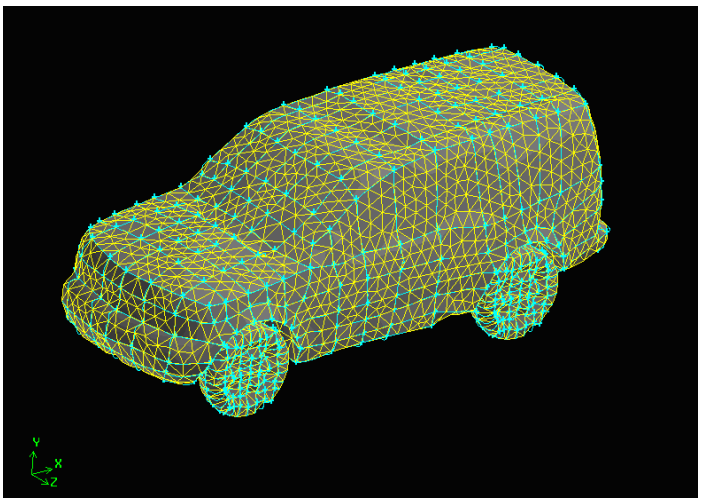

Figure 5.2 Coarse mesh applied to laser-scanned model with wheels

The model was solved with both static and rotating wheels with a moving ground plane. The speeds of the wheels were calculated to be 403rad/s for the scale model to travel at 25m/s with a wheel radius of 0.062m.

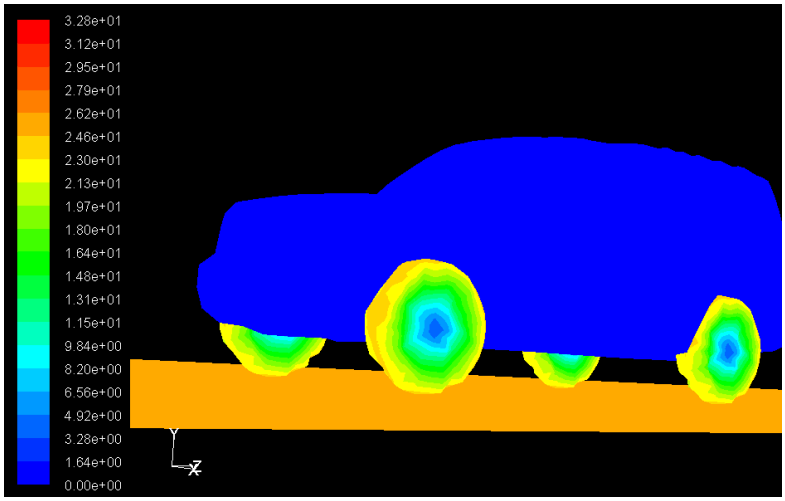

Figure 5.3 Velocity plot showing ground and wheel movement

Figure 5.3 shows the velocity magnitude of the moving ground and vehicle and verifies that the wheels were rotating at the desired speed.

To improve the results, Grid adaption was used. Wall y^+ is a non-dimensional parameter defined by Equation 7:

Equation 7

$$y^+ = \frac{\rho \upsilon_\tau y_P}{\mu}$$

Where υ_τ is the friction velocity,

y_P is the distance from point *P* to the wall,

ρ is the fluid density,

μ is the fluid viscosity at point *P*

The friction velocity can be calculated using Equation 8:

Equation 8

$$\upsilon_\tau = \sqrt{\tau_w / \rho_w}$$

Where τ_w is the wall shear stress

The wall unit, y^+, is the ratio of turbulent to laminar influences in a cell and has different values depending on which part of the boundary layer is being considered when investigating the wall region [29]:

- the viscous sub-layer ($y^+ < 5$)
- the blending region ($5 < y^+ < 30$)
- the fully turbulent or log-law region ($y^+ > 30$ to 60).

A wall-function simulation, as used here with a k-ε model, normally requires that y^+ of the first cell outside the walls is in the log-law region. In this region, there is

equilibrium between production and dissipation of the turbulent kinetic energy, therefore decreasing turbulent instability in near-wall simulations.

"Wall-function boundary conditions for parallel velocities are activated automatically within Fluent whenever a wall entity is prescribed as a boundary condition and a turbulence model has been activated. In order for the wall function approach to operate in a satisfactory manner it is essential that the value of y+ falls within the range $50 < y+ < 500$ for any wall entity" [23]. Grid adaption was particularly necessary around the wheels and the front of the car to ensure this was the case, as shown in Figure 5.4:

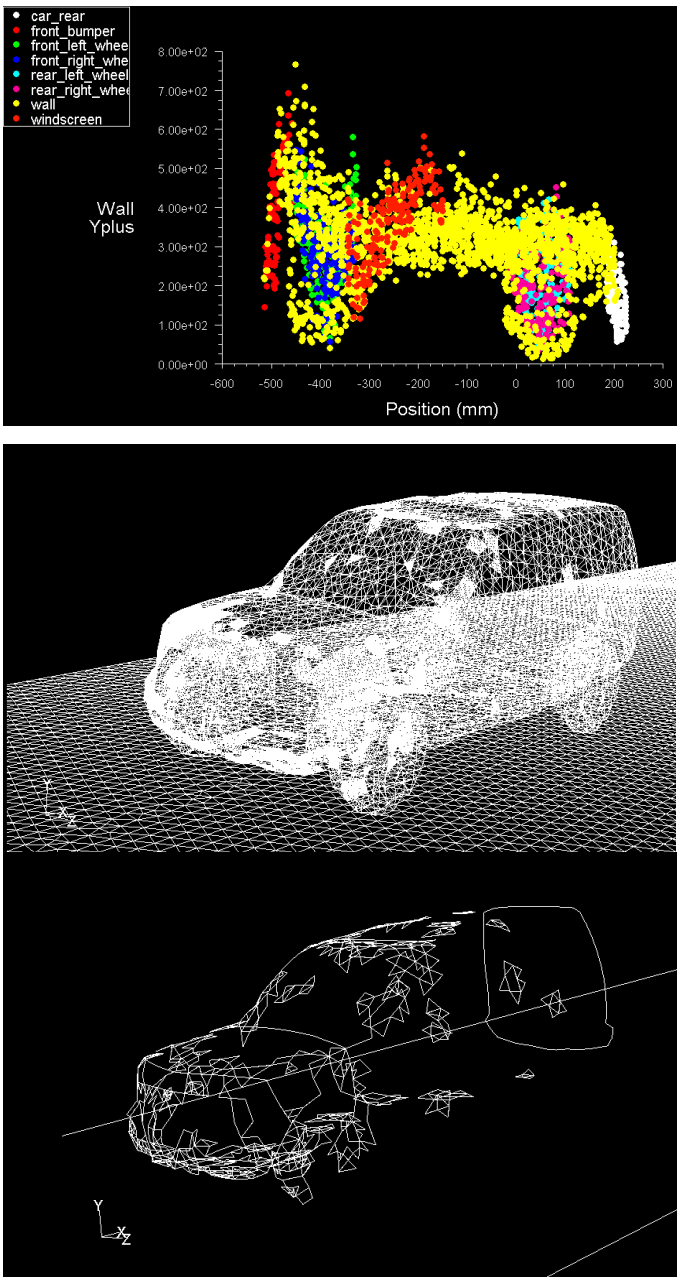

Figure 5.4 Plot of Y+ values prior to adaption and images showing areas of grid adaption

These processes were followed for any further analysis carried out in Fluent.

5.2 Half Model

Typically, in vehicle analysis, pressure or form drag is dominant over skin friction; therefore, the accuracy of the results obtained from CFD is largely determined by the accuracy of the calculated static pressure distribution on the body. As pressure distribution is strongly affected by the locations of flow separation and reattachment, incorporating a fine surface mesh allows accurate prediction of such phenomenon and improves the results. A coarser mesh tends to lead to inaccuracies in the model geometry, and therefore commonly increases the size of protrusions and sharpens angle sizes – usually resulting in an increased drag coefficient.

General CFD practice dictates that in vehicle analysis, a mesh of around 2-4 million elements is considered to be a coarse mesh. A moderate mesh should consist of between 4 and 10 million elements, and a fine mesh will contain more than 10 million elements [30].

Although the model was not exactly symmetrical, a half model was employed to allow a finer mesh to be applied. It was expected that the benefits of a finer mesh would far outweigh the loss of the asymmetrical features of the vehicle in producing an accurate results. By halving the model size and applying a symmetry plane to the centreline (as done with the basic model, described in Chapter 4), the number of elements that can be applied to the remaining geometry can be doubled without increasing the computational intensity. This allows a finer mesh or a larger control volume to be utilised without compromising the processing time for each study.

The model was cut using a Boolean command in Gambit. Care was taken to ensure that this was done through the centre of the vehicle and that no yaw angle was incorporated. The mesh was graded, with a fine mesh of 3mm being applied around the vehicle, becoming gradually coarser towards the edge of the control volume. The control volume size was set according to Fluent's best practice guide for vehicle analysis [30]. The domain extended around three times the vehicle length to the

front and five times to the rear. The width and height of the control volume were set so that the cross section of the vehicle did not exceed 1.5% of the domain area. With a graded unstructured tetrahedral mesh, approximately 2.2 million elements were used. Figure 5.5 and Figure 5.6 show the mesh used on the car surface and the control volume respectively.

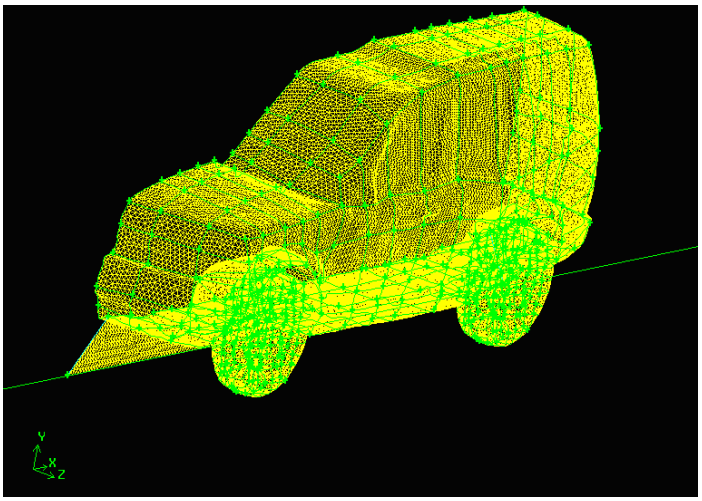

Figure 5.5 Mesh applied to half model

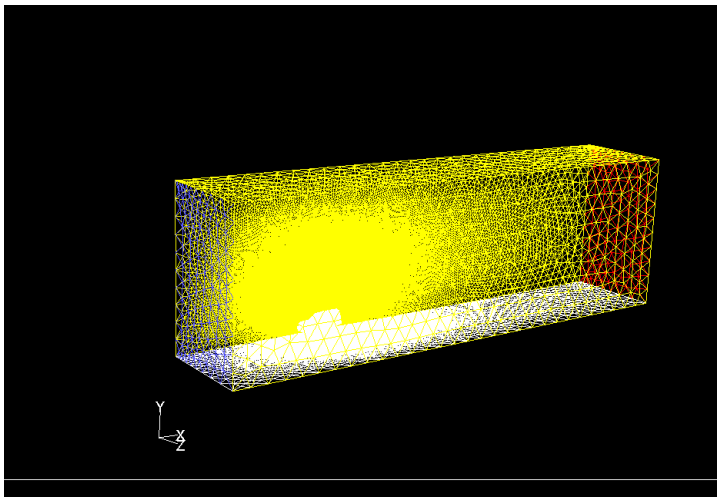

Figure 5.6 Mesh applied to control volume

The model was imported to Fluent 6.3.26. Interestingly, the finer mesh meant that the model shape imported to Fluent more closely related to the original scanned

geometry. This meant that the reference area reduced by 5.87% relative to half the model with the coarse mesh. This change in reference area is reflected in the results shown in Table 5.1. The model was run in Fluent for initial results to which all base bleed tests could be compared. The convergence criteria of the residuals were set to $1e^{-5}$ and a k- ε turbulence model was used. Using Equations 2 and 3, initial values of K and ε were calculated to be:

$k_i = 2.8125$

$\boldsymbol{\varepsilon}_i = 3.4442$

The model was set up to allow analysis of the change to forces on different areas of the vehicle. Tests were carried out with a static ground plane and both static and turning wheels for the sake of comparison with wind tunnel tests, as well as with both ground plane and wheels moving as done previously.

5.3 Model Scale

For the effects of the air flow to be examined properly, it was important that the CFD analysis being carried out was mechanically similar to the vehicle in question. Studying a small-scale model requires investigation at much higher inlet velocities to give a comparable Reynolds number with a real-life situation, as Reynolds number is a function of vehicle geometry and free-stream velocity[31]:

Equation 9

$$\mathrm{Re} = \frac{\rho V l}{\mu}$$

Where ρ is the air density,

V is the free-stream velocity

l is the characteristic length

μ is the dynamic viscosity

The Reynolds number characterises whether flow conditions lead to laminar or turbulent flow. As the Reynolds number is increased, the structure and location of boundary layer separation often changes. This can sometimes result in a reduction of overall drag. The Reynolds number particularly affects skin friction drag (generated by the shear stresses within the boundary layer) which on a bluff vehicle of this nature is likely to be around 10% but can account for up to 30% of the drag of a modern car [1]. For illustrative purposes, a flat plate of equivalent exposed planform area can represent the flat surfaces of a simple vehicle as skin friction drag is unaffected by rotation of the surface along the axis of the airflow. Equations 10 and 11 show the relationship between Reynolds number and skin friction drag that would be generated with a fully turbulent boundary layer:

Equation 10

$$C_f = 0.455(\log_{10} \mathrm{Re})^{-2.58}$$

Equation 11

$$D = qC_f S$$

Where q is the dynamic pressure

Cf is the skin friction coefficient

S is the equivalent flat plate area

As the wind tunnel could not achieve the high speeds necessary to create equivalent values of Reynolds number on a scale model, it would therefore not simulate skin friction accurately. Therefore, it was felt more advantageous to perform CFD analysis on a full-scale model with further CFD tests being run on a small-scale model for comparison with wind tunnel studies.

Furthermore, it was felt that analysis should be done on a full-scale simulation for the sake of comparison with other studies, giving realistic force readings for the Land Rover Discovery Mk 3. It was therefore important to investigate the effects of changing the scale of the CFD model and establishing the sensitivity of the results to Re effects.

Both the full and half models were scaled-up to actual size in Fluent and tested again. The control volumes were increased proportionately and the mesh designs were unaltered. Values of y+ were maintained for boundary layer studies ($50<y+<500$). The Reynolds number increased from approximately 1.4×10^6 to 8.3×10^6 with reference lengths of 0.806m and 4.835m for the small-scale and full-scale models respectively. Additionally, the wheel speed reduced to 67 rad/s – the radius having been increased from 0.062m to 0.372m. It was considered that the rotational speed

of the wheels may have a significant bearing on the overall drag values. The inlet velocity was kept at 25m/s on the full-scale simulation.

5.4 Results and Discussion of Model Testing

Table 5.1 shows the results of the CFD model testing. All reference areas were read from Fluent.

	Moving Road	Turning Wheels	Reference Area	Total Drag (N)	Cd
Full Model 1/6 Scale	Y	No Wheels	0.06756	19.61847	0.759
Full Model 1/6 Scale	Y	N	0.06756	18.68	0.722
Full Model 1/6 Scale	Y	Y	0.06756	18.894	0.731
Full Model Large-scale	Y	Y	2.433784	620.6261	0.666
Half Model 1/6 Scale	N	N	0.0318	6.85	0.563
Half Model 1/6 Scale	N	Y	0.0318	6.78	0.557
Half Model 1/6 Scale	Y	Y	0.0318	7.12	0.585
Half Model Large-scale	Y	Y	1.147066	230.65	0.525

Table 5.1 Results of Model Testing

As the full model necessitated a coarse mesh, it was apparent that the C_d values were unrealistic. However, this case established that the model could be imported in Fluent and Gambit and solved successfully.

Using a half-model is more common in CFD analysis, and with the finer mesh and larger control volume that could consequently be applied, the resulting C_d was likely to be far more accurate. Indeed, when a finer mesh was applied, the resulting values were closer to the expected range for a vehicle of this geometry. For any further analysis, it was felt that the benefits of a finer mesh were likely to outweigh the disadvantage of losing the flow patterns around the rear windscreen wipers and similar asymmetric features. However, were crosswinds or yaw to be investigated, a full model would be required due to the asymmetry.

The drag coefficient decreased by 10% and 14% for the half and full models respectively when the model was scaled-up. This may be due to the increase in near-

wall mesh resolution, as y+ values were kept constant while the vehicle size was increased, giving results that were more accurate. The Reynolds number at large-scale would also be more realistic, possibly affecting the contribution of skin friction drag. The resulting force values of the large-scale model are more comparable to production vehicles and therefore were more useful in this investigation.

Although the CFD model was of a very similar geometry to a production SUV, there were a number of inaccuracies in the scale model used for scanning which translated to the CFD model. The most prominent of these was the lack of airflow through the engine bay, which would contribute to cooling drag, often producing around 10-15% of total drag [6]. However, in this case it is possible that the lack of heat exchange flow could actually increase drag as air was redirected around the large bluff front [24]. Furthermore, the placement of the wheels may not have been accurate, contributing to a higher drag coefficient. A factor that could have lowered C_d, however, was the floor of the vehicle, which, while containing some detail such as the exhaust pipe, was smoother than that of a real vehicle and therefore was unrealistic.

The resolution of the mesh applied to the half-model was far more suitable than that of the full model. It should be noted that, were a structured mesh such as hexcore or locally trimmed hexahedral to have been applied, the results may have been more accurate. However, due to the non-regular nature of the geometry, only an unstructured mesh could be used without far more time being dedicated to the pre-processing stage. This would have been an inappropriate allocation of time as once a base model with reasonable accuracy had been established it would be suitable for comparison in the testing phase of the project.

5.5 Conclusions

This method was effective in producing an adaptable 3D model for CFD purposes. It is easily replicable using the software mentioned and could be applied to projects outside of vehicle aerodynamics and design.

This study showed that the laser-scanned model could successfully be solved at full-scale with turning wheels. As expected, the half model was far more accurate than the full model due to the finer mesh and larger control volume used and was therefore implemented in all base bleed testing.

It was also found that increased mesh resolution at the near-wall region as the model scale was increased brought an overall reduction in the drag reading. These readings were deemed more useful and the full-scale model was therefore used for all further CFD analysis.

The final C_d value of 0.53 was higher than that of a production vehicle of this geometry; however, this was expected due to processing constraints resulting in poor mesh design and resolution. However, this model was deemed suitable as a base result for comparison with base bleed designs.

These results can also serve as a comparison to wind tunnel tests described later in this report.

6 Base Bleed Analysis

At a vehicle velocity of 25m/s, there was a large pressure force ($0.35C_d$) in the positive x-direction acting on the rear of the vehicle. This draws the car rearwards and contributes greatly to the overall drag force acting on the car. To reduce this pressure value as far as possible was desired, but in doing this consideration must be given to the overall effect and the pressure forces acting on other areas of the car.

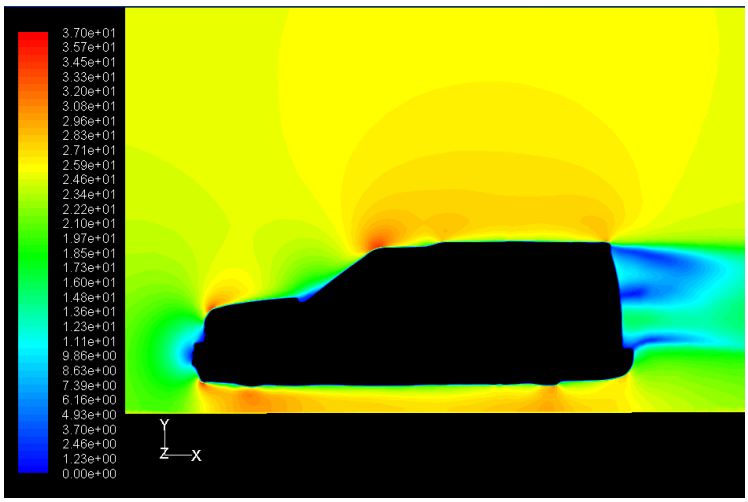

Figure 6.1 Velocity plot of airflow over standard model

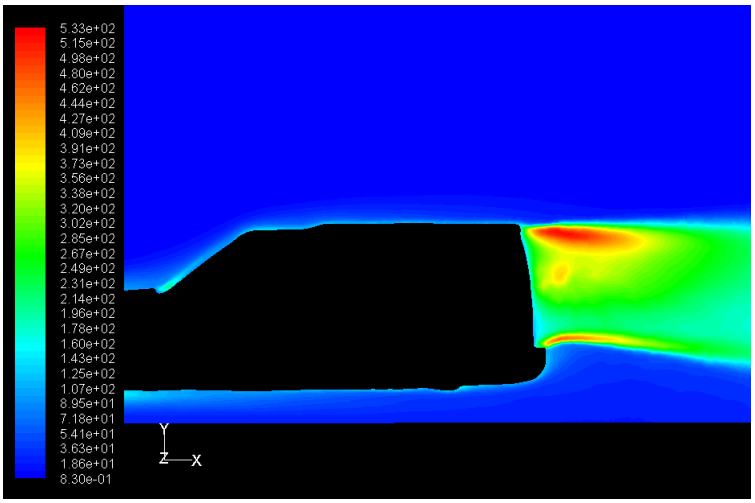

Figure 6.2 Turbulent intensity plot of standard model

Figure 6.1 and Figure 6.2 show a large turbulent region at the upper portion of the rear of the vehicle and so investigation was carried out to see if implementing base bleed in this area could control the airflow and reduce the size of this turbulent wake, resulting in a pressure increase and drag decrease.

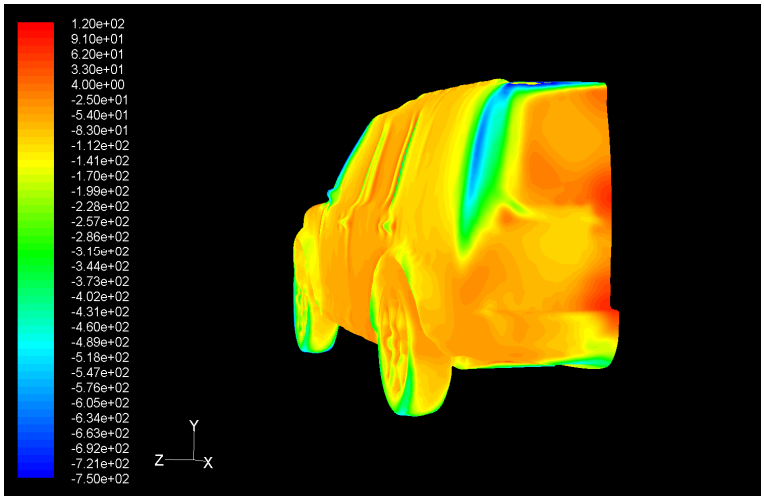

Figure 6.3 Static pressure plot of rear of standard model

Figure 6.3 shows that there are large areas of low pressure acting on the rear of the vehicle. Areas of particular interest are the upper and side trailing edges where boundary layer separation occurs. This low pressure retards the movement of the vehicle and so is undesirable.

Initially, three 'bleed configurations' were considered. Howell [8] found that the most effective locations for a bleed outlet are at the top, side and bottom of the base region. He found that very little drag reduction could be obtained using a centrally located outlet. Due to the inaccurate representation of a smooth vehicle floor, the lower portion of the base region has a large bumper to which the flow remains attached particularly well (see Figure 6.1), base bleed configurations in this region may therefore give misleading results. Therefore, investigation was carried out with the three configurations shown in Figure 6.4 to Figure 6.6:

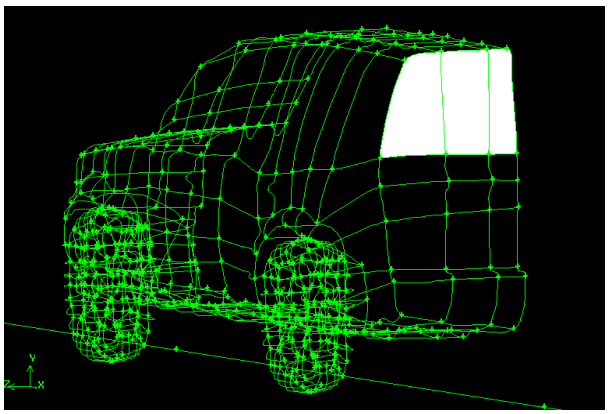

Figure 6.4 Bleed configuration 1 – outlet area 0.279m^2

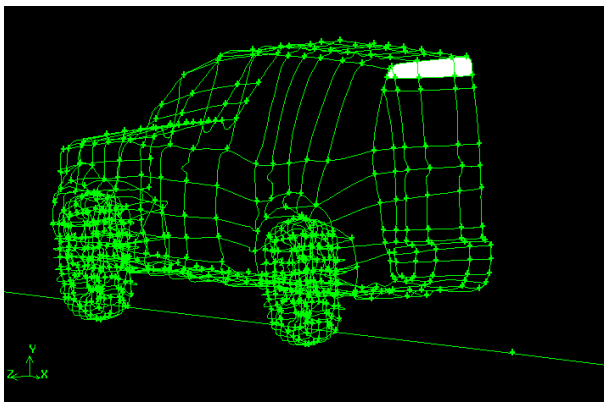

Figure 6.5 Bleed configuration 2 – outlet area 0.04733m^2

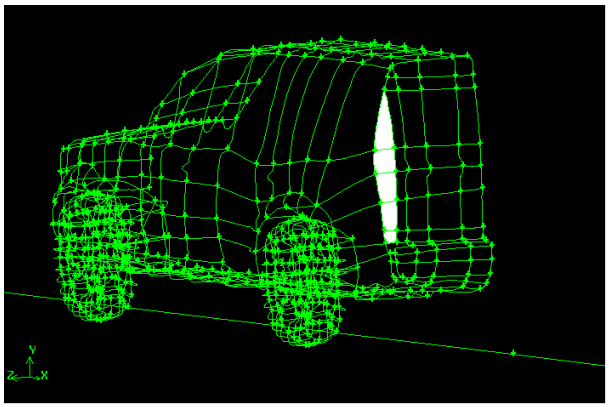

Figure 6.6 Bleed configuration 3 – outlet area 0.06388m^2

The white areas in the images show the cavity through which the bleed air was blown. All outlet areas given are the projected areas in the x-direction. It should be noted that, as a half model was used, all values for bleed area and hence mass flow would need to be doubled for a full vehicle. The bleed outlets were set-up as 'velocity inlets' in Fluent, simulating a supplementary source of air. The disadvantage of this method is that the cavity that would be present in a real system was not simulated and may have had a bearing on the overall result. Furthermore, the flow from the outlet does not account for the boundary layer that would be established within the duct and was therefore completely uniform.

These three configurations were investigated under varying outlet velocities (mass flow rates) as well as varying outlet flow angles (β) to asses the effect on the flow characteristics in the base region. The outlet velocities in each case were varied between 0m/s and 25m/s. For cases 1 and 2, the flow was expelled at 90°, 60° and 45° to the Y-Z plane with a downward bias. For case 3, the flow was tested at 90°, 60° and 45° to the X-Y plane with a bias towards the centreline of the vehicle. This is shown in Figure 6.7 and Figure 6.8 respectively.

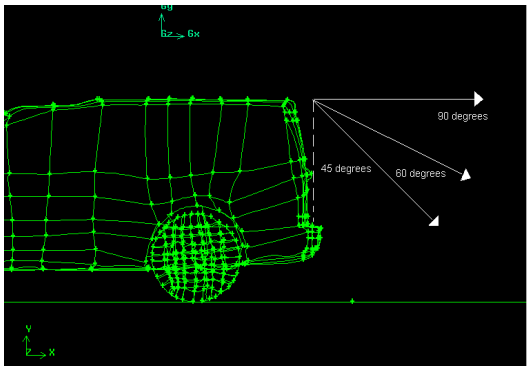

Figure 6.7 Flow angle diagram for Config. 1 and 2

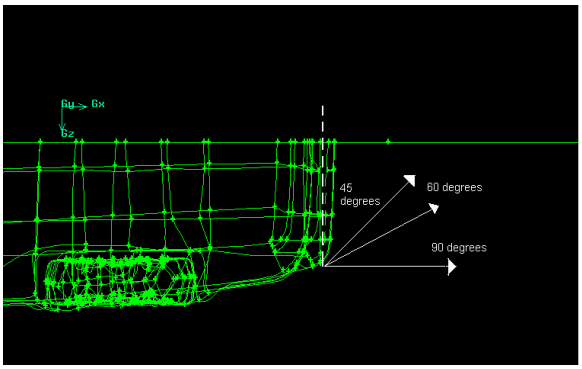

Figure 6.8 Flow angle diagram for Config. 3

It was noted that as the bleed air was deflected, the resultant outlet area was reduced. This is most effectively explained by examining Figure 6.9:

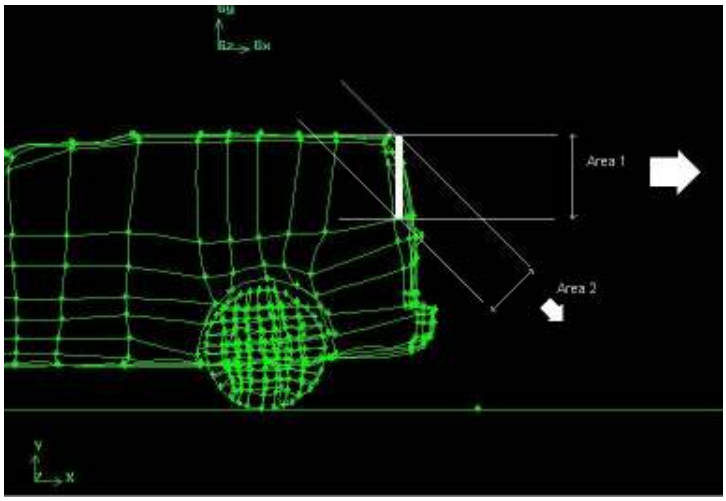

Figure 6.9 Area change diagram for deflected flow

The lines show the flow direction from configuration 1. Area 1 represents the outlet area when the flow is undeflected i.e. it is discharged at 90° to the vertical. Area 2 represents the outlet area when the flow has been deflected at 45°. It can be seen that Area 2 is slightly smaller than Area 1. This reduction in area corresponds to a reduction in mass flow rate of air when the velocity of air remains constant, according to Equation 12:

Equation 12

$$\dot{m} = \rho A v$$

Where $\dot{m}$ is mass flow rate

ρ is fluid density

A is outlet area

v is fluid velocity

This effect is greater with a larger bleed outlet area, such as configuration 1, and at steeper outlet angles.

6.1 Bleed Configuration 1 Results and Discussion

Howell [8] found that drag reduced linearly with mass flow rate and also decreased as bleed outlet area increased. Bleed configuration 1 was used as a test case to establish if base bleed could reduce the drag of a road vehicle in the most extreme of circumstances i.e. with a large bleed outlet area that would be unachievable in a practical sense due to the high mass flow rates required.

It was found that for a bleed velocity of 5m/s, the retarding pressure force on the rear of the vehicle decreased from 80.16N to 37.91N. Although the pressure increased over other parts of the vehicle, there was a net decrease in drag (C_d reduced to 0.503) showing that base bleed could be successfully implemented. However, this was found to be the optimum bleed velocity. As the bleed mass flow rate was increased, it was found that the drag started to rise (Figure 6.10). This is compatible with the findings of Wood [13] and Bearman [14] and was likely due to the high mass flow rates reducing the base pressure due to turbulence.

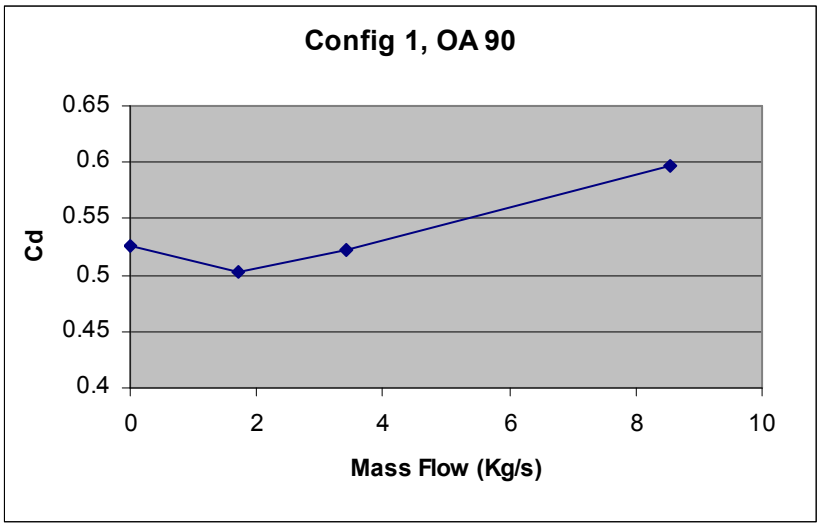

Figure 6.10 C_d against Mass flow for config. 1 with flow angle of 90°

Figure 6.11 helps to give a comparison of the results with other studies by showing C_d against the bleed coefficient Cq, defined in Chapter 2.2.

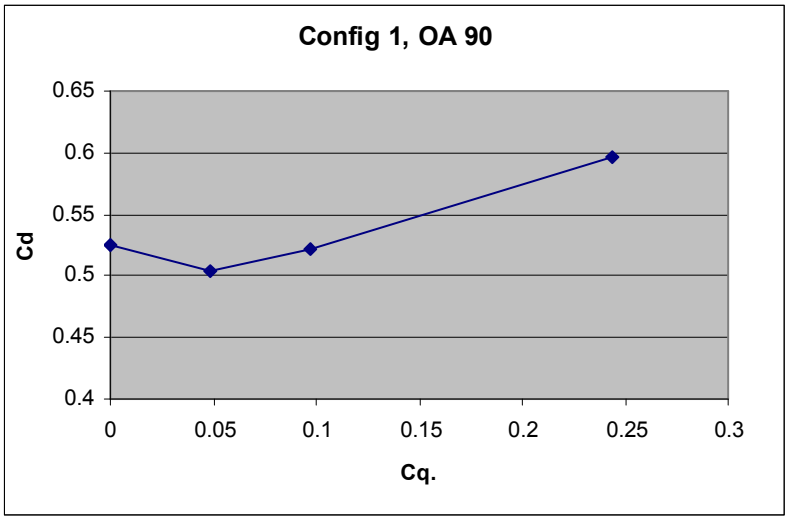

Figure 6.11 C_d against Cq for config. 1 with flow angle of 90

It can be seen that the greatest drag reduction occurred when Cq was around 0.04. It was cited by Bearman [14] that the reported optimum for drag reduction was in the range $0.12 < Cq < 0.15$, however with these Cq values for this configuration it was found that C_d had actually increased. Further investigation could have been done to increase Cq by increasing the outlet area, however a larger outlet would have been unfeasible for a production vehicle.

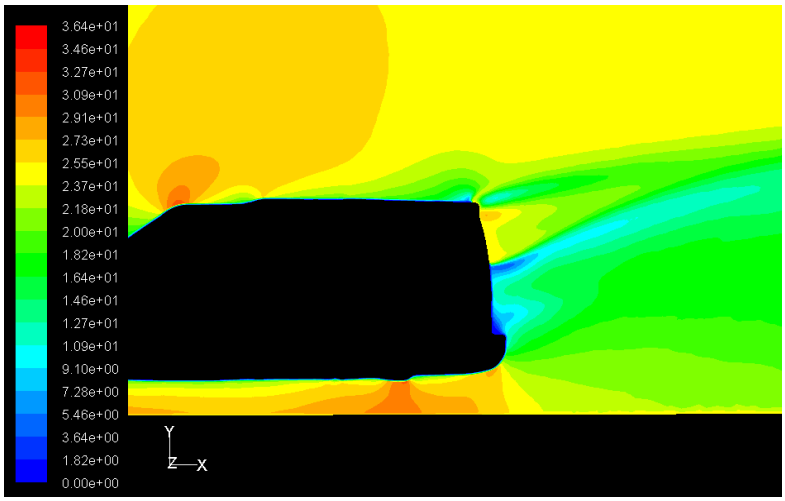

Figure 6.12 Velocity plot of bleed at 25m/s for config. 1 with flow angle of 90°

To help explain the trend found, contour plots from Fluent were examined. Figure 6.12 shows that base bleed in this configuration appears to draw the wake upwards, moving forward the boundary layer separation on the upper surface and increasing the overall size of the turbulent wake. This effect increases as the bleed velocity increases. As a real-life system would likely be based on passive ducting from a high pressure region and mass flow would increase with increasing forward speed, mass flow would need to be regulated as, without flow control, drag could increase as vehicle speed increased.

The angle of the flow was then altered to see if a more desirable effect could be achieved. As the flow angle was altered through 45° and 60°, the results shown in Figure 6.13, 6.14 and Figure 6.15 respectively were obtained:

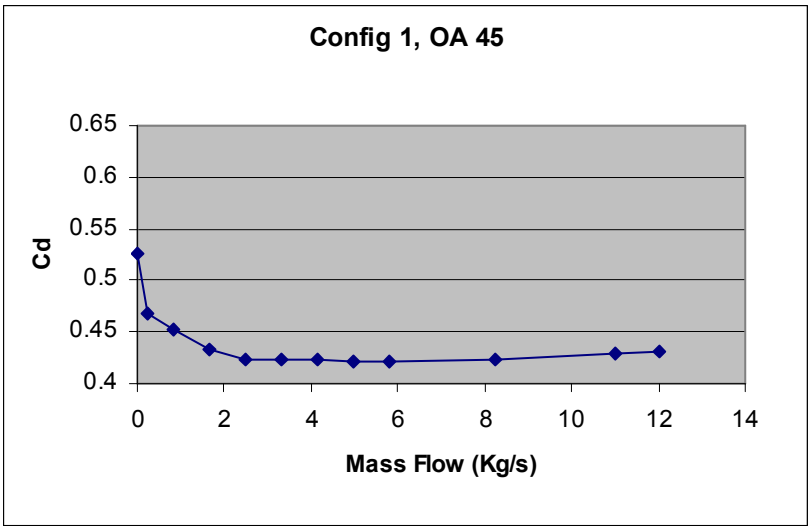

Figure 6.13 C_d against mass flow for config. 1 with flow angle of 45°

By angling the flow, base bleed was shown to significantly reduce drag. The best result achieved was a C_d of 0.421 with a mass flow rate of 3.3kg/s, a decrease of 19.8%. This occurred when the ratio of bleed outlet velocity to free-stream velocity (V_d/V) was 0.8 and Cq was 0.15. This is in line with the finding of Bearman [14].

Although potentially unobtainable in a ducting system for this configuration, values of $V_d/V>1$ were also investigated (Figure 6.14). It was found that above $V_d/V = 0.8$

the drag began to increase from the optimum value, but with the flow deflected a large drag reduction was still produced when $V_d/V = 2$.

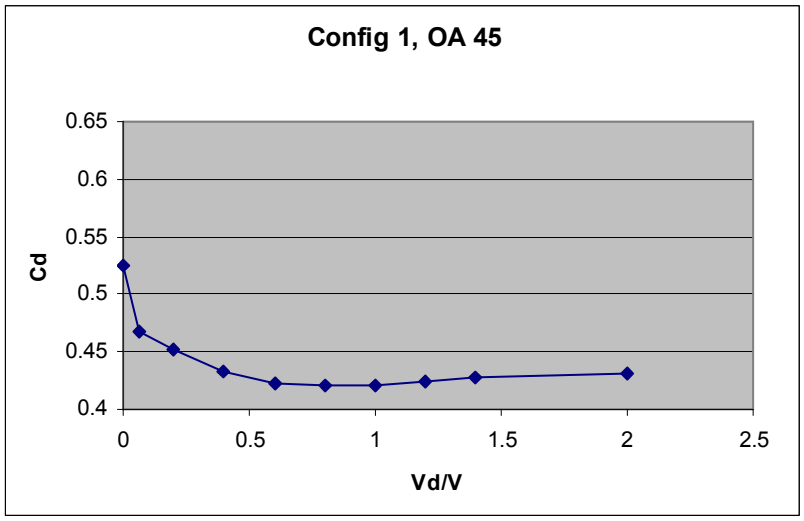

Figure 6.14 C_d against V_d/V for config. 1 with flow angle of 45°

A point of interest of these initial studies was that large drag reductions could be achieved with very low mass flow rates. With a mass flow rate of only 0.827kg/s at β=45°, the C_d was reduced to 0.451, a 14% reduction from the original vehicle. Furthermore, increasing the mass flow rate beyond this point did not produce a linear reduction in drag.

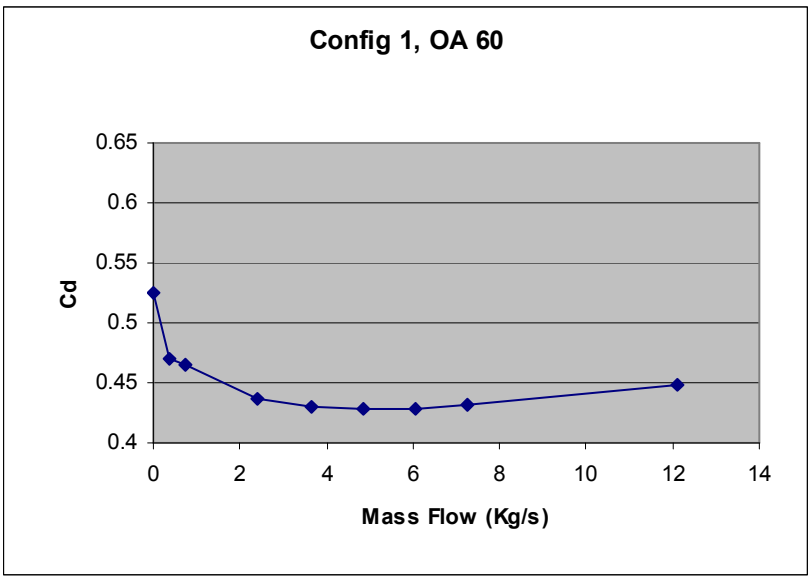

Figure 6.15 C_d against mass flow for config. 1 with flow angle of 60°

When the flow angle was decreased to 60° similar results were found (Figure 6.15), although the angle of the flow did influence the effectiveness of the system. Although the results are comparable at similar outlet velocities, with a flow angle of 60° the mass flow rates are significantly higher than at 45°. This is an important point as, depending on the mass flow through the duct, one system may be preferable to the other to achieve an optimum drag reduction depending on the vehicle velocity.

Again, the optimum result was found when $V_d/V = 0.8$, with a C_d value of 0.428. Investigation into the pressure distribution around $V_d/V=0.8$ showed a significant change in the pressure distribution on the rear of the vehicle. Figure 6.16 shows that at low values of V_d/V there are particular areas of high and low pressure on the lower half of the rear of the vehicle (the upper half being the bleed outlet). Figure 6.17 shows a plot of static pressure under the optimum condition for drag reduction. It can be seen at this stage that the specific areas of high pressure have reduced in value; however base bleed has increased the base pressure more evenly around the rear of the vehicle resulting in a net reduction in drag. Figure 6.18 shows that as V_d/V was increased, the pressure distribution became irregular. Although there were areas of higher pressure (the dark red areas in the centre of the vehicle and on the rear bumper), the net pressure force on the rear surface increased from 17.68N to

24.83N when compared with V_d/V =0.8. On the rear sidewall and rear underside, the drag force increased by around 1N. On the remainder of the vehicle, the pressure forces remained almost identical.

This irregularity in the pressure distribution results from turbulence caused by the injection of high volumes of air at high speed into the rear wake of the vehicle.

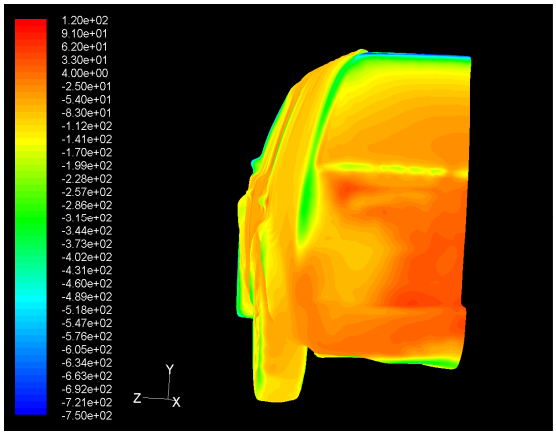

Figure 6.16 Static pressure plot of config 1, V_d/V=0.2 at 45°

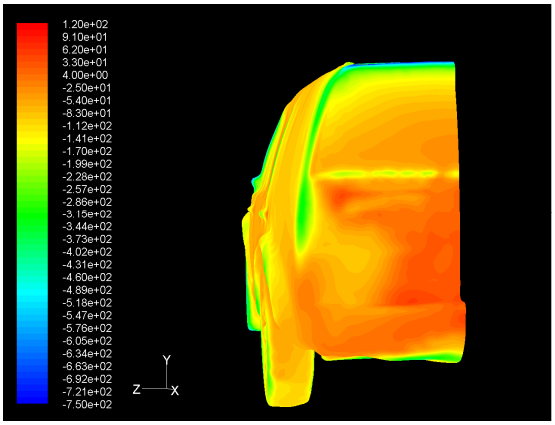

Figure 6.17 Static pressure plot of config 1, V_d/V=0.8 at 45°

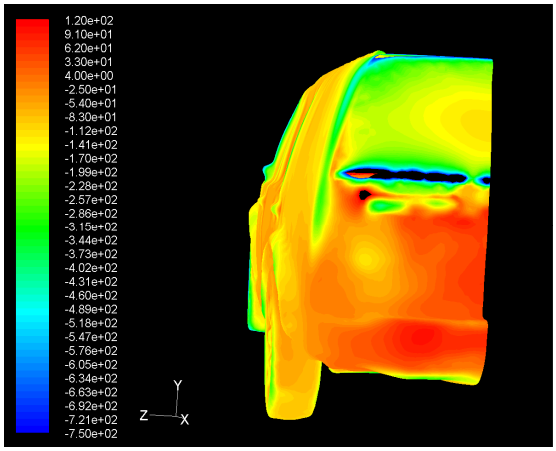

Figure 6.18 Static pressure plot of config 1, V_d/V=2 at 45°

It should be noted that to obtain an outlet velocity close to 25m/s at a vehicle velocity of 25m/s using passive ducting, the inlet might have to be significantly larger than the outlet due to duct losses. For this configuration, this would almost certainly be impractical and so with such a large outlet, the optimum value of V_d/V=0.8 would be unobtainable.

6.2 Bleed Configuration 2 Results and Discussion

By reducing the size of the bleed outlet, the possibility of implementing such a system increases. As it has been found that significant results can be achieved from a relatively low mass flow rate, the bleed outlet area was reduced to 0.04733m^2 and low mass flow rates were studied. The bleed outlet remained situated on the upper portion of the base region (Figure 6.5). Similar results were found when no deflection was applied to the bleed air, with the forces ultimately increasing with mass flow (Figure 6.19).

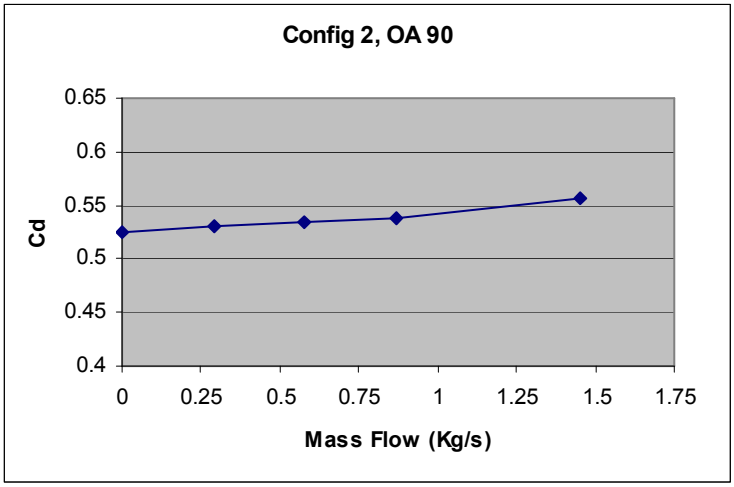

Figure 6.19 C_d against Mass flow rate for config. 2 with no deflection

With such low mass flow rates, Cq values were no longer comparable to that of other literature mentioned previously (Figure 6.20).

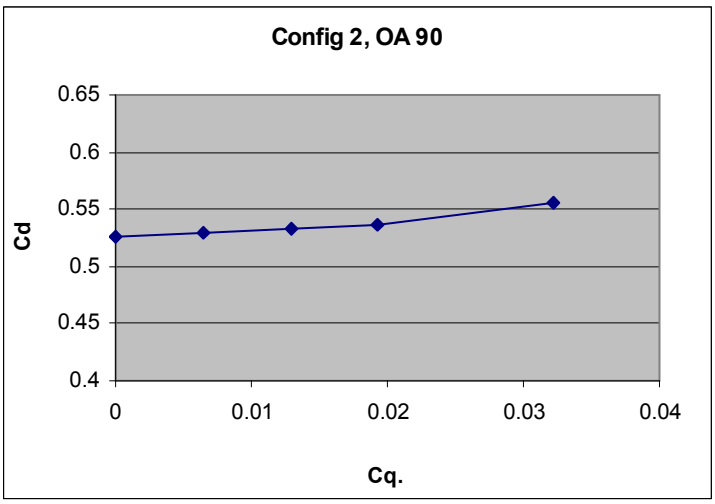

Figure 6.20 C_d against Cq for config. 2 with no deflection

Figure 6.21 shows the results obtained with a deflection of 45°:

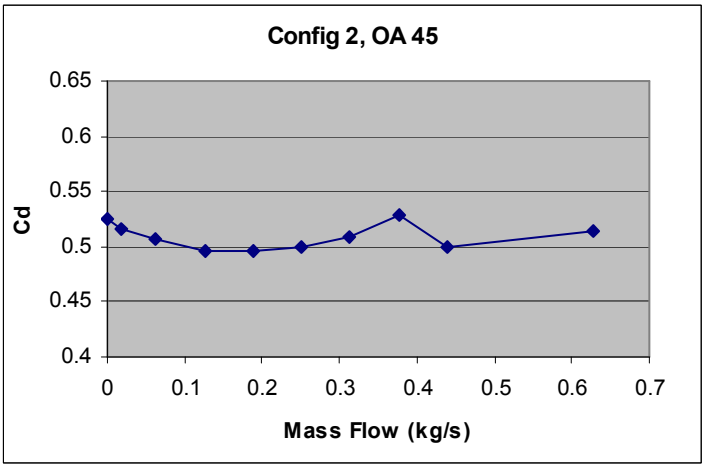

Figure 6.21 C_d against Mass flow rate for config. 2 with flow angle of 45°

Varying the outlet velocity from 0m/s to 25m/s, it was found that C_d could be reduced to 0.496 with a bleed outlet velocity of 15m/s and a 45° outlet angle. For this, a mass flow rate of only 0.188kg/s was required. This was a decrease of 5.5% in the drag coefficient.

Beyond this value, however, the drag coefficient began to increase with mass flow. Again, bleed outlet velocities of up to 50m/s were studied and it was found that an

outlet velocity of 30m/s produced an overall increase in C_d even with the flow deflected. This appeared to be for similar reasons as in configuration 1 with no deflection, where the high flow velocities cause turbulence and decreased the overall pressure on the rear of the vehicle.

Figure 6.22 shows C_d against the ratio of bleed velocity to vehicle velocity:

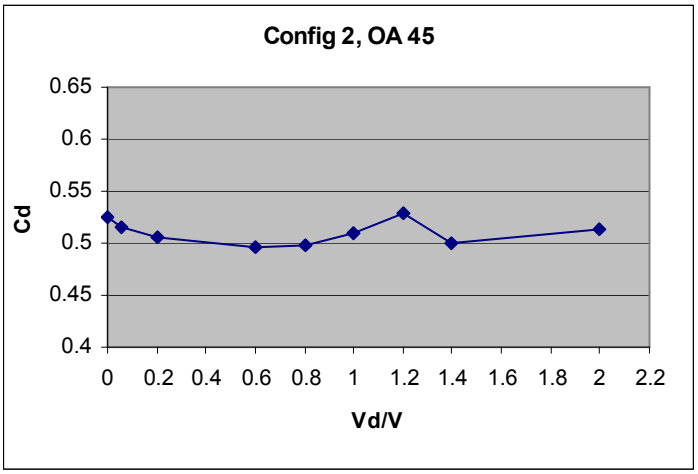

Figure 6.22 C_d against V_d/V for config. 2 with flow angle of 45°

It was interesting to note that with this configuration the optimum value of V_d/V had decreased to 0.6 with a 45° deflection.

The drop in C_d as the outlet velocity was increased beyond 30m/s was interesting.

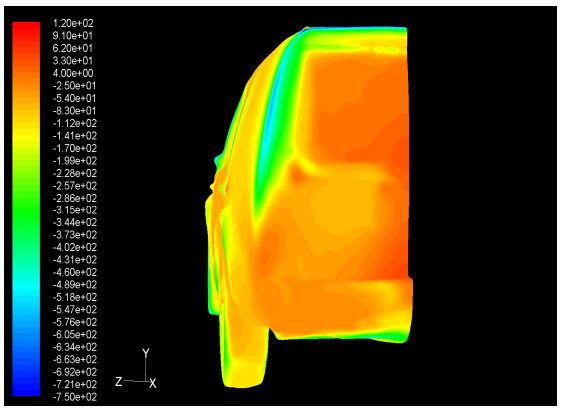

Figure 6.23 Static pressure plot of config 2, V_d/V=0.8 at 45°

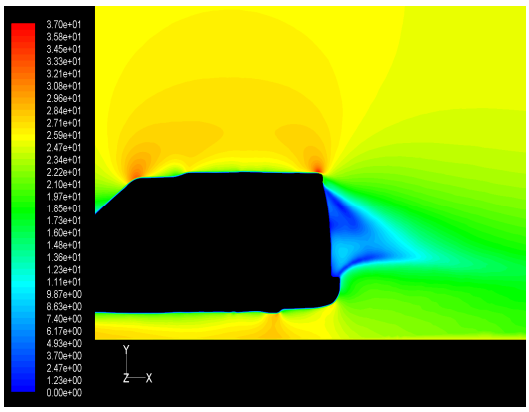

Figure 6.24 Velocity plot of config 2, V_d/V=0.8 at 45°

At V_d/V=0.8, base bleed was seen to increase the base pressure across most of the base region. It can be seen from Figure 6.24 that the wake is being controlled by the bleed air and the lower bumper, reducing the turbulence and increasing the base pressure. This image can be compared to Figure 6.3 for further emphasis.

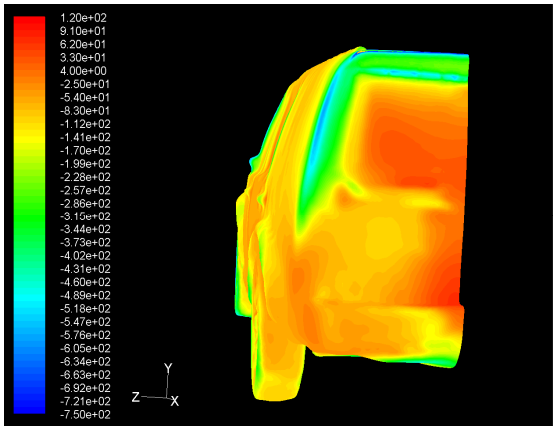

Figure 6.25 Static pressure plot of config 2, V_d/V=1.2 at 45°

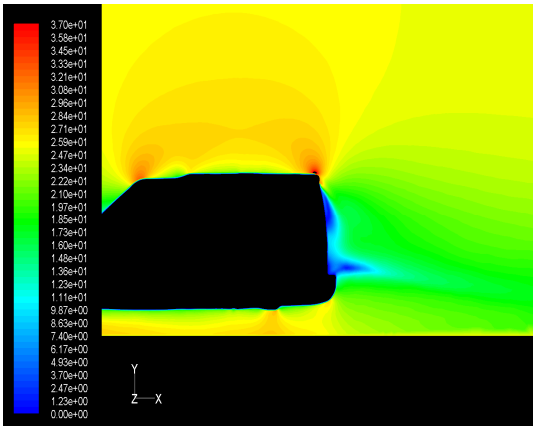

Figure 6.26 Velocity plot of config 2, V_d/V=1.2 at 45°

When V_d/V reached 1.2 (V_d = 30m/s) there were still particular areas of high pressure, but a large area of low pressure became prevalent towards the lower outside surface. Examining the velocity profile along the centreline (Figure 6.26) showed a

significant change in the shape of the wake. It can be seen that the velocity magnitude of the air has increased in all but a small area, resulting in reduced base pressure and higher drag.

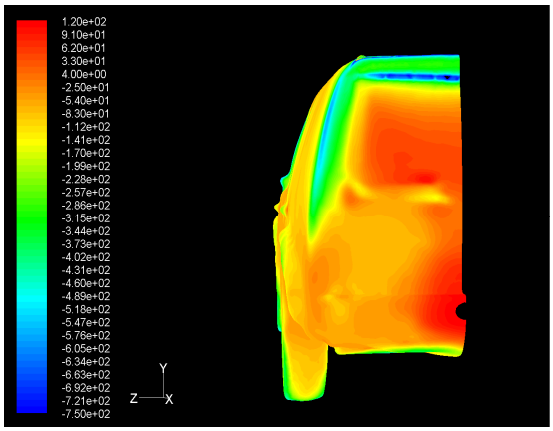

Figure 6.27 Static pressure plot of config 2, V_d/V=1.4 at 45°

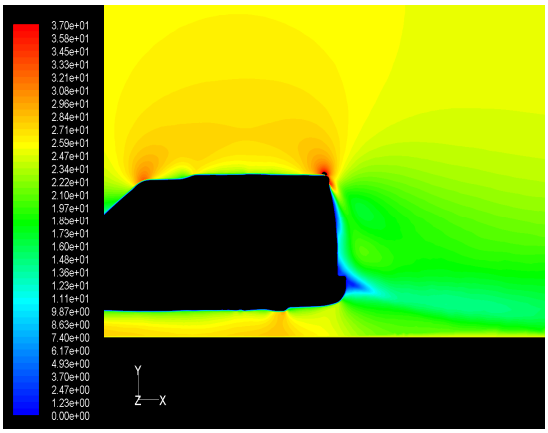

Figure 6.28 Velocity plot of config 2, V_d/V=1.4 at 45°

As the bleed velocity increased further, Figure 6.28 shows that the increase in air velocity in the base region continued. This, it would be expected, should have caused further increases in base drag; however, this was not the case.

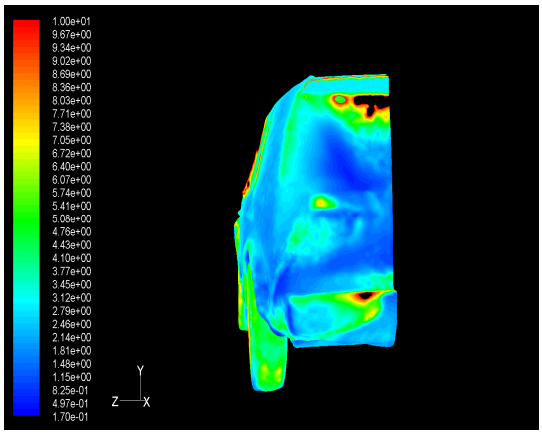

Figure 6.29 Turbulent kinetic energy plot of config 2, V_d/V = 1.2 at 45°

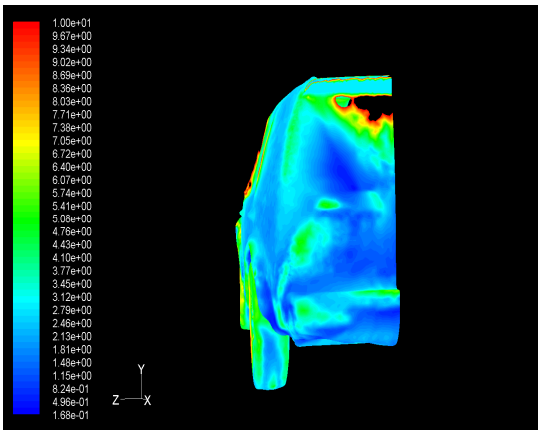

Figure 6.30 Turbulence plot of config 2, V_d/V = 1.4 at 45°

Figure 6.29 and Figure 6.30 show areas of high and low turbulence. Comparing Figure 6.29 to Figure 6.25, it can be seen that areas of high turbulence correspond to areas of low pressure[1]. As the bleed mass flow was increased, the turbulent regions remained constant or, in some areas, increased in magnitude and area. The main contribution to the net decrease in drag came from the increase in pressure on the bumper. From Figure 6.28 it can be seen that there is a region of low velocity air surrounding the centre of the bumper as the higher bleed outlet velocity allows the bleed air to control the wake around this section, resulting in a point of particularly high pressure. Figure 6.30 shows that there is also a significant reduction in turbulence across the length of the bumper. In fact, the increase in pressure on the bumper accounted for 77% of the total reduction in drag.

This is significant as it shows that the drop in C_d beyond V_d = 30m/s occurred by chance due to the specific shape of the rear bumper of this vehicle and its contribution to the total drag force. Slight changes to the vehicle design would likely have mean that this drop in C_d would not occur, and would result in a constant increase in drag beyond the optimum bleed rate.

At β=60°, the peak in the graph was not present as the bleed air did not reach the low bumper as it did at β=45°. Instead, beyond the optimum mass flow there was a steadier rise in C_d.

[1] The black areas in the image correspond to turbulent kinetic energy values above the maximum value on the scale. This has been done to give more detail in areas of interest.

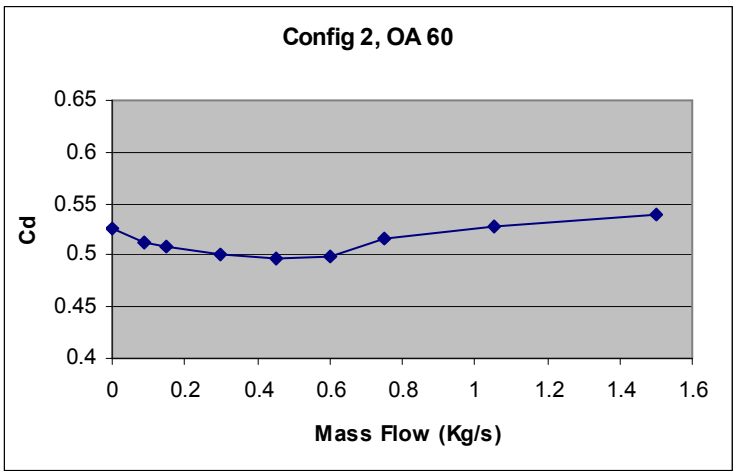

Figure 6.31 C_d against Mass flow rate for config. 2 with flow angle of 45°

Comparing configuration 2 with configuration 1, it was observed that for similar mass flow rates and deflection angles, there was a significant increase in C_d. For example, at $\dot{m} = 0.75$ at 60°, C_d was 0.517 compared with 0.465 for configurations 2 and 1 respectively. Therefore, for a real system to be designed, a large bleed outlet is desirable. This is in line with the findings of Bearman [14]. However, with this small outlet, even with an outlet velocity of 5m/s (a mass flow of 0.063kg/s) the C_d value was decreased to 0.451 for configuration 2 at β=45°.

6.3 Bleed Configuration 3 Results and Discussion

A final configuration was investigated. Were a ventilation system to be implemented, it may be most practical to bleed air from a scoop on the underside or side of the vehicle. Therefore, a bleed outlet on the upper portion of the rear may not be as practical as one implemented on the side. There was a key difference in this configuration - where the bleed was implemented at the side of the vehicle there were two outlets blowing towards each other and interacting.

A similar process was followed to the previous cases and it was found that, where no deflection was applied, the C_d increased to 0.59 with an outlet velocity of 25m/s. Figure 6.32 shows the resulting curve with no deflection applied to the bleed air:

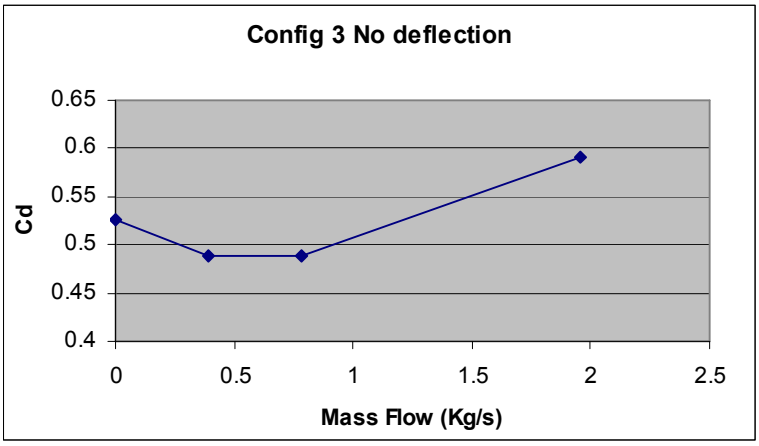

Figure 6.32 C_d against Mass flow rate for config. 3 with no deflection

Figure 6.3, Figure 6.33 and Figure 6.34 allow comparison of the static pressure distribution on the rear of the vehicle under varying bleed angles.

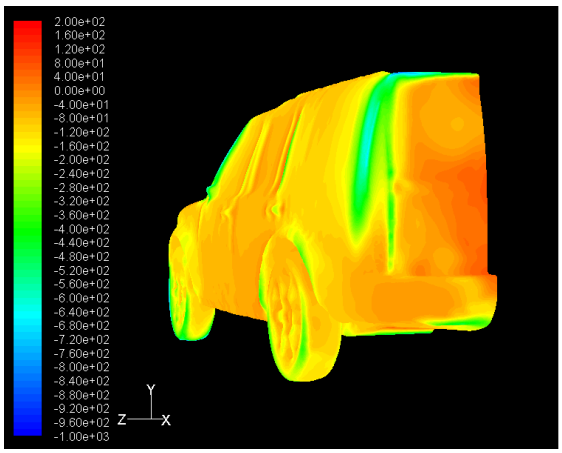

Figure 6.33 Pressure contour plot for config. 3 at 25m/s with 45° deflection

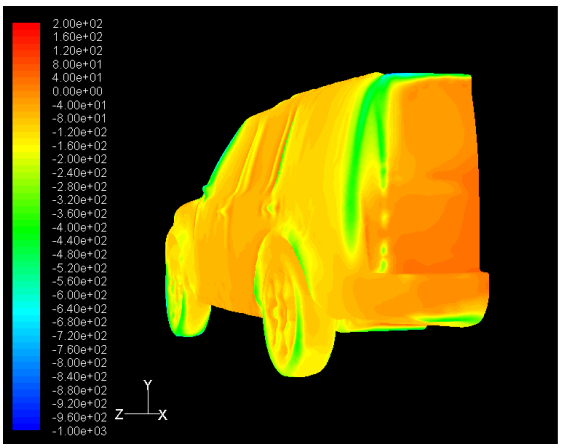

Figure 6.34 Pressure contour plot for config. 3 at 25m/s with 60° deflection

At the sharp angle of 45°, the flow at the rear of the vehicle was accelerated around the rear edge due to entrainment, creating a low pressure zone towards the outside of the vehicle (Figure 6.33). However, a region of high pressure was created around the centreline of the vehicle where the two air jets met and slowed, and overall the base pressure did increase. The optimum result was achieved with a very low bleed velocity; however a C_d of 0.508 was achieved when the outlet velocity was 25m/s (Figure 6.35).

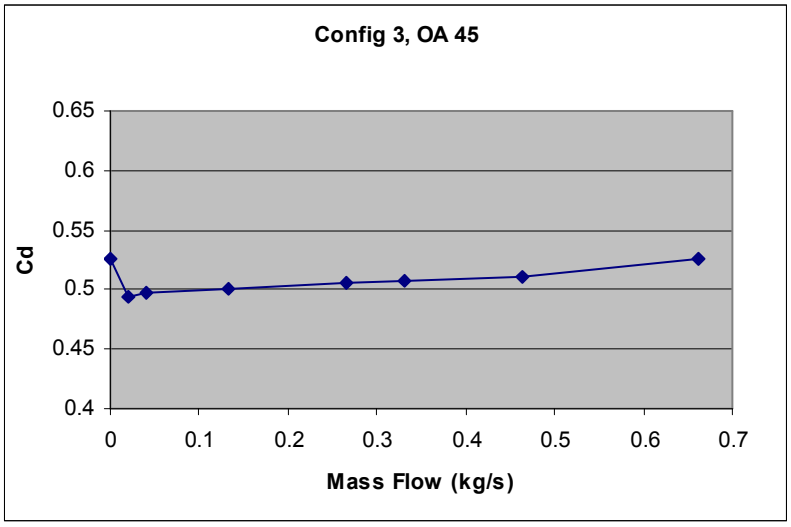

Figure 6.35 Cd against Bleed Velocity for config. 3 with flow angle of 45°

Again, when the velocity was increased significantly, turbulence at the rear of the vehicle reduced the base pressure giving an overall negative effect. This outlet velocity would not likely be approached through a passive ducting system for a vehicle velocity of 25m/s with such a large outlet configuration.

For a bleed angle of 60°, the region of fast moving, low pressure air was controlled and the sub atmospheric pressure acting on the rear of the vehicle was increased more evenly giving better results on the overall drag. This emphasises that the effect on the base region is not uniform and the importance of analysis on a real vehicle shape and not a generic bluff body.

Interestingly, with a bleed mass flow of 0.7599kg/s, a drag coefficient of 0.477 was achieved, and with a mass flow of only 0.114kg/s, the effect on the flow was similar with a C_d reduction to 0.485. For this configuration, the interaction of the two bleed outlets meant that higher mass flow rates caused turbulence and ultimately did not decrease the drag coefficient linearly. This is shown in Figure 6.36:

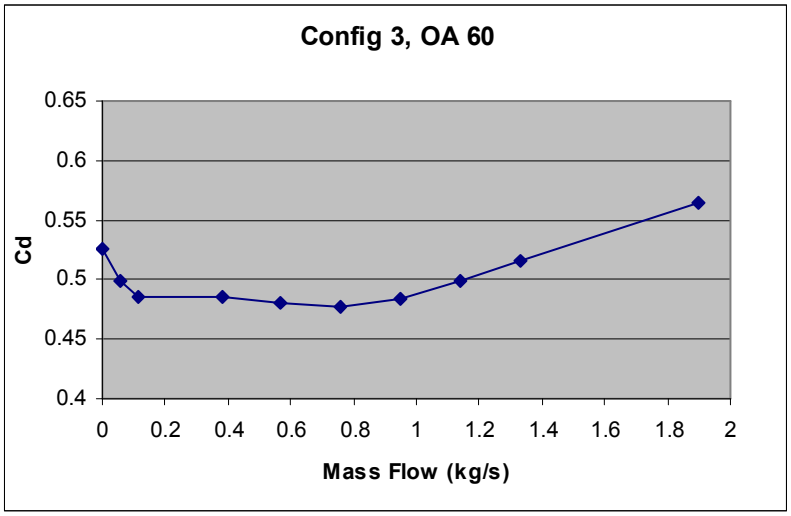

Figure 6.36 Cd against Mass Flow Rate for config. 3 with flow angle of 60°

Furthermore, the optimum result was achieved at $V_d/V=0.8$ (as with configuration 1), however varying V_d/V between 0.1 and 1 had little effect, as shown in Figure 6.37.

Above $V_d/V=1$, the high bleed velocity caused a significant amount of turbulence that caused a linear increase in drag coefficient with bleed velocity.

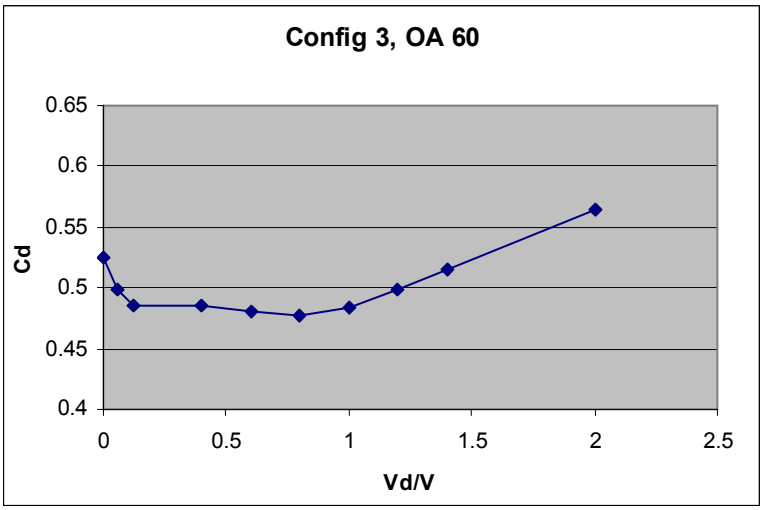

Figure 6.37 Cd against V_d/V for config. 3 with flow angle of 60°

The findings for this configuration are particularly relevant not only because it is possibly easier to implement for some vehicle shapes, but also because a reduction in C_d can be obtained from very low mass flow rates and C_d does not subsequently increase as mass flow increases until high values of V_d/V. This could be a major advantage when incorporating base bleed to a production vehicle.

6.4 Deflection Study Results and Discussion

Particular interest was taken in this investigation of the effect of deflecting the flow angle from the bleed outlet. Redirecting the airflow from the outlet towards the centre of the rear of the vehicle had had a significant effect in each of the three configurations studied. However, to this point in the investigation the full effect of the deflection angle, β, had not been understood and so further work was carried out to see if an optimum angle could be discovered for a particular configuration while keeping the outlet velocity, V_d, constant.

This study was carried out for configuration 2, being that this was a more practical outlet size than configuration 1. Tests were done for three different outlet velocities: 5m/s, 15m/s and 25m/s. The same procedure was followed in Fluent as done previously, varying the velocity components to produce a deflected flow from the velocity outlet faces on the rear of the model. The data for each outlet velocity is listed in Table 6.1:

Outlet Velocity	Cq.	V_d/V
25	0.032	1
15	0.019	0.6
5	0.006	0.2

Table 6.1 Outlet Velocity Data for Deflection Study

Tests were done for angles between 40° and 90° at 10° intervals with an extra test included at 45° (see Figure 6.7 for a schematic of bleed angle). The minimum angle examined was 40° as the rear of the vehicle was set at an angle greater than 30°.[2] Figure 6.38 shows the results when the bleed velocity was 25m/s:

[2] Tests were carried out for angles between 10° and 30° for each configuration and it was found that, for a constant velocity, a negative mass flow rate was reported by Fluent.

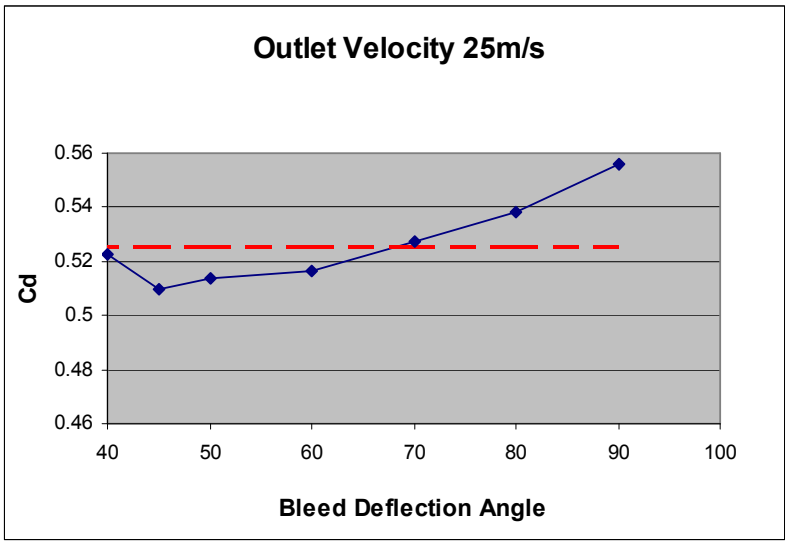

Figure 6.38 C_d against Bleed Deflection Angle for bleed velocity of 25m/s

The red line indicates C_d when no base bleed has been applied. At 65° base bleed starts to have a negative effect on the drag coefficient. For the steeper outlet angles, the mass flow rate of bleed air was extremely low (as explained on page 61) and so it was surprising how effective base bleed was at the steeper outlet angles[3]. This result emphasises the benefits of deflecting the bleed air as it exits the vehicle and indicates that optimising the deflection angle may be more beneficial than optimising the mass flow rate.

[3] Graphs of mass flow against bleed angle for each test can be found in Appendix C – Mass Flow Data for Deflection Study

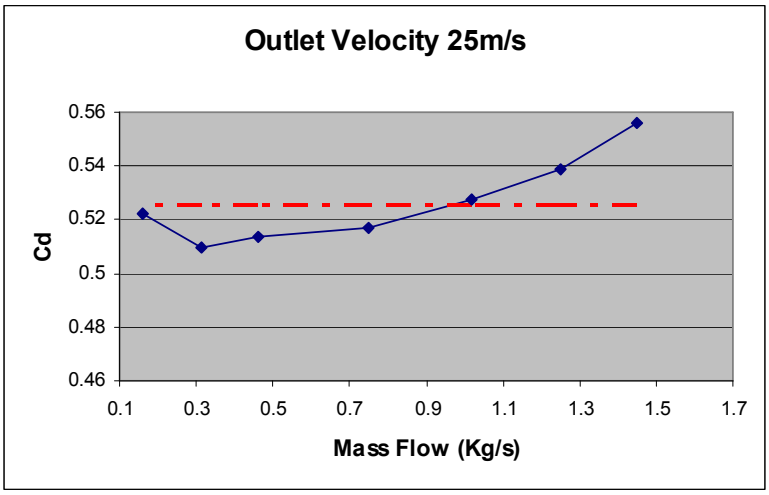

Figure 6.39 C_d against Mass Flow for bleed velocity of 25m/s

Figure 6.38 shows there was an almost linear relationship between drag and the deflection applied to the bleed air with the exception of $\beta = 40°$ where there was a higher C_d than at 45°.

Upon examination of the drag force distribution on the vehicle between 40° and 45°, there was an increase in base drag of 7N at 45° with virtually no change the remaining forces. Examining the contour plots from Fluent helped gain an understanding of this.

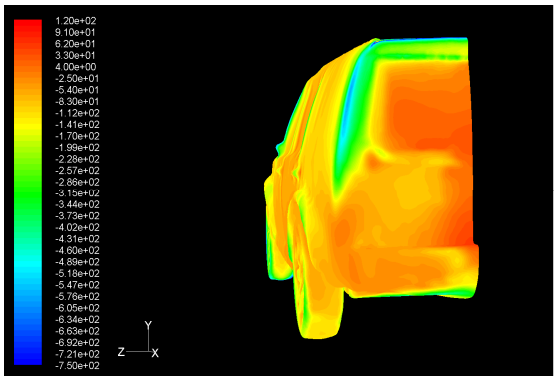

Figure 6.40 Pressure distribution for outlet velocity of 25m/s at 45°

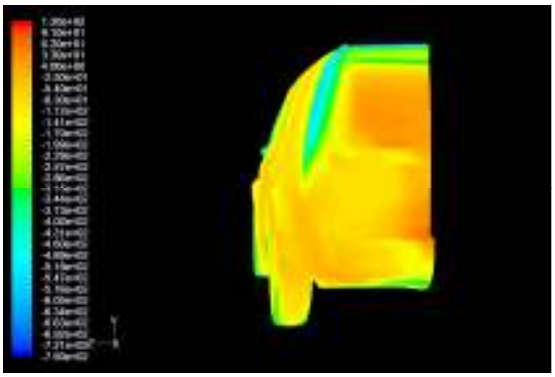

Figure 6.41 Pressure distribution for outlet velocity of 25m/s at 40°

Comparing Figure 6.40 with Figure 6.41shows that when the flow was deflected to 40°, base bleed was less effective at increasing the base pressure and large yellow areas of low pressure were widespread.

Examining the turbulent kinetic energy at the rear of the vehicle helps to explain this:

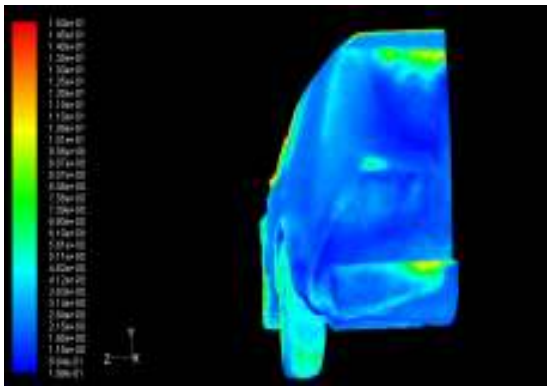

Figure 6.42 Turbulent kinetic energy plot for outlet velocity of 25m/s at 45°

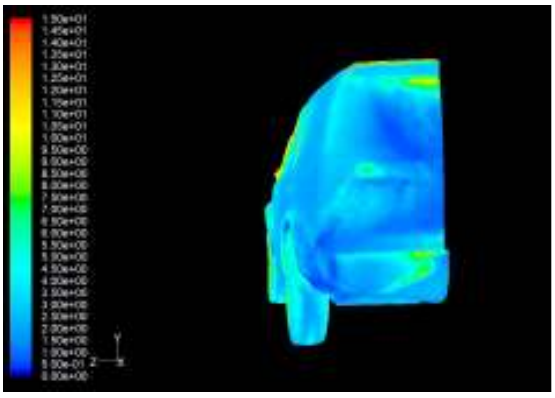

Figure 6.43 Turbulent kinetic energy plot for outlet velocity of 25m/s at 40°

There was a clear transition in the way the turbulence was distributed on the rear of the vehicle at around 40°. At $\beta = 45°$, the rear of the vehicle is predominantly dark blue, indicating low turbulence. However, there were large green areas prevailing at the top trailing edge and the protrusions on the rear of the vehicle (such as the top edge of the rear bumper) where the turbulent kinetic energy has increased to around $9m^2/s^2$. When β was decreased to 40°, the air was being blown down the surface of the vehicle. It can be seen that although the green areas of high turbulence seem to have reduced in magnitude, there is a wider distribution of turbulence at around $5.5m^2/s^2$ (the pale blue areas). These areas of medium turbulence create lower pressure and therefore a net increase in drag.

As the deflection angle was increased beyond 45°, a similar effect occurred on a more gradual scale as the air was blown into the wake of the vehicle. The turbulent kinetic energy began to increase in what were formerly areas of low turbulence, and the base pressure began to decrease on the rear surface of the vehicle. It was

observed that the net value of turbulent kinetic energy increased and the pressure force therefore decreased. At 70° the effects of base bleed became negligent and between 70° and 90° base bleed caused the drag to increase as the base region became largely turbulent.

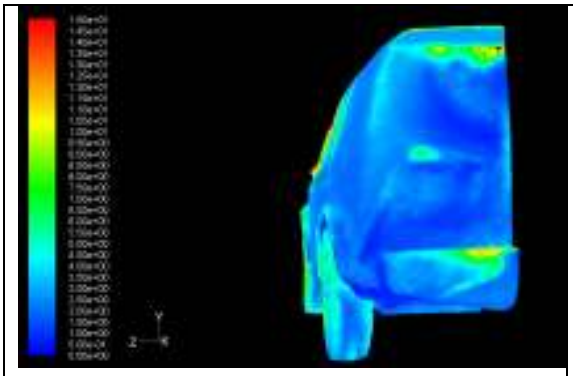

Figure 6.44 Turbulent kinetic energy plot for outlet velocity of 25m/s at 50°

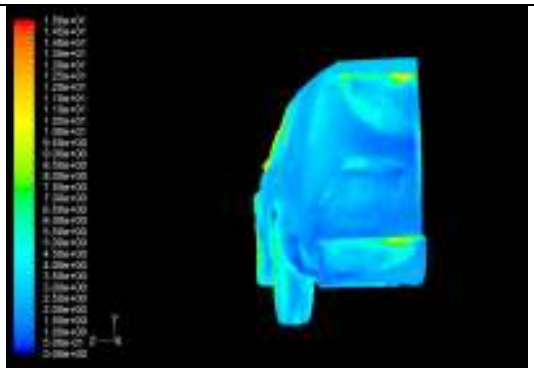

Figure 6.45 Turbulent kinetic energy plot for outlet velocity of 25m/s at 70°

Further examination was then carried out to discover whether these same effects would occur at lower bleed velocities:

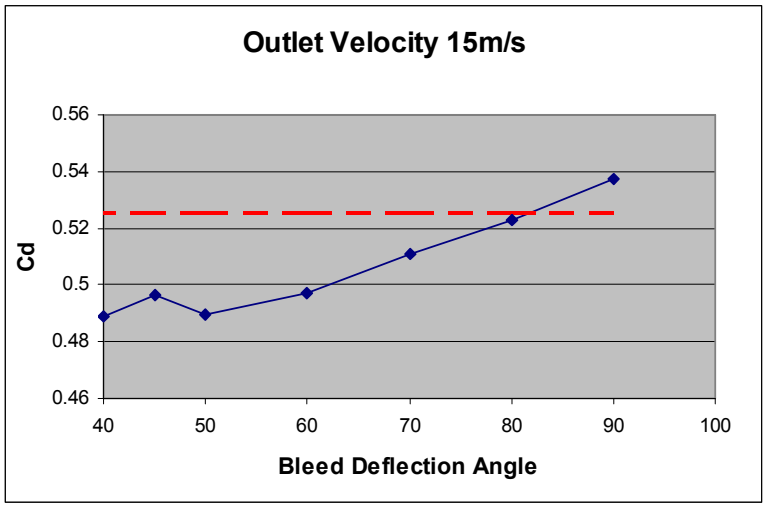

Figure 6.46 C_d against Bleed Deflection Angle for bleed velocity of 15m/s

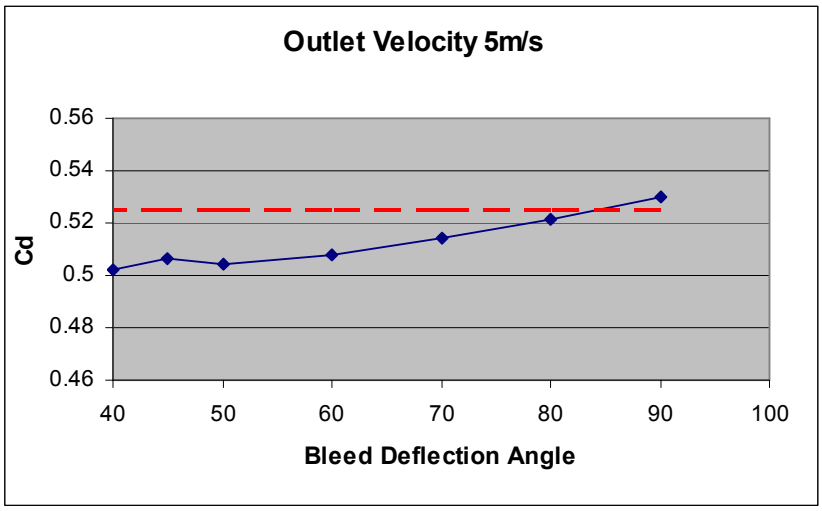

Figure 6.47 C_d against Bleed Deflection Angle for bleed velocity of 5m/s

As the velocity of the bleed air reduced, the gradient of the trend line decreased. This meant that base bleed was effective to much higher deflection angles. These tests also concurred with the previous results, showing that the lowest C_d could be achieved when $0.6 \leq V_d/V \leq 0.8$.

A particular point of interest for this study was the observation of how changing the deflection angle can influence the effects of extremely low mass flow rates. Figure 6.48 shows that for mass flow rates of as low as 0.032kg/s a significant drag reduction could be achieved.

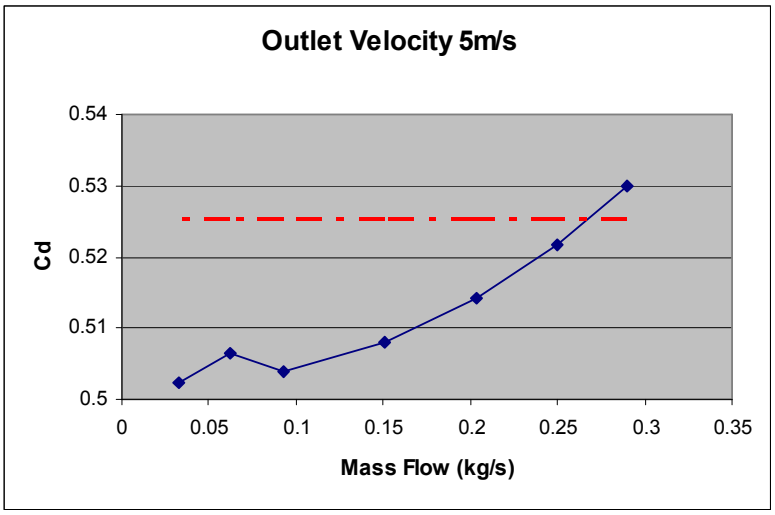

Figure 6.48 C_d against Mass Flow for bleed velocity of 5m/s

6.5 Effects of Base Bleed on Down Force

It has been noted that steeper outlet angles produced greater drag reductions for this system, with the exception of β=40°. It should also be noted, however, that there was a significant decrease in down force as the bleed air was deflected at these steeper angles. At 45°, the total down force was 60N for the half model. This can be compared to 96N for the standard half model and 147.5N when the bleed air was undeflected. Figure 6.49 shows the trend:

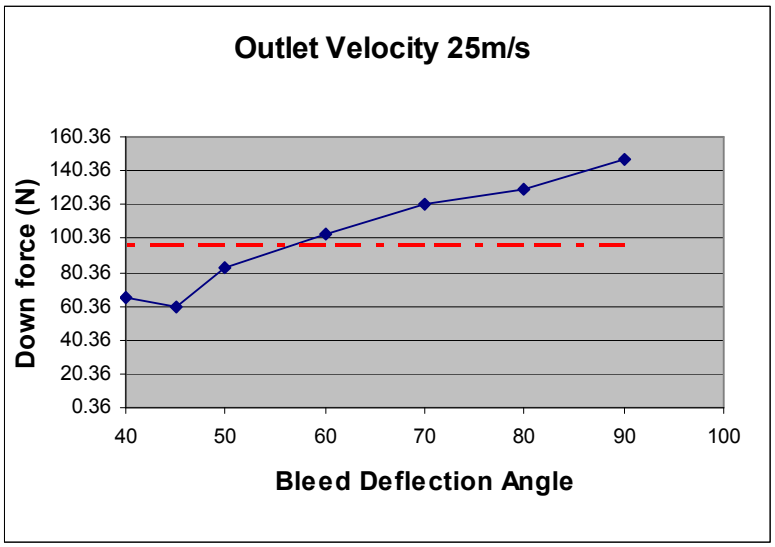

Figure 6.49 Down Force against Bleed Deflection Angle for bleed velocity of 25m/s

Reducing drag by increasing the deflection angle meant increasing the lift forces acting on the vehicle. This effect is extremely important as increasing lift force can have implications on the safety of the vehicle. Handling performance data was not available at the time of writing and so further discussion of acceptable lift force limits is not possible, however it should be noted that when $\beta=60°$, not only was C_d decreased from 0.525 when no base bleed was applied to 0.517, down force was actually increased from 96N to 103N for the half model. This demonstrates that through careful design and optimisation, base bleed could be used to decrease both drag and lift forces acting on a vehicle even at high outlet velocities.

The effects of base bleed on down force were also examined at lower outlet velocities, shown in Figure 6.50.

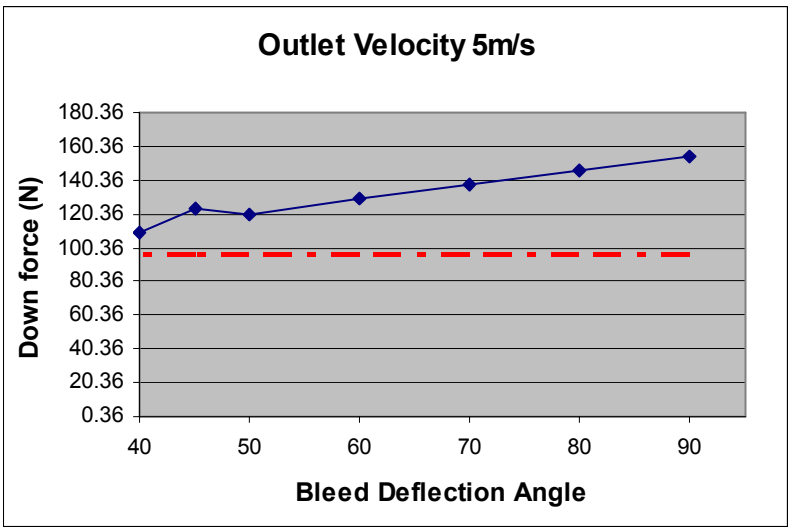

Figure 6.50 Down Force against Bleed Deflection Angle for bleed velocity of 5m/s

With lower outlet velocities, base bleed was found to increase net down force, even at the steepest angles studied. More down force over the rear axle is not always a good thing. However, the handling characteristics of this class of vehicle do benefit from negative lift at the rear axle, relative to the front.

The same relationship between down force and drag is apparent, where one must be sacrificed in order to benefit the other. To investigate further, choosing a particular deflection angle was necessary:

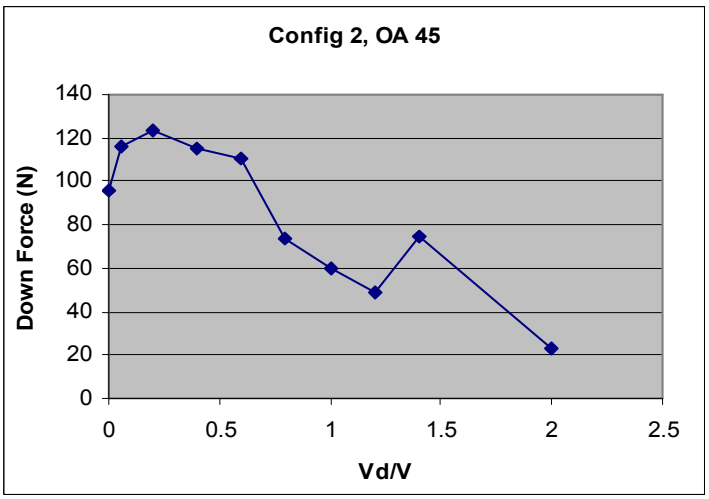

Figure 6.51 Down Force against V_d/V for config 2 for flow angle of 45°

Figure 6.51 shows the variation in down force as outlet velocity was increased for a flow angle of 45°. For this angle, base bleed increased down force until $V_d/V = 0.65$ ($V_d = 16.25$m/s). It was interesting to note that the drop in C_d that occurred at $V_d/V=1.2$ (shown in Figure 6.22) also inversely affected the down force.

To confirm the theory that base bleed could be beneficial to down force below a particular outlet velocity, examination was done at a flow angle of 60° for configuration 2.

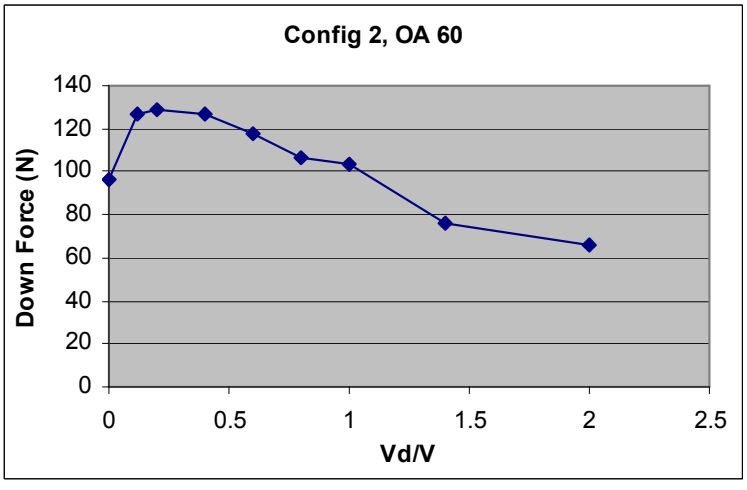

Figure 6.52 Down Force against V_d/V for config 2 for flow angle of 60°

At the shallower angle of 60°, higher outlet velocities increased down force. Base bleed was found to increase down force until $V_d/V=1$, beyond which point the effects were adverse.

Configuration 3 was investigated to see how a side outlet with inward deflection affected down force. As expected, variation in bleed velocity and mass flow had a far more subtle effect than with a high outlet. There was still some increase to the down force when using configuration 3 however, as shown in Figure 6.53:

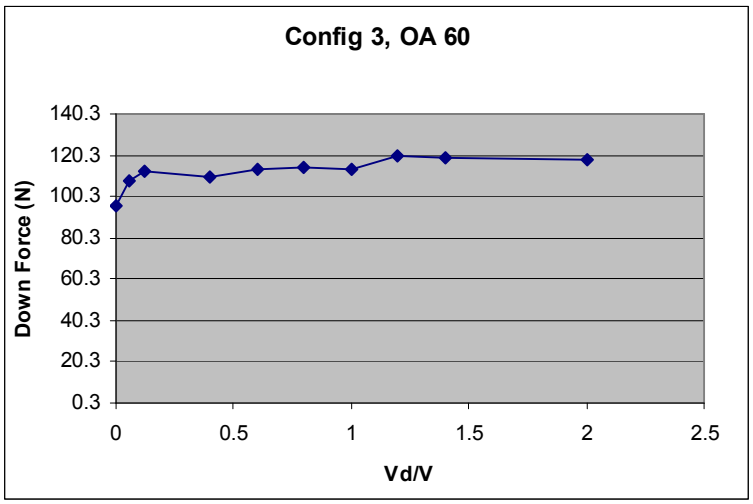

Figure 6.53 Down Force against V_d/V for config 3 for flow angle of 60°

In this case, down force increased with mass flow due to control of the turbulent wake, which can often contribute to lift. Similar results were obtained for a flow angle of 45°. This may be a significant advantage of a side outlet.

6.6 Conclusions

It has been shown that base bleed can significantly decrease drag when applied to the geometry of a real SUV. Mass flow rates of under 0.76kg/s can reduce drag coefficient by 9.1% with an outlet on the side of the vehicle, and a mass flow rate of under 0.2kg/s can reduce the drag coefficient by 5.5% for a small outlet on the upper section of the rear of the vehicle.

It was concluded that a large outlet with a lower bleed velocity was more effective for the same mass flow rate than a smaller outlet with greater bleed velocity. This is particularly relevant if applying a ventilation system where the mass flow is limited.

For the geometry studied, a bleed outlet applied to the upper portion is most effective in reducing drag. It may be difficult to implement this, however, as bleeding air from a high pressure region towards the top would be difficult. For this configuration, investigation may have to be carried out into bleeding air from an inlet on the roof of the vehicle.

It was found that bleed through the sides of the base region is also effective. This would allow venting from the sides, underside or roof.

It was also found that deflecting the flow has a large impact on the drag reduction achieved. As bleed angle changed, in each case there was a transition in turbulence intensity on the rear of the vehicle. At around 40-45° there was a change from specific areas of high and low turbulence caused by protrusions on the rear of the vehicle to a more evenly distributed medium turbulence that resulted in a base pressure decrease. This phenomenon occurred at each bleed velocity investigated at approximately the same angle.

For outlet velocities of 5 and 15m/s, the drag was lower than if base bleed had not been implemented until around 83°, whereas for a higher outlet velocity, base bleed was only effective when $\beta<65°$.

Further to this, the outlet velocity and flow angle both had a significant bearing on the down force acting on the vehicle. Increasing the outlet velocity reduced the down force but, to a certain point, increased drag reduction. Decreasing the flow angle at the outlet also had a negative effect on the down force, but improved drag reduction. When the outlet velocity remained below a certain value for each outlet angle, it was possible to improve down force and drag reduction simultaneously. Further to this, a side outlet did not show any negative effect on down force, regardless of outlet velocity or flow angle. It was concluded that through proper optimisation, base bleed could be used to reduce drag and increase down force, thus improving economy and the handling and safety characteristics of the vehicle.

It was reasoned that the flow angle should be optimised for any system implemented. As the flow around the rear of any real vehicle is largely non-uniform, investigation into the optimum angle would have to be carried out for the vehicle in question. Also, it should be noted that there is not one single optimum angle, but that the optimum angle will vary with outlet velocity. For lower bleed velocities, steeper outlet angles are less effective than they are for high bleed velocities ($V_d/V\approx1$). Were a ducting system to be implemented, it may therefore be recommended that a variable outlet be used to produce an optimum system for a number of different vehicle velocities.

Were this system to be implemented, the cavity of the bleed outlet may in fact increase drag reduction further [8]. Wind tunnel testing or a more detailed computer model would be required to investigate this.

7 Wind Tunnel Testing

Wind tunnel testing is widely regarded to be a cheaper and quicker way of performing drag analysis, particularly where numerous iterations are involved [24]. There are clearly some strong advantages in using wind tunnel data in an investigation such as this. Turbulence modelling in a CFD environment, whilst its realism is progressing rapidly, is not always entirely realistic. This is not the case with wind tunnel testing where for macroscopic flows turbulence is inherent in any real system. Further to this, even a fine mesh applied to a CFD model will distort the vehicle geometry to some extent. There will also be compromises with flow paths, where it may be overly complex to model ducts such as in the engine bay. Wind tunnel testing, in theory, can avoid these problems with far more accurate models or real vehicles being used in large-scale tunnels.

When testing full-scale vehicles, wind tunnel testing can be far more realistic as the material properties are also more easily considered. Deformation of the vehicle under mechanical or aerodynamic loading can affect flow paths and resulting drag readings, as can surface roughness. Unfortunately, as only a scale model was used for this investigation, these implications could not be tested in the wind tunnel, however it was still felt advantageous to test the drag reading of the scale model used for the laser-scanned CFD model and compare it with the CFD results.

For reasons described in chapter 3.3, wind tunnel testing was not be used as a primary means of investigation. However, as there is limited published information on base bleed in vehicle applications, it was intended that wind tunnel testing be used as a method of verifying the accuracy of the CFD model. It was hoped that wind tunnel testing may also be used if any unexpected phenomena arose that could not clearly be explained through the outputs available from Fluent, or that may have been a result of errors during the set-up procedure in Fluent.

7.1 Procedure

The model used for wind tunnel testing was created using two different 1/6 scale models. The four wheel drive system and body shell was taken from one vehicle and incorporated onto the chassis and wheels from another. This created a model that was geometrically the same as the CFD model while allowing all four wheels to turn in the wind tunnel by means of a remote control.

Figure 7.1 Wind tunnel model chassis and wheels

Figure 7.2 Wind tunnel model shell

Figure 7.3 Inside of wind tunnel model shell

Figure 7.4 Complete wind tunnel model

All gaps in the model shell were sealed using strong tape. Wheels arches were created inside the shell from cardboard. Tape was also used to seal horizontally from the wooden board shown in Figure 7.1 to the vehicle shell, simulating the passenger compartment of the vehicle which was unaffected by the external air flow. A vertical

seal was also placed across the centre of the vehicle to further restrict airflow inside the vehicle.

Generally, the wind tunnel at Strathclyde University is used for testing of scale model aircraft. Therefore, preparations for wind tunnel testing began through design of a rig to which the Land Rover model was mounted. Engineering drawings of this rig are included in Appendix B of the report, along with a colour image of the car mounted to the rig. A fairing was used around the rig stand to ensure that the drag of the exposed area was minimised.

The model was mounted to the rig via a wooden board attached to the chassis which also acted as a lower surface for the vehicle. This meant that the underside of the vehicle was smooth around the mounting, however the underside of the model was not sealed completely so air could flow up into the shell (Figure 7.5).

Figure 7.5 Underside of wind tunnel model

When mounting the model, careful consideration was given to the roll, pitch and yaw angles of the vehicle to ensure it was aligned with the airstream.

The balance to which the rig was mounted was set to output the drag force acting on the vehicle. An MDF board was mounted 2mm under the vehicle's wheels to simulate the ground. It was ensured that the ground board was level.

Figure 7.6 Model on rig and balance

Figure 7.7 Model with ground board in place

Figure 7.6 and Figure 7.7 show the model mounted in the wind tunnel. It can be noted that the hole in the ground board through which the rig was inserted was sealed using tape and card. There were no gaps between the ground board and the fairing around the rig. A splitter plate was incorporated in the design of the ground board to ensure that the resulting boundary layer developing at the front of the board did not affect the flow around the vehicle.

The wind tunnel allows for testing at various speeds, with a maximum limit of around 30m/s. For the purposes of this investigation, a wind speed of 25m/s was required. The wind speed in the tunnel was calculated using a pitot static tube which measured the pressure in the free-stream at the inlet to the system. Pressure measurements were taken using a calibrated inclinometer with water as the working fluid at a density of 1000kg/m^3.

The velocity was calculated using Bernoulli's equation as follows:

Equation 13

$$P_1 + \frac{1}{2}\rho_a v_1^{\,2} + \gamma h = P_2 + \frac{1}{2}\rho_a v_2^{\,2} + \gamma h$$

Where P_1 is the static pressure and P_2 is the stagnation/total pressure

v_2=0 at the stagnation point. Therefore, by rearranging:

Equation 14

$$v = [2\frac{(P_2 - P_1)}{\rho_a}]^{\frac{1}{2}}$$

$(P_2 - P_1)$ is known as the dynamic pressure, P_d.

Equation 15

$$P_d = \rho g h$$

Where the height of the water, h, is corrected using an appropriate scale factor.

The ambient air density was calculated as follows:

Equation 16

$$\rho_a = \frac{P_a}{RT_a}$$

A digital barometer was used to measure ambient air pressure.

Before testing was carried out, the balance in the wind tunnel was tested to ensure that the forces present on the model would translate into the balance correctly. A pulley system was mounted to the top of the rig and a series of weights were hung from the mounting board of the model (Figure 7.8).

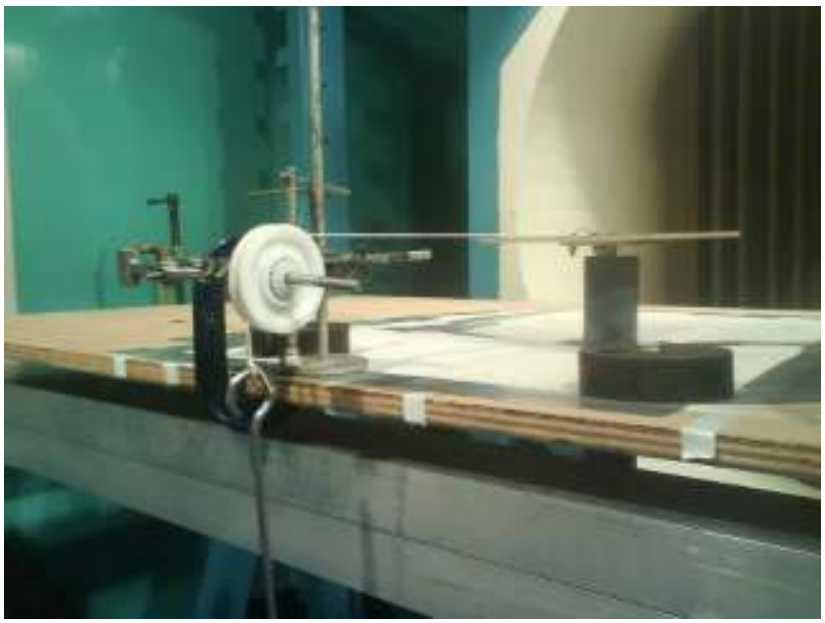

Figure 7.8 Wind tunnel balance test

Care was taken to ensure that the string used in the pulley system was completely horizontal to ensure that the full force of the weights was converted into a drag reading. Readings were then taken from the balance and compared with the known forces applied to the system. It was found that there was a percentage and a constant error in the balance so all readings were calculated using Equation 17:

Equation 17

$$F_A = 0.176F_r + 0.35$$

Where F_A is the actual force on the model and F_r is the force read from the balance.

C_d was calculated using Equation 6. All calculations were done using the reference area produced by Fluent. This was felt to be the most accurate representation of the projected area of the vehicle. The reference area of the model was also measured, however, to ensure accuracy. Average dimensions are given in Table 7.1 Wind tunnel model dimensions:

Vehicle Height	23.5cm
Vehicle Width	23.5cm
Exposed Wheel Height	7cm
Exposed Wheel Width	3.5cm
Reference Area	$0.06m^2$

Table 7.1 Wind tunnel model dimensions

The calculated area was known to be approximate but was similar to that given by Fluent and so the Fluent value was used.

With the airflow in the tunnel set, readings were taken for the model using the sliding scale on the balance, the scale of which was in lbs with a resolution of $\pm 0.025 lbs$. All tests were carried out three times, and an average reading was recorded.

7.2 Testing of Vehicle Drag Coefficient

Testing was done in the wind tunnel to measure the drag coefficient of the scale-model used for the laser-scanning procedure. This served to establish the accuracy of the CFD method used and ensure the results of the base bleed analysis were truthful.

Tests were done on a static ground board with both static wheels and turning wheels. The wheel speed was not measure, however based on the power of the motor was estimated to be a forward velocity of around 15m/s. The effect of turning wheels on the model was also briefly examined.

7.3 Bleed Outlet/Cavity Test

Many studies have indicated that a cavity to the rear of a vehicle can influence the drag coefficient [6][8][32]. As this cavity was not simulated by the CFD methods

used in this investigation, wind tunnel tests were carried out to try to establish if the absence of the cavity would have contributed to the drag reduction. For each test, the outlet was also altered to see how far the size of the outlet hole affected the results.

The procedure involved removing the rear window panel of the vehicle shell to create an outlet that approximately match that of each of bleed configuration 1. Tape was then used to create an outlet that matched bleed configuration 2. First, a test was carried out with a cavity extending to the seal across the centre of the vehicle. Then, the interior cavity was reduced in length by taping across the inside of the vehicle. Three cavity sizes were tested. The vehicle was approximately 40cm in length. Cavities of 50%, 25% and 12.5% of this were examined, measurements being approximate due to the camber at the rear section of the car. All measurements were taken along the floor of the cavity.

Tests were carried out with static and turning wheels to see if the outlet hole and cavity affected their influence on the vehicle drag.

7.4 Results and Discussion

Table 7.2 shows the findings of all wind tunnel tests. All tests were carried out three times and the mean values were used.

	Turning Wheels	Reading (lb)	Actual (lb)	Force (N)	Cd
No outlet	N	2.3	3.055	13.829	0.568
	Y	2.2	2.937	13.296	0.546
Config 1 21cm Cavity	N	2.275	3.025	13.696	0.563
	Y	2.175	2.908	13.163	0.541
Config 1 11cm Cavity	N	2.275	3.025	13.696	0.563
	Y	2.15	2.878	13.030	0.535
Config 1 5cm Cavity	N	2.225	2.967	13.43	0.552
	Y	2.125	2.849	12.897	0.53
Config 2 21cm Cavity	N	2.3	3.055	13.829	0.568
	Y	2.2	2.937	13.296	0.546
Config 2 11cm Cavity	N	2.3	3.055	13.829	0.568
	Y	2.175	2.908	13.163	0.541
Config 2 5cm Cavity	N	2.25	2.996	13.563	0.557
	Y	2.125	2.849	12.897	0.53

Table 7.2 Wind Tunnel Results

7.4.1 Testing of Vehicle Drag Coefficient

C_d of the model was within 1% of that found using CFD for the 1/6 scale model without turning wheels, and 2% with turning wheels (Table 5.1). This helps to verify the CFD results, as the small increase in C_d can be accounted for by dissimilarities in the model due to the mounting on the rig.

As expected, the rotation of the wheels over a static ground board reduced the total drag force on the vehicle. Again, this is consistent with general theory [33] and the CFD results.

It can be noted that there is a slightly larger decrease in drag in the wind tunnel tests. The reduction in C_d for the CFD tests was 1.023%, whereas for the wind tunnel tests it was 3.85%. Due to the nature of the suspension in the vehicle, the wheels were observed to have oscillated slightly due to unsteady lift force during the testing, affecting the overall result. This was particularly prevalent in all tests where the wheels were rotating and may partly explain the slight change.

Furthermore, the wheels were not completely sealed off from the body shell and therefore rotating the wheels would have affected the airflow around a larger portion of the car than in the CFD tests. Finally, the rotational speed of the wheels could not be measured precisely and so any error would also have contributed to a discrepancy in the drag reduction.

As the wind tunnel model used was a hybrid of two different scale models, the underside of the model did not exactly match that used in the CFD process. This was particularly the case where the chassis had to be constructed to incorporate the four-wheel drive system and mounting rig for the balance. However, the similarity in C_d showed that the model could reasonably be used for further testing and justifiably supports the accuracy of the CFD tests.

7.4.2 Bleed Outlet/Cavity Test

In the case of the bleed outlet cavity test, it must first be noted that the results do not exactly simulate a real base bleed system but were merely an indication as to whether the outlet and cavity would affect the results with no bleed air. In a real system, the cavity would either lead to a gas generator or, more likely, an inlet located at a high pressure region on the vehicle. This would significantly affect the internal shape of the duct and therefore the amount by which the drag is reduced.

It should also be stated that each time the internal cavity was reduced in size the test was repeated with no bleed outlet to ensure that the drag was not affected by changing the internal configuration of the vehicle alone. In each case, no change was recorded without a bleed outlet present.

First, the results of the cavity test were examined.

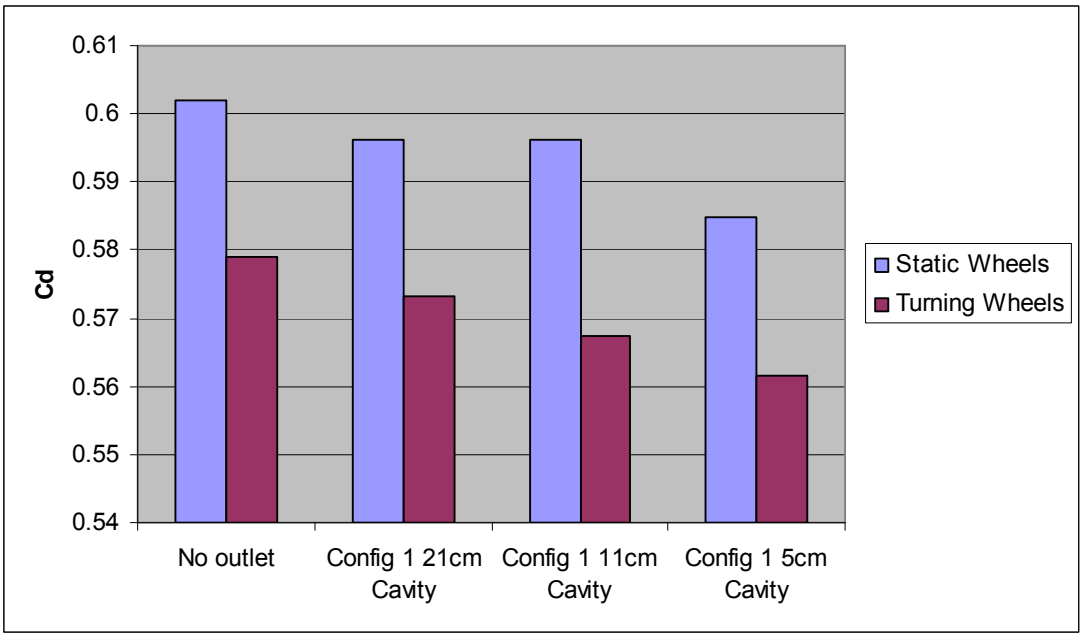

Figure 7.9 C_d against varying cavity depth for configuration 1

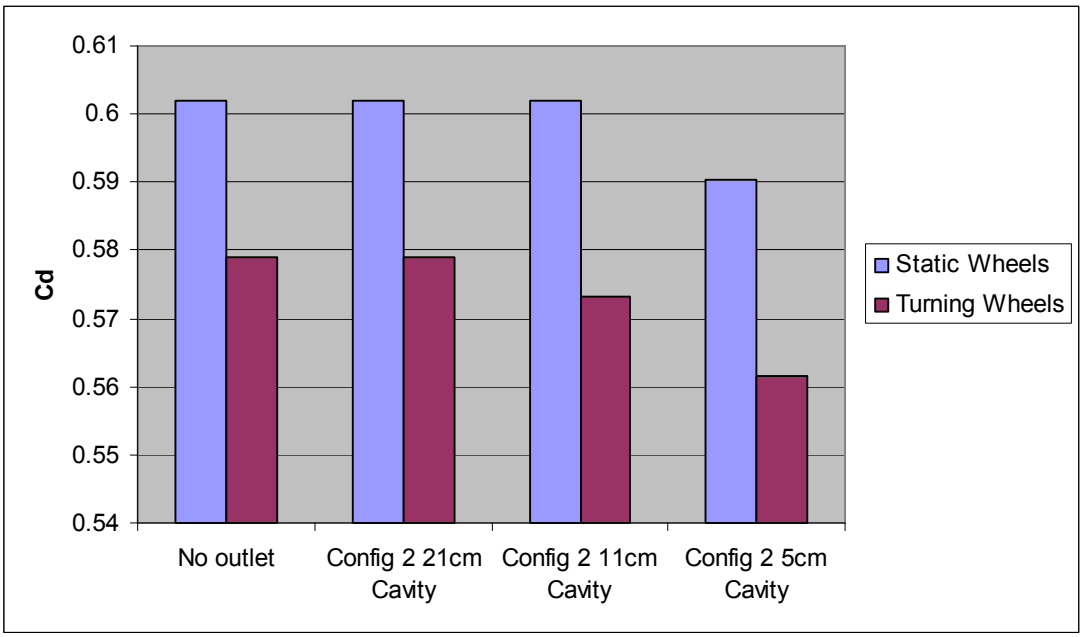

Figure 7.10 C_d against varying cavity depth for configuration 2

The cavities were tested with outlets matching bleed configurations 1 and 2. Figure 7.9 and Figure 7.10 shows a steady decrease in C_d as the cavity size is approximately halved. It was found that the smallest cavity produced the greatest drag reduction. The smallest cavity tested was approximately 10% of total length, which, interestingly, was found to be the optimum cavity depth by Howell for a generic bluff body shape [8]. In terms of base bleed application to vehicle design, this finding is beneficial to duct design where consideration would have to be given to the interior space of the vehicle. A smaller duct would be easier to implement and would not restrict the practicality of the vehicle as much as a larger duct design.

In comparing Figure 7.9 and Figure 7.10, these results also confirm that the size of the outlet affects the drag reduction when no bleed air is present. With the large cavity present, configuration 1 reduced C_d by around 3.5% with static wheels and 3.1% with turning wheels when compared with the original values. For configuration 2, C_d reduced by only 0.5% and 1% for static and turning wheels respectively. This shows that, for the same internal cavity size and shape, the larger bleed outlet creates a larger drag reduction.

A comparison of the two outlet configurations is most easily made using Figure 7.11, where the results for each configuration are shown side by side.

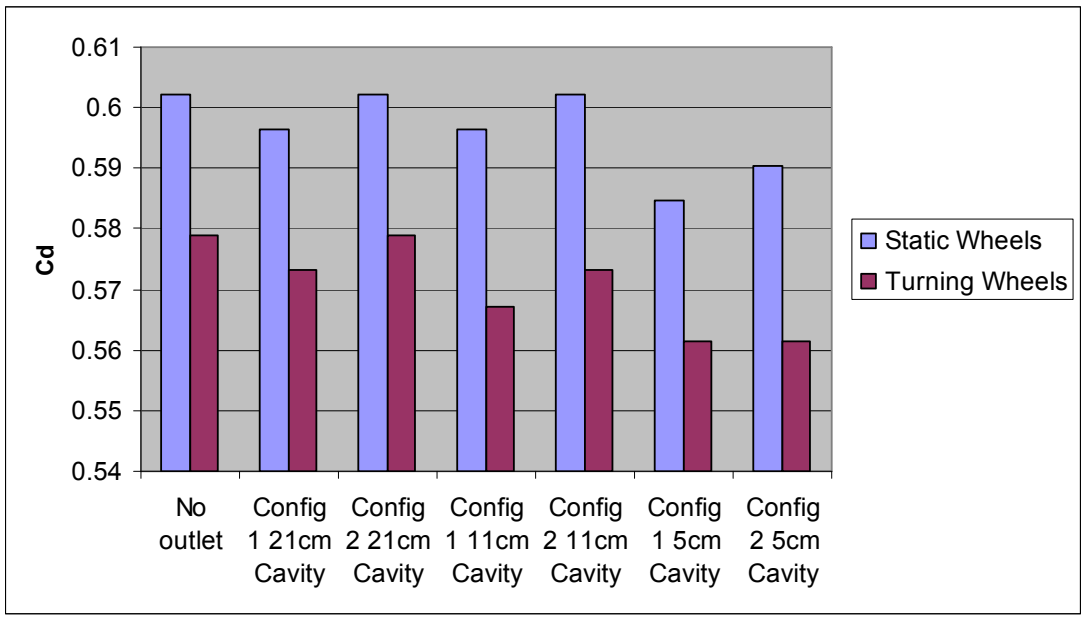

Figure 7.11 C_d against varying cavity depth for outlet configurations 1 and 2

It can be seen that for each cavity size the drag increased with a smaller outlet size, and was highest with no outlet.

For both tests carried out, a number of generic errors may have affected the results. Changes in the local environment between setting up the experiment and measuring the results could have affected the overall readings. Pressure and temperature within the laboratory could have changed slightly over time, however as an average reading was taken for each measurement it is unlikely that this had a significant bearing on the results.

Fluctuations of the fluid in the inclinometer also meant that the velocity in the tunnel had a degree of inaccuracy which may have affected readings and C_d calculations. Further to this, the orientation of the pitot static tube may have affected the velocity calculation in the tunnel through inaccuracy of the static pressure reading.

Although care was taken to align the vehicle into the airstream in roll, pitch and yaw angle, inaccuracies in the model and alignment of the body shell with the chassis and wheels may have affected the results.

7.5 Conclusions

Firstly, the wind tunnel tests acted as verification of the accuracy of the CFD tests. The drag coefficient of the model was very similar to that found using CFD, indicating that each has produced precise data.

The work carried out in the wind tunnel was also important as it helped further realise the benefits of base bleed. Although the CFD results show that base bleed can be used to decrease drag, the CFD method used does not replicate a real system exactly. The wind tunnel tests showed that, were a system to be modelled more accurately in CFD, it would possibly show further drag reduction due to the cavity and outlet present on the rear of the vehicle.

The wind tunnel tests show that optimisation of the duct design is important as the duct in itself can reduce drag. It was found that the optimum duct length was around 10% of total vehicle length, as had been found in other work on similar shaped bluff bodies [8].

The wind tunnel work also showed that the size of the outlet significantly affected the drag reduction. Where a larger outlet was present, the drag reduced by a significantly higher amount – even with the same size and shape of duct present. This shows that it is beneficial to design an outlet to be as large as possible when applying base bleed to vehicle design.

8 Conclusions and Recommendations for Further Work

The work that has been carried out during this investigation may serve as a preliminary basis for the application of base bleed into vehicle design. It has been shown that base bleed can produce favourable results under particular conditions; however, there are many factors that have not been considered that may influence the effectiveness of such a system.

Each case in this investigation has been carried out under constant atmospheric conditions. In a real system, changes to air temperature, pressure or density would affect the airflow around the vehicle and thus the influence base bleed may have. For example, it is likely that optimum values of V_d/V would alter with atmospheric conditions for the same vehicle velocity and geometry. Further to this, the CFD and wind tunnel work did not simulate weather. For a real system, a vehicle would not drive through still air and would be subject to unsteady headwinds or crosswinds. This may have a major impact on the effectiveness of the system, particularly as the bleed air interacts with crosswinds. An interesting study may be to see if the effects of crosswinds can be countered by deflecting the bleed airflow using side outlets.

Another interesting advancement on the work discussed in this report would be to vary the vehicle velocity. The vehicle speed in this investigation was chosen as it was deemed equivalent to motorway driving speed in the UK. It was felt that under motorway driving conditions, base bleed would be most effective as at high speeds pressure drag is the predominant force acting against the motion of the vehicle. In addition, journeys done by motorway tend to be for long distances where fuel economy is a primary consideration when choosing a car. Higher and lower driving speeds could be investigated to establish if base bleed can increase fuel economy as effectively, or to discover if there is an optimum driving speed that base bleed should be used for. This is not to say, however, that base bleed may not also be effective at much lower speeds. SUVs are commonly used for inner-city motoring due to their

aesthetic appeal, and so to reduce drag at speeds around 30mph would be advantageous.

Under varying vehicle speeds, it would be interesting to establish whether similar bleed deflection angles or mass flow rates are required and if the optimum angles or mass flow rates are different under varying speeds. This could have a significant impact on an accelerating vehicle, where variable outlets could be used to improve the performance of a vehicle both in terms of fuel efficiency and rate of acceleration.

Vehicle direction is also a consideration that would require further study. It is rare that a vehicle will drive for any extended period without turning and introducing a yaw angle to the air flow. This may have a similar effect on base bleed to crosswinds and would likely diminish the drag reduction and so study into how to offset this would be worthwhile.

Although the wind tunnel tests that were carried out in this investigation showed that the results of base bleed may have been improved had the duct been modelled in the CFD simulations, they do not fully show the effect that a duct may have. For example, the tests showed that varying the duct length changed the overall drag reduction, but it was not possible to conclude if this was due to varying the duct length or if a change in volume was the main contributor. Further tests could confirm the ideal duct shape and size for optimum drag decrease, and confirm whether this duct design coincides with the requirements for maximum bleed air flow efficiency. This work may significantly influence the effectiveness of a base bleed system when applied to an SUV. Duct design is also extremely important as it significantly affects the feasibility of incorporating such a system to a production vehicle, where limitations are present due to interior capacity requirements. Therefore, any work done on duct design and optimisation should take into account the practical limitations of a real vehicle, with testing done on a production vehicle shape as has been done in this investigation.

In the same way, work done on designing an inlet for a base bleed system would be required for each vehicle to which base bleed could be applied. This study has highlighted some areas of high pressure around the vehicle surface, but most of these occur in areas would be difficult to efficiently channel the bleed air from to the rear of the vehicle. Therefore, clever inlet design on areas of lower pressure nearer to the rear of the vehicle, alongside optimised duct design, would be required to create an efficient system.

Because of time constraints, only three outlet configurations could be studied in any detail in this investigation. Furthermore, these outlets were chosen as they were very different in shape and size, allowing conclusions to be easily drawn on what may be most effective. Based on these conclusions, it is recommended that further investigation be done to discover if the outlet design can be optimised. For example, it was shown that a larger outlet is more effective than a smaller one for similar mass flow rates and outlet shapes, but it was not confirmed whether altering the shape of the outlet could improve drag reduction for a constant area. It may also be interesting to assess the effect of slight alterations to the outlet location on base bleed effectiveness.

In conclusion, this study has shown that a base bleed system must be taken as a whole. Each change to the system influences the total air flow around the vehicle and therefore the individual variables cannot be optimised independently. Knowledge of the available mass flow rates as vehicle velocity changes is vital in designing a full system. To properly establish the effectiveness of a system, the source and conditions of the bleed air should be known. This should include knowledge of the air quality, whether it is laminar or turbulent, its temperature and density etc. Knowledge of the available technology for use in the system is also essential. For example, a controllable mass flow could significantly benefit a system if the means were available. Once these parameters are known, an efficient ducting system could be designed, leading to design and placement of the outlet(s). Without sufficient knowledge of all parameters forward of the outlet, this investigation has

shown that optimisation of the outlet design would not be possible. Even so, it would be likely that a single outlet design would be unlikely to create an optimum drag reduction under varying driving conditions.

One of the most crucial points in the design of a vehicle base bleed system is that the work is done specifically for a particular geometry. The interaction of small details of the vehicle can have a large bearing on the results, as found in the study of bleed configuration 2 where at a particular angle of deflection the rear bumper caused a large increase in drag for a particular mass flow rate to a system that otherwise had better performance than the other angles studied.

Knowing the geometry of the vehicle also helps define the constraints within which the designer can work. Legal constraints, such as the placement of rear lighting on the vehicle or the strength that a vehicle must have to withstand crash or roll damage, may severely restrict the placement of a duct or outlet within the vehicle. Further to this, the optimum outlet position may be made impossible by physical features of the vehicle, such as the rear windscreen or passenger compartment. Furthermore, the vehicle must remain practical, a particular point of interest for a vehicle such as an SUV for reasons explained in the introduction.

For these reasons, this investigation did not set out to fully design and optimise a base bleed system for a bluff two-box SUV, but merely was intended to serve as a basis upon which further study could continue. Restrictions on time, computational processing power and manpower have meant that a more detailed study could not be completed, however it was hoped that the work done would contribute to the useful literature currently available on such technology.

This report intended to discuss the investigation and detail the methods used, highlighting both the strengths and weaknesses of the work. The work carried out has quantitatively shown that base bleed could, in theory, significantly reduce the drag of a production SUV and has detailed some of the key factors that could

contribute to this reduction. The modern methods used during this investigation (such as CFD and laser scanning) differed in many ways from those used in the other literature mentioned throughout the report, and it was hoped that the way in which the work has been carried out has allowed a greater insight into the effects of base bleed in vehicle design than had more traditional methods been used.

The work has also highlighted some of the problems and constraints designers may face in incorporating base bleed into a production vehicle. It was hoped that these brief comments will be useful in the future and help towards base bleed becoming commonplace as a drag reduction method on bluff two-box SUVs.

9 References

1. Aerodynamics of Road and Racing Vehicles; M Stickland; 16598-1-1 - Aerodynamic Performance SEM2-07-08

2. http://www.edmunds.com/advice/fueleconomy/articles/106954/article.html

3. Experiments on the flow past spheres at very high Reynolds numbers; Aachenbach E.; 1972; Fluid Mech. 62, 209-221

4. The effect of base slant on the flow pattern and drag of three-dimensional bodies with blunt ends; R. T. Jones; in Aerodynamic drag mechanism of blunt bodies and vehicles, Plenum Press, NY, 1978

5. Motor vehicle dynamics: modeling and simulation; Giancarlo Genta; Published by World Scientific, 1997; ISBN 9810229119, 9789810229115

6. Reduction of Aerodynamic drag with base bleed system; Itsuhei Kohri, Takuya Kataoka; Journal of JSAE Vol., 45, No. 4, 1991, pp 78-83

7. Predicted Flight Performance of Base-Bleed Projectiles; James E. Danberg and Charles J. Nietubicz; U.S. Army Ballistic Research Laboratory, Aberdeen Proving Ground, Maryland

8. Aerodynamic Drag Reduction for a Simple Bluff Body Using Base Bleed; Jeff Howell and Andrew Sheppard -Land Rover; Alex Blakemore -Loughborough University; SAE Technical Paper Series 2003-01-0995

9. A ground based Research vehicle for base drag studies at subsonic speeds - Corey Diebler and Mark Smith

10. Fluid-Dynamic Drag: Practical Information on Aerodynamic Drag and Hydrodynamic Resistance; Hoerner, F. Sighard; Self-published work, Library of Congress Card Number 64-19666, Washington, D. C., 1965.

11. Wake and base bleed flow downstream of bluff bodies with different geometry - Chin-Yi Wei, Jeng-Ren Chang

12. Bluff-body drag reduction by passive ventilation; G. K. Suryanarayana, Hemming Pauer, G. E. A. Meier; 1993; Experiments in Fluids 16, 73-81

13. The effect of base bleed on periodic wake; Wood, C. J. 1964; Royal Aeronautical Society, Vol. 68, 477-482

14. The effect of base bleed on the flow behind a two-dimensional model with a blunt trailing edge; Bearman, P. W; 1967; The Aeronautical Quarterly, 207-224

15. Passive and Active Controls of 3D Wake of Bluff Body; Hiroshi Higuchi; Syracuse University, Department of Mechanical and Aerospace Engineering

16. Drag Reduction Techniques for Axisymmetric Bluff-Bodies. Mair. W. A. 1978: Aerodynamic drag mechanisms of bluff bodies and road vehicles, pp 161-187. New York: Plenum Press.

17. The COANDA Flow Control and Newtonian concept approach to achieve drag reduction of passenger vehicles Jung-Do Kee, Moo-Sang Kim, Byung-Cheon Lee - Hyundai Motor Co.

18. An introduction to computational fluid dynamics: the finite volume method; Henk Kaarle Versteeg, Weeratunge Malalasekera; Edition: 2, illustrated; Published by Pearson Education, 2007; ISBN 0131274988, 9780131274983

19. Computational Fluid Dynamics For Engineers: From Panel to Navier-Stokes; By Tuncer Cebeci, Jian P. Shao, Fassi Kafyeke; Horizon Publishing Inc.; ISBN 3-540-24452-4

20. ME405-1-1 - Heat And Flow 4 SEM1-06-07 notes; T Scanlon; University of Strathclyde

21. 16597 Computational Fluid Dynamics (CFD) notes; M Wheel; University of Strathclyde

22. Turbulence: an introduction for scientists and engineers; Peter Alan Davidson; Published by Oxford University Press, 2005; ISBN 019852948 1;

23. TURBULENT FLOW - 16597 Computational Fluid Dynamics notes; T Scanlon; University of Strathclyde

24. The Appropriate Use of CFD in the Automotive Design Process; A P Gaylard; Jaguar Land Rover; 2009-01-1162

25. Performance evaluation of three active vision systems built at the National Research Council of Canada; J.-A. Beraldin, S. F. El-Hakim and F. Blais; Proceedings of the Optical 3D Measurement Techniques III, NRC Technical Report 39165. Vienna: pp. 352–361. 1995.

26. Scientific Canadian: Invention and Innovation from Canada's National Research Council; Roy Mayer; Vancouver: Raincoast Books, 1999.

27. 3D Digitizing KONICA MINOLTA 3D Laserscanner *Applications in medical science*; 2004 Konica Minolta Photo Imaging Europe GmbH

28. The 3D Model Acquisition Pipeline; Fausto Bernardini, Holly E. Rushmeier; Comput. Graph. Forum 21(2): 149-172; 2002

29. Wall y^+ Strategy for Dealing with Wall-bounded Turbulent Flows; Salim M Salim and S. C. Cheah; Proceedings of the International MultiConference of Engineers and Computer Scientists 2009 Vol II, IMECS 2009, March 18 - 20, 2009, Hong Kong

30. '3. Meshing', *Best practice guidelines for handling Automotive External Aerodynamics with FLUENT*, Version 1.2; Lanfrit,M; Fluent Deutschland GmbH Birkenweg 14a64295 Darmstadt/Germany,19; 2005

31. Boundary-layer theory; Hermann Schlichting, K. Gersten, Egon Krause, Katherine Mayes, Herbert Oertel; Translated by Katherine Mayes; Contributor Egon Krause, Herbert Oertel; Edition: 8, illustrated; Published by Springer, 2000; ISBN 3540662707, 9783540662709

32. A New Aerodynamic Approach to Advanced Automobile Basic Shapes; A. Morelli; SAE 2001-01-0491; 2001.

33. Drag reduction mechanisms due to moving ground and wheel rotation in passenger cars; Per Elofsson, Mark Bannister; SAE 2002 World Congress

Appendix A - CFD Errors and Resolutions

Throughout this process, a number of other criteria were checked to ensure that they would not affect the results output.

Double Precision Solver

The double precision solver was used to ensure that the results would not be affected. This was done using a full model and static wheels and convergence criteria of 0.001.

Force vector: (1 0 0)

zone name	pressure force n	viscous force n	total force n	pressure coefficient	viscous coefficient	total coefficient
car_rear	3.7124817	0.0099105949	3.7223923	6.0611947	0.016180563	6.0773752
front_bumper	7.0289913	0.056649197	7.0856405	11.475904	0.092488484	11.568393
front_left_wheel	1.0529121	0.039578401	1.0924905	1.7190401	0.064617797	1.7836579
front_right_wheel	1.0853557	0.039825156	1.1251808	1.7720092	0.065020662	1.8370299
rear_left_wheel	0.5808528	0.025840919	0.60669372	0.9483311	0.042189255	0.99052035
rear_right_wheel	0.63595227	0.025704379	0.66165665	1.0382894	0.041966333	1.0802557
wall	2.8310695	0.83612439	3.6671939	4.6221543	1.365101	5.9872554
windscreen	0.62648457	0.086176638	0.71266121	1.0228319	0.14069655	1.1635285
net	17.5541	1.1198097	18.67391	28.659755	1.8282607	30.488016

The model converged after 161 iterations. This took considerably longer to solve and produced exactly the same results as previously calculated. This solver was not used again within this investigation.

Appendix B – Wind Tunnel Rig Diagrams

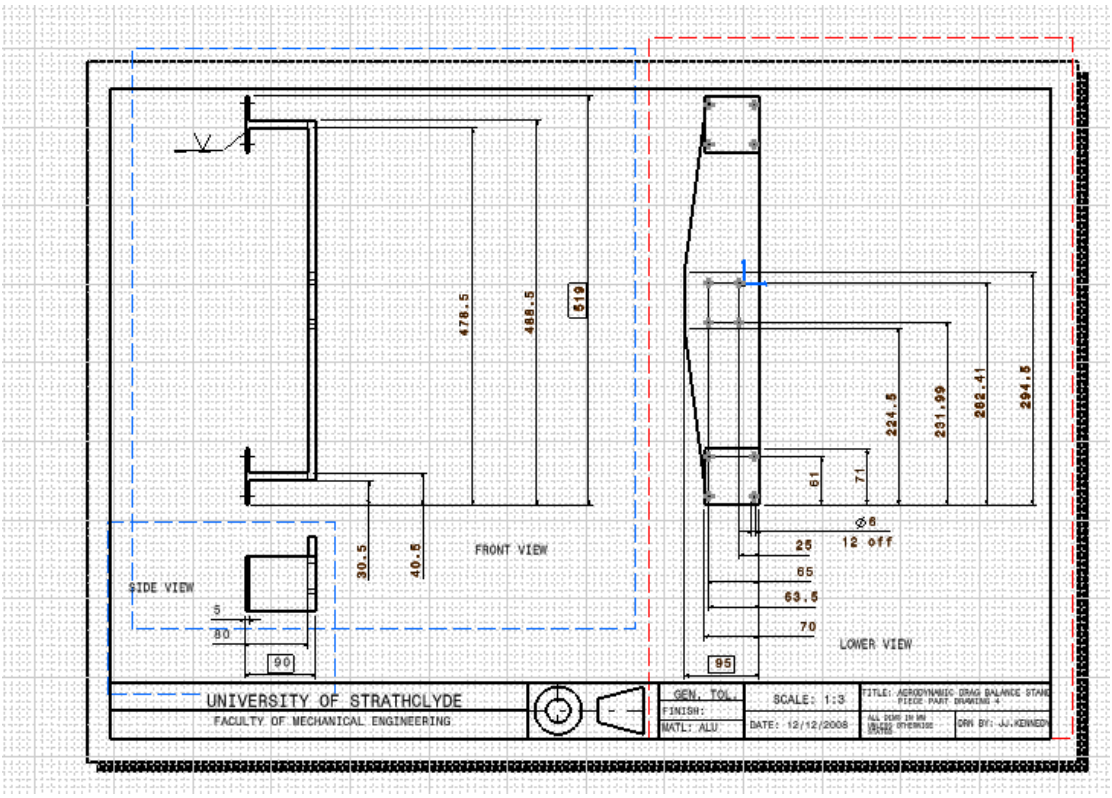

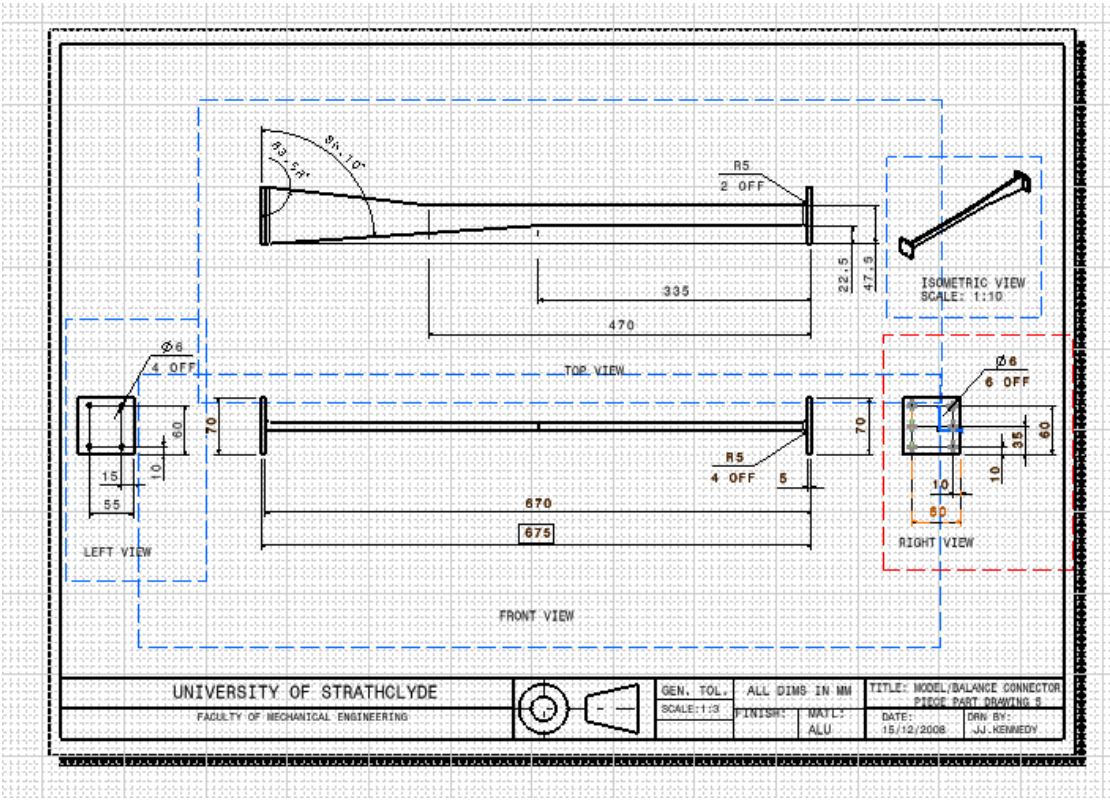
R5
2 OFF
335
470
22.5
47.5
ISOMETRIC VIEW
SCALE: 1:10
Ø6
4 OFF
TOP VIEW
Ø6
6 OFF
70
60
15
10
55
LEFT VIEW
R5
4 OFF
5
670
675
RIGHT VIEW
FRONT VIEW
UNIVERSITY OF STRATHCLYDE
FACULTY OF MECHANICAL ENGINEERING
GEN. TOL.
SCALE: 1:3
ALL DIMS IN MM
FINISH:
MATL: ALU
TITLE: MODEL/BALANCE CONNECTOR PIECE PART DRAWING 8
DATE: 15/12/2008
DRN BY: JJ.KENNEDY

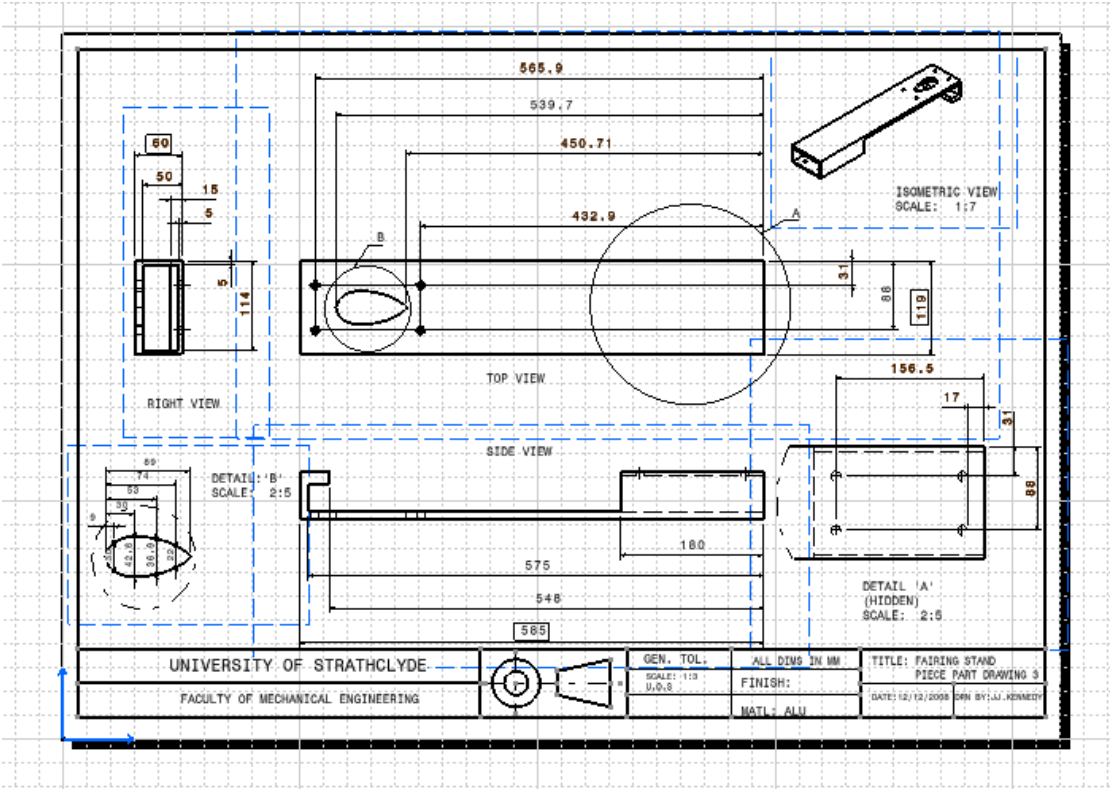
565.9
539.7
450.71
432.9
ISOMETRIC VIEW
SCALE: 1:7
60
50
15
5
5
114
B
A
31
86
119
TOP VIEW
156.5
17
31
RIGHT VIEW
SIDE VIEW
DETAIL 'B'
SCALE: 2:5
180
575
548
585
DETAIL 'A'
(HIDDEN)
SCALE: 2:5
UNIVERSITY OF STRATHCLYDE
FACULTY OF MECHANICAL ENGINEERING
GEN. TOL.
ALL DIMS IN MM
FINISH:
MATL: ALU
TITLE: FAIRING STAND PIECE PART DRAWING 3

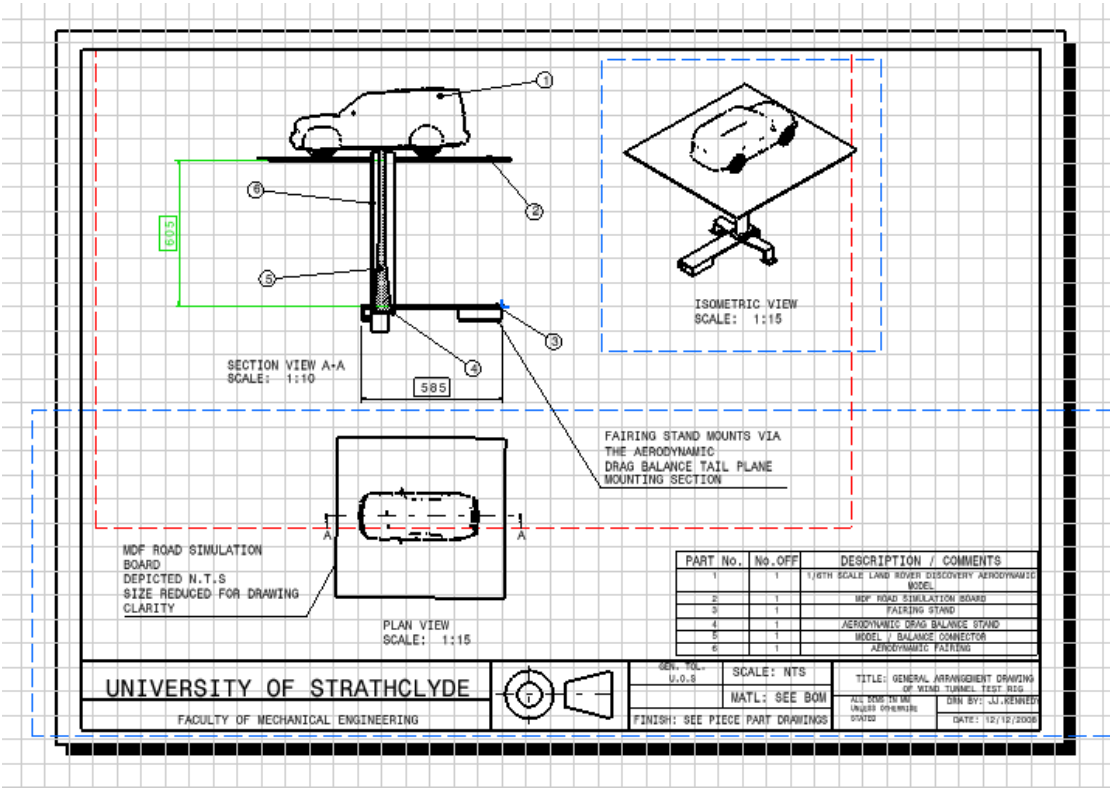
ISOMETRIC VIEW
SCALE: 1:15
SECTION VIEW A-A
SCALE: 1:10
615
585
FAIRING STAND MOUNTS VIA THE AERODYNAMIC DRAG BALANCE TAIL PLANE MOUNTING SECTION
MDF ROAD SIMULATION BOARD DEPICTED N.T.S SIZE REDUCED FOR DRAWING CLARITY
PLAN VIEW
SCALE: 1:15
PART No. | No.OFF | DESCRIPTION / COMMENTS
1 | 1 | 1/6TH SCALE LAND ROVER DISCOVERY AERODYNAMIC MODEL
2 | 1 | MDF ROAD SIMULATION BOARD
3 | 1 | FAIRING STAND
4 | 1 | AERODYNAMIC DRAG BALANCE STAND
5 | 1 | MODEL / BALANCE CONNECTOR
6 | 1 | AERODYNAMIC FAIRING
UNIVERSITY OF STRATHCLYDE
FACULTY OF MECHANICAL ENGINEERING
SCALE: NTS
MATL: SEE BOM
FINISH: SEE PIECE PART DRAWINGS
TITLE: GENERAL ARRANGEMENT DRAWING OF WIND TUNNEL TEST RIG
DRN BY: JJ.KENNEDY
DATE: 12/12/2008

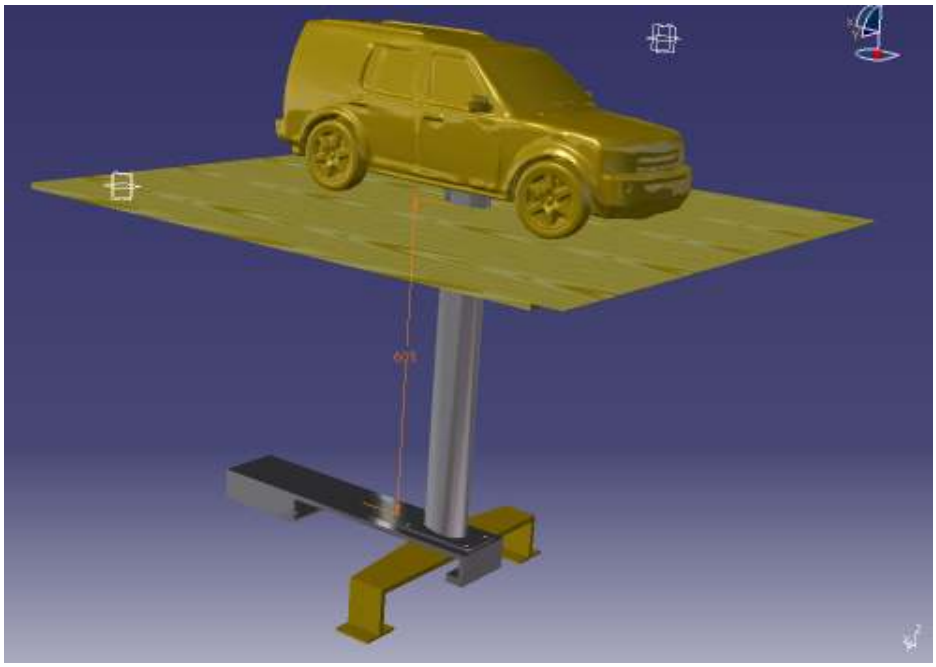

Appendix C – Mass Flow Data for Deflection Study

Outlet Velocity 25m/s

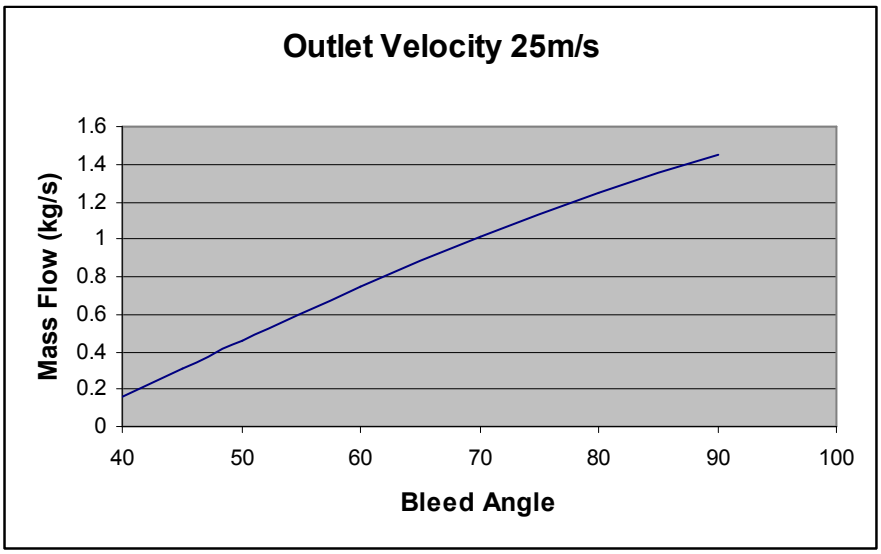

Bleed Outlet Angle	X Component	Y Component(-ve)	Mass Flow (kg/s)
90	25	0	1.44948125
80	24.62019383	4.341204442	1.251635
70	23.49231552	8.550503583	1.016992
60	21.65063509	12.5	0.7515244
50	19.15111108	16.06969024	0.4632032
45	17.67766953	17.67766953	0.313247
40	16.06969024	19.15111108	0.160938

Outlet Velocity 15m/s

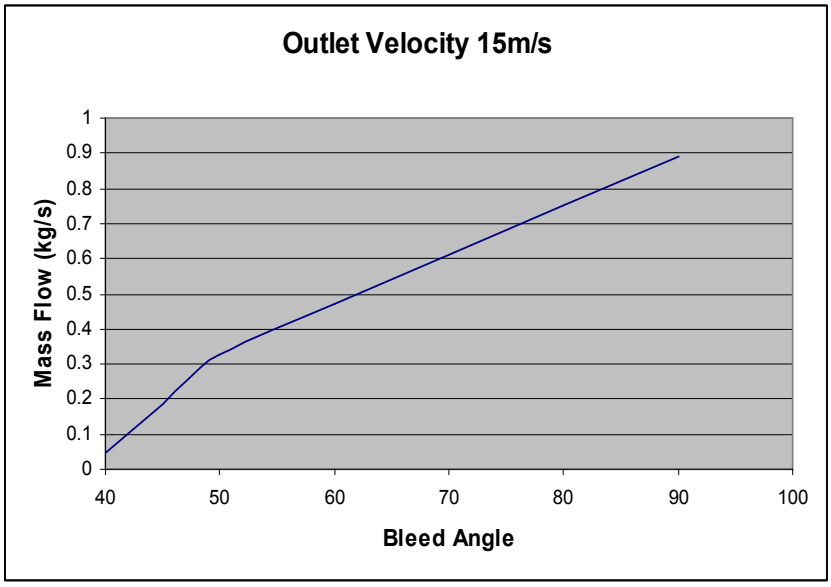

Bleed Outlet Angle	X Component	Y Component(-ve)	Mass Flow (kg/s)
90	15	0	0.8915223
80	14.7721163	2.604722665	0.750865
70	14.09538931	5.13030215	0.6102077
60	12.99038106	7.5	0.4695504
50	11.49066665	9.641814145	0.3288931
45	10.60660172	10.60660172	0.1882358
40	9.641814145	11.49066665	0.0475785

Outlet Velocity 5m/s

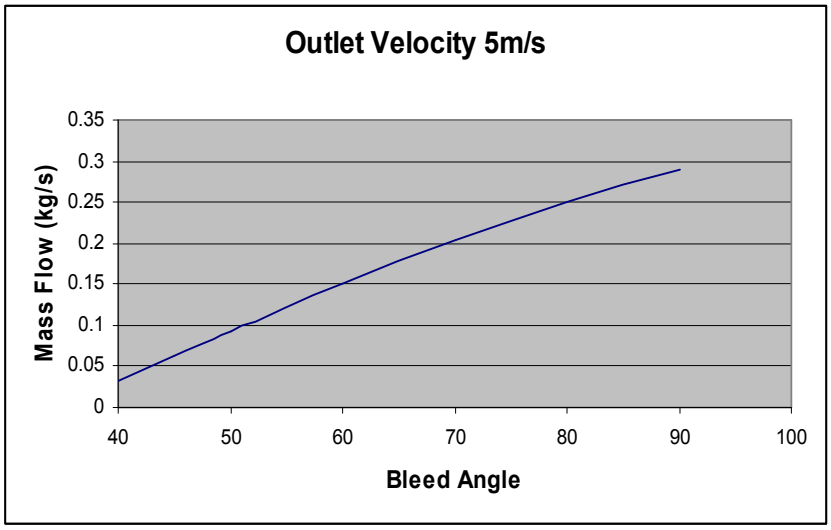

Bleed Outlet Angle	X Component	Y Component(-ve)	Mass Flow (kg/s)
90	5	0	0.2896272
80	4.924038765	0.868240888	0.2500953
70	4.698463104	1.710100717	0.2033833
60	4.330127019	2.5	0.15030485
50	3.830222216	3.213938048	0.09279672
45	3.535533906	3.535533906	0.06265101
40	3.213938048	3.830222216	0.03218762